

Robust Coordinated Control of FACTS Devices in Large Power Systems

Von der Fakultät für Ingenieurwissenschaften der
Universität Duisburg-Essen
zur Erlangung des akademischen Grades eines

Doktoringenieurs (Dr. -Ing.)

genehmigte Dissertation

von

Lijun Cai

aus

Hebei, P.R. China

Referent: Prof. Dr.-Ing. habil. István Erlich

Korreferent: Prof. Dr.-Ing. Edmund Handschin

Tag der mündlichen Prüfung: 16.02.2004

Bibliografische Information Der Deutschen Bibliothek

Die Deutsche Bibliothek verzeichnet diese Publikation in der Deutschen Nationalbibliografie; detaillierte bibliografische Daten sind im Internet über <http://dnb.ddb.de> abrufbar.

©Copyright Logos Verlag Berlin 2004

Alle Rechte vorbehalten.

ISBN 3-8325-0570-9

Logos Verlag Berlin
Comeniushof, Gubener Str. 47,
10243 Berlin
Tel.: +49 030 42 85 10 90
Fax: +49 030 42 85 10 92
INTERNET: <http://www.logos-verlag.de>

Lijun Cai, Robust Coordinated Control of FACTS Devices in Large Power Systems

Published by Logos Verlag Berlin 2004, ISBN 3-8325-0570-9

Gedruckt mit Unterstützung des Deutschen Akademischen Austauschdienstes

献给我亲爱的妈妈，爸爸，姐姐
和我可爱的妻子

*This work is gratefully dedicated to:
my dear mother, my father, my sister
and my lovely wife*

Acknowledgement

Foremost, I would like to express my sincere gratitude and appreciation to my advisor, Univ. Professor Dr.-Ing. habil. István Erlich, for his support, patience, and encouragement throughout my Ph.D study. His technical and editorial advice was essential to the completion of this dissertation. He is not only my supervisor but also encouraged and challenged me throughout my academic researches.

I am also grateful to my co-advisor, Univ. Professor Dr.-Ing. Edmund Handschin from the university of Dortmund, for reading previous drafts of this dissertation and providing many valuable comments that improved the presentation and contents of this dissertation.

My thanks also go to the other members of my examination board, Professor Dr.-Ing. G. Zimmer, Professor Dr.-Ing. S.X. Ding and Professor Dr.-Ing. A. Czulwik for their valuable comments and suggestions.

Furthermore, I would like to thank all members of the institute for contributing to such an inspiring and pleasant atmosphere. Special thanks go to Dipl.-Ing. Georgios Stamtsis and Dipl.-Ing. Getachew Befekadu for the discussions, cooperation and reading of the manuscript.

Finally, I would like to acknowledge the financial support of the German Academic Exchange Service (DAAD) for giving me the opportunity to pursue my doctoral degree in Germany.

Lijun Cai
Duisburg Germany
February , 2004

Abstract

With the rapid development of power electronics, *Flexible AC Transmission Systems* (FACTS) devices have been proposed and implemented in power systems. FACTS devices can be used to control power flow and enhance system stability. There is an increasing interest in using FACTS devices in the operation and control of power systems. However, their coordination with the conventional damping controllers in aiding of power system oscillation damping is still an open problem. Therefore, it is essential to investigate the coordinated control of FACTS devices and traditional power system controllers in large power systems.

The followings are areas of research achieved in this thesis:

- **FACTS modeling and controller design:** FACTS devices are modeled using the current injection method and the FACTS damping controllers are developed using the residue method in this thesis. This residue approach is a practical method for FACTS damping controller design in large power systems.
- **Optimal choice and allocation of FACTS devices:** FACTS devices can be used to control power flows. Therefore, provided optimal locations, FACTS devices can be used to achieve the optimal power flow without any constraint violation and thus to increase the utilization of the lowest cost generation in power systems. FACTS types and locations should be reasonably chosen according to their contribution to the general objective of power system economic generation and dispatch. In this research, using the genetic algorithms, the locations of the FACTS devices, their types and rated values are optimized simultaneously. The objective cost function, which consists of the investment costs for FACTS devices and the generation costs, is minimized.
- **Adaptive FACTS transient controller design using ANFIS technology:** This research deals with the development of adaptive FACTS transient

stability controller using Adaptive Network based Fuzzy Inference System (ANFIS) technology. The approach adaptively activates the FACTS transient stability controller in large power systems during large disturbances. The design aspects and their implementation in form of fuzzy-adaptive switching controller are presented. Furthermore, ANFIS technology is employed for the parameter optimization of the proposed controller. This approach is realized in a large power system and it is proved to be an effective method for the adaptive transient control of FACTS devices.

- **Simultaneous coordinated tuning of FACTS damping controller and conventional Power System Stabilizers (PSSs):** In this research, using the linearized power system model and the parameter-constrained non-linear optimization algorithm, interactions among FACTS controller and PSS controllers are considered. The controller parameters are optimized simultaneously to achieve a global optimal damping behavior. By realizing in a large power system, this approach is proved to be a general optimal tuning method for multi-controller parameters.
- **Robust FACTS loop-shaping POD (Power Oscillation Damping) controller design in large power systems:** This study deals with the FACTS robust loop-shaping POD controller design in large power systems. By applying the model reduction and modern robust loop-shaping control technique, the FACTS robust loop-shaping POD controller is realized. This controller exploits the advantages of both conventional loop-shaping and modern H_∞ robust control technique. Moreover, it is a decentralized approach and suitable for FACTS controller design in real large power systems. The performance of the proposed control scheme has fulfilled the robust stability and robust performance criteria. Furthermore, non-linear simulation has proved that using the proposed controller, the power oscillation damping behavior is also satisfactory under large disturbances.

Contents

LIST OF FIGURES AND TABLES	vii
List of Figures	vii
List of Tables	ix
CHAPTER 1 INTRODUCTION	1
1.1 Introduction of FACTS devices	1
1.2 Practical application of FACTS devices	5
1.3 Objectives of the dissertation	7
1.4 Outlines of the dissertation	9
CHAPTER 2 FACTS MODELING AND CONTROLLER DESIGN	11
2.1 FACTS modeling	11
2.1.1 FACTS devices	11
2.1.2 Current injection model for FACTS devices	12
2.2 FACTS controllers	16
2.2.1 FACTS steady-state controller.....	17
2.2.2 FACTS transient stability controller.....	18
2.2.3 FACTS POD controller	19
2.3 Single FACTS POD controller design	19
2.3.1 FACTS POD controller design – linear approach	19
2.3.1.1 Modal analysis for power system	20
2.3.1.2 FACTS POD controller design.....	25
2.3.2 FACTS POD controller design–non-linear approach.....	29
2.3.2.1 Non-linear parameter optimization for FACTS controller	29
2.3.2.2 Simulation result.....	31
2.4 Multi-FACTS coordinated POD controller design	32
2.4.1 Traditional sequential design	32
2.4.2 Fuzzy-logic based coordinated controller design	33
2.4.2.1 Fuzzy approach for coordination of POD controllers.....	35

2.4.2.2	Simulation results.....	39
2.4.2.3	Conclusion of fuzzy coordinated control scheme	41
2.5	Comments on the FACTS damping controller design.....	42
CHAPTER 3 SELECTION OF THE PROPER LOCATIONS FOR FACTS		
	DEVICES.....	43
3.1	Introduction	43
3.2	ATC criterion.....	44
3.3	Steady-state stability criterion	45
3.4	Economic criterion	49
3.4.1	Cost functions.....	50
3.4.1.1	Generation cost function	50
3.4.1.2	Cost functions for FACTS devices	51
3.4.2	Optimal FACTS allocation.....	52
3.4.3	Genetic algorithm.....	54
3.4.3.1	Encoding	54
3.4.3.2	Initial population	56
3.4.3.3	Fitness calculation.....	58
3.4.3.4	Reproduction	58
3.4.3.5	Crossover.....	59
3.4.3.6	Mutation	61
3.4.4	Case study	63
3.4.4.1	Case 1 — Voltage congestion at bus 2.....	64
3.4.4.2	Case 2 — Active power flow congestion.....	64
3.4.5	Conclusions of GA optimization method.....	65
3.5	Comments on the allocation of FACTS devices.....	66
CHAPTER 4 ADAPTIVE FACTS TRANSIENT CONTROLLER DESIGN		
	USING ANFIS TECHNOLOGY	67
4.1	Introduction	67
4.2	Switching strategy for FACTS transient controller.....	68
4.3	Fuzzy adaptive switching controller	69
4.3.1	Structure of the fuzzy adaptive switching controller	69
4.3.2	Fuzzy-logic loop.....	71

4.3.2.1	Fuzzification	71
4.3.2.2	Inference	72
4.3.2.3	Defuzzification	72
4.3.3	Protection loop	73
4.4	ANFIS training.....	73
4.4.1	ANFIS structure	73
4.4.2	ANFIS training	75
4.4.2.1	Fine-tuning of the membership functions.....	76
4.4.2.2	Training of the fuzzy inference system	76
4.4.3	Training data	76
4.4.4	Training results	78
4.4.4.1	Membership functions	78
4.4.4.2	Fuzzy inference system.....	79
4.5	Simulation results	80
4.6	Conclusion	81
 CHAPTER 5 SIMULTANEOUS COORDINATED TUNING OF FACTS POD		
AND PSS CONTROLLERS FOR DAMPING OF POWER		
SYSTEM OSCILLATIONS		
		83
5.1	Introduction.....	83
5.2	PSS and FACTS POD controller.....	84
5.2.1	PSS controller	84
5.2.2	FACTS POD controller	84
5.2.3	Conventional approach	85
5.3	Simultaneous coordinated tuning method.....	86
5.3.1	Linearized system model	87
5.3.2	Non-Linear optimization technique	88
5.3.3	Practical application.....	90
5.4	Simulation results	90
5.4.1	Dominant eigenvalues.....	90
5.4.2	Root-locus	91
5.4.3	Optimized system performance	92
5.4.4	System performance under different operating condition	93

5.4.5	Non-linear simulation results	93
5.5	Conclusion.....	94
CHAPTER 6 ROBUST FACTS LOOP-SHAPING POD CONTROLLER		
	DESIGN IN LARGE POWER SYSTEMS	95
6.1	Introduction	95
6.2	System model and performance criteria	96
6.2.1	General concepts of feedback control system	96
6.2.1.1	General model	96
6.2.1.2	Loop transfer function and sensitivities	97
6.2.1.3	Loop-shaping.....	98
6.2.2	Robust performance criteria	99
6.2.2.1	Normalization of inputs and outputs	99
6.2.2.2	Power system performance under uncertainties.....	99
6.3	FACTS robust loop-shaping POD controller design	104
6.3.1	Model reduction	105
6.3.2	FACTS loop-shaping controller design.....	107
6.3.3	Robust loop-shaping design using coprime factors.....	108
6.4	Simulation results.....	111
6.4.1	Nominal stability	111
6.4.2	Nominal performance.....	113
6.4.3	FACTS robust loop-shaping controller design.....	114
6.4.3.1	System model reduction	114
6.4.3.2	FACTS robust loop-shaping controller design	115
6.4.4	Robust stability and robust performance.....	118
6.4.5	Non-linear simulation results	121
6.5	Summary	122
CHAPTER 7 CONCLUSIONS AND FUTURE WORKS		
7.1	Conclusions	123
7.2	Future works.....	125
APPENDICES		
	Appendix 1	127
	Appendix 2	130

Appendix 3..... 130

Appendix 4..... 131

REFERENCES 133

LIST OF SYMBOLS 139

Latin Symbols..... 139

Greek Symbols 147

LIST OF ABBREVIATIONS..... 149

CURRICULUM VITAE 151

PUBLISHED PAPERS 153

DEVELOPED PROGRAMS..... 154

List of Figures and Tables

List of Figures

Figure 1.1	Functional diagrams of FACTS devices.....	3
Figure 2.1	Equivalent circuit diagrams of the considered FACTS devices	12
Figure 2.2	TCSC mathematical model for dynamic analysis	14
Figure 2.3	Mathematical model of TCPST	14
Figure 2.4	Mathematical model of SVC	15
Figure 2.5	Mathematical model of UPFC	16
Figure 2.6	Series FACTS steady-state power flow controller	17
Figure 2.7	Shunt FACTS steady-state controller	17
Figure 2.8	FACTS transient stability controller.....	18
Figure 2.9	FACTS POD controller	19
Figure 2.10	Power system with FACTS POD controller.....	26
Figure 2.11	Eigenvalue displacement after FACTS POD control action	27
Figure 2.12	Flow chart of the parametric optimization.....	31
Figure 2.13	Single machine infinite bus power system model	31
Figure 2.14	Non-linear simulation results.....	32
Figure 2.15	Three-area power system model.....	34
Figure 2.16	Fuzzy coordinated POD controllers.....	35
Figure 2.17	Block diagram of the fuzzy coordinated controller	36
Figure 2.18	Membership function.....	36
Figure 2.19	Simulation result - case 1	40
Figure 2.20	Simulation result - case 2.....	40
Figure 2.21	Simulation result - case 3.....	41
Figure 3.1	Simplified New England Power System.....	46
Figure 3.2	Dominant eigenvalues of the power system	47

Figure 3.3	Bode plot of the FACTS POD controller.....	48
Figure 3.4	Root-locus of the FACTS POD controller.....	49
Figure 3.5	Cost functions of the FACTS devices: SVC, TCSC and UPFC	52
Figure 3.6	Individual configuration of FACTS devices.....	55
Figure 3.7	Calculation of the entire population.....	57
Figure 3.8	Roulette wheel selection	59
Figure 3.9	Two points crossover	61
Figure 3.10	Flow chart of the GA optimization	63
Figure 3.11	Modified IEEE 14-bus test system.....	64
Figure 3.12	Simulation results.....	65
Figure 4.1	FACTS comprehensive control scheme.....	68
Figure 4.2	Fuzzy adaptive switching controller	70
Figure 4.3	Membership functions.....	71
Figure 4.4	ANFIS structure	75
Figure 4.5	Training data	78
Figure 4.6	Optimized membership functions of ΔP_{Line}	79
Figure 4.7	Training result.....	80
Figure 4.8	Simulation results.....	81
Figure 5.1	PSS controller.....	84
Figure 5.2	FACTS POD controller.....	85
Figure 5.3	Movements of eigenvalues.....	88
Figure 5.4	Flow chart of optimization based coordinated tuning method.....	89
Figure 5.5	Results of the conventional controller tuning	91
Figure 5.6	Root-locus of the FACTS POD controller.....	92
Figure 5.7	Optimization based coordinated tuning results	92
Figure 5.8	Non-linear simulation results	94
Figure 6.1	General SISO feedback control system model.....	96
Figure 6.2	General feedback control system with uncertainty	100
Figure 6.3	Controlled plant with uncertainty loop	101
Figure 6.4	Block diagram for the evaluation of nominal performance: N_{22} ...	103
Figure 6.5	Different routines of model reduction.....	106
Figure 6.6	Loop-shaping of the plant	107

Figure 6.7	Plant with controller and coprime factor uncertainty	108
Figure 6.8	The dominant eigenvalues of the power system.....	112
Figure 6.9	Root-locus of the FACTS POD controller.....	113
Figure 6.10	Maximum singular value plot of N_{22}	113
Figure 6.11	Bode diagram of the original and the reduced order system	114
Figure 6.12	Power system with FACTS robust POD controller.....	115
Figure 6.13	Root-locus of the FACTS robust loop-shaping controller.....	117
Figure 6.14	Feedback control system with multiplicative output uncertainty .	118
Figure 6.15	System performances.....	120
Figure 6.16	Non-linear simulation results.....	121

List of Tables

Table 2.1	Fuzzy inference table for fuzzy coordinated POD controller 1	38
Table 2.2	Fuzzy inference table for fuzzy coordinated POD controller 2	38
Table 3.1	The residues associated with the inter-area mode 2	47

Chapter 1

Introduction

1.1 Introduction of FACTS devices

With the rapid development of power electronics, *Flexible AC Transmission Systems* (FACTS) devices have been proposed and implemented in power systems. FACTS devices can be utilized to control power flow and enhance system stability. Particularly with the deregulation of the electricity market, there is an increasing interest in using FACTS devices in the operation and control of power systems with new loading and power flow conditions. A better utilization of the existing power systems to increase their capacities and controllability by installing FACTS devices becomes imperative.

Due to the present situation, there are two main aspects that should be considered in using FACTS devices: The first aspect is the flexible power system operation according to the power flow control capability of FACTS devices. The other aspect is the improvement of transient and steady-state stability of power systems. FACTS devices are the right equipment to meet these challenges.

1.1.1 Definition of FACTS

According to IEEE, FACTS, which is the abbreviation of *Flexible AC Transmission Systems*, is defined as follows [1]:

Alternating current transmission systems incorporating power electronics based and other static controllers to enhance controllability and power transfer capability.

Since the "other static controllers" based FACTS devices are not widely used in current power systems, this thesis focuses only on the power electronics based FACTS devices.

1.1.2 FACTS categories and their functions

1.1.2.1 FACTS categories

In general, FACTS devices can be divided into four categories [1,2]:

i Series FACTS devices:

Series FACTS devices could be a variable impedance, such as capacitor, reactor, etc., or a power electronics based variable source of main frequency, subsynchronous and harmonic frequencies (or a combination) to serve the desired need. In principle, all series FACTS devices inject voltage in series with the transmission line.

ii Shunt FACTS devices:

Shunt FACTS devices may be variable impedance, variable source, or a combination of these. They inject current into the system at the point of connection.

iii Combined series-series FACTS device:

Combined series-series FACTS device is a combination of separate series FACTS devices, which are controlled in a coordinated manner.

iv Combined series-shunt FACTS device:

Combined series-shunt FACTS device is a combination of separate shunt and series devices, which are controlled in a coordinated manner or one device with series and shunt elements.

1.1.2.2 Typical FACTS devices and their functions

In this thesis, four typical FACTS devices are considered in detail: TCSC (Thyristor Controlled Series Capacitor), TCPST (Thyristor Controlled Phase Shifting Transformer), UPFC (Unified Power Flow Controller) and SVC (Static Var Compensator). Their functional diagrams are shown in Figure 1.1.

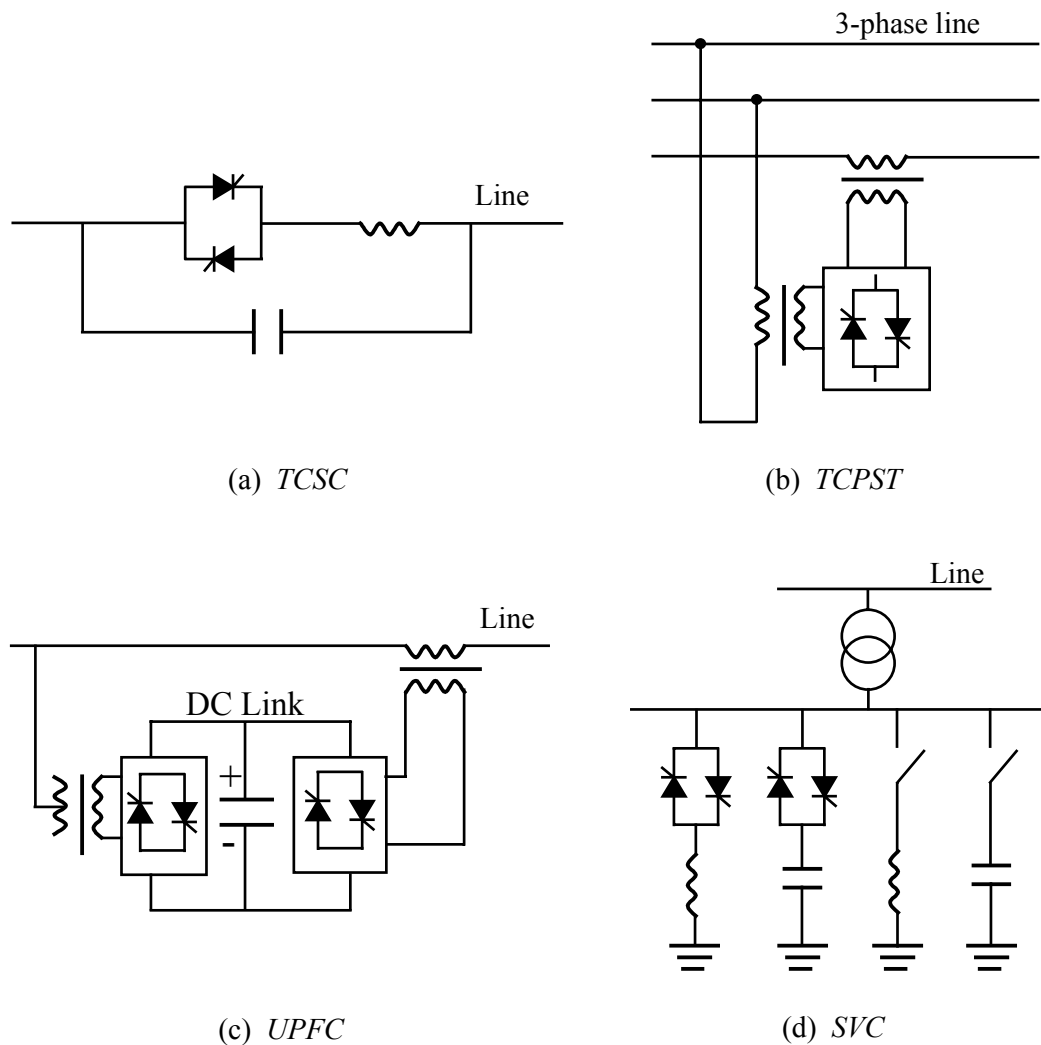


Figure 1.1 Functional diagrams of FACTS devices

TCSC is a typical series FACTS device that is used to vary the reactance of the transmission line. Since TCSC works through the transmission system directly, it is

much more effective than the shunt FACTS devices in the application of power flow control and power system oscillation damping control [1,2].

The UPFC is the most powerful and versatile FACTS device due to the facts that the line impedance, terminal voltages, and the voltage angles can be controlled by it as well. Similar to the UPFC, TCPST is also a typical combined series-shunt FACTS device, which can be used to regulate the phase angle difference between the two terminal voltages.

SVC is a shunt FACTS device that can be used to control the reactive compensation.

1.1.3 Possible benefits from FACTS technology

Within the basic system security guidelines, the FACTS devices enable the transmission system to obtain one or more of the following benefits [1-4,9]:

- Control of power flow as ordered. This is the main function of FACTS devices. The use of power flow control may be to follow a contract, meet the utilities' own needs, ensure optimum power flow, ride through emergency conditions, or a combination of them.
- Increase utilization of lowest cost generation. One of the principal reasons for transmission interconnections is to utilize the lowest cost generation. When this cannot be done, it follows that there is not enough cost-effective transmission capacity. Cost-effective enhancement of capacity will therefore allow increased use of lowest cost generation.
- Dynamic stability enhancement. This FACTS additional function includes the transient stability improvement, power oscillation damping and voltage stability control.
- Increase the loading capability of lines to their thermal capabilities, including short term and seasonal demands.
- Provide secure tie-line connections to neighboring utilities and regions thereby decreasing overall generation reserve requirements on both sides.
- Upgrade of transmission lines.

- Reduce reactive power flows, thus allowing the lines to carry more active power.
- Loop flows control.

1.2 Practical application of FACTS devices

Many projects are succeeded to prove the benefits of FACTS devices over the last years. Although there are numerous successful installation examples, for the sake of highlight, only four main new applications are briefly discussed in this section: WAPA's Kayenta ASC, BPA's Slatt TCSC, TVA's Sullivan STATCOM and AEP's Inez UPFC [1].

WAPA's Kayenta advanced series capacitor (ASC)

The total ASC system, dedicated in 1992, which includes a TCSC and a conventional series capacitor, was installed at the Kayenta 230 kV substation in Western Area Power Administration (WAPA) in Northeast Arizona. This ASC was employed to increase the reliable transmission capacity of a 230 kV line between Glen Canyon and Shiprock. The ASC consists of two 55 Ω series capacitor banks each rated for 165 Mvar and 1000 A. The results of the project have proved that the ASC is a reliable means of using existing transmission capacity while maintaining system security.

BPA's Slatt TCSC

The BPA's Slatt TCSC, dedicated in September 1993, is installed at the Slatt 500 kV substation in Bonneville Power Administration (BPA) in Oregon. It was put into economic operation in 1995. This TCSC is in series with the Slatt-Buckley 500 kV transmission line. The location for the installation was selected to expose the TCSC to severe operating conditions and to gain sufficient operating benefits and experience. The maximum dynamic range of capacitive reactance is 24 Ω and the nominal three-

phase compensation is 202 MVar. The results of this project show that TCSC is not only an effective means of impedance and current control but also a powerful means for increasing power system stability. Furthermore, TCSC also provides powerful damping against subsynchronous resonance (SSR).

TVA's Sullivan STATCOM

This first high-power STATCOM (Static Synchronous Compensator) in the United States was commissioned in late 1995 at the Sullivan substation of the Tennessee Valley Authority (TVA) for transmission line compensation. The STATCOM is employed to regulate the 161 kV bus voltage during the daily load buildup so that the tap changer on the transformer bank will be used less often. The nominal capacity of the STATCOM is ± 100 MVar. This application shows that STATCOM is a versatile equipment with outstanding dynamic capability, that will find increasing application in power transmission systems.

AEP's Inez UPFC

This first UPFC in the world was commissioned in mid-1998 at the Inez station of the American Electric Power (AEP) in Kentucky for voltage support and power flow control. This UPFC was designed to provide fast reactive shunt compensation with a total control range 320 MVar, and control power flow in the 138 kV high-capacity transmission line. Furthermore, it can be applied to force the transmitted power, under contingency conditions, up to 950 MVA.

The application proved that the UPFC has the unique capability to provide independent and concurrent control for the real and reactive line power flow, as well as the regulation of the bus voltage. Moreover, it has a flexible circuit structure to be reconfigured for independent shunt and series compensation, as well as for only shunt or only series compensation at double rating.

There are also many other successful applications of FACTS devices. Particularly, in recent years, with the improvements in power electronics, the costs of FACTS devices

could be reduced considerably and thus the practical application of FACTS devices becomes more favorable.

1.3 Objectives of the dissertation

As mentioned in the previous sections, FACTS devices can be effectively utilized for the steady-state power flow control and dynamic control of power systems. Even if many researches have already been made on these subjects, the following points need to be investigated in detail:

- FACTS controller design in large power systems
- Proper allocation of FACTS devices
- Coordinated design and tuning of FACTS and conventional PSS (Power System Stabilizer) controllers
- Adaptive FACTS transient control
- Robust control of FACTS damping controller

To address the above-mentioned points, the following five general objectives are considered in this dissertation:

➤ **FACTS modeling and controller design**

This fundamental objective focuses on the FACTS modeling and FACTS controller design methods. In this research, the FACTS devices are modeled using the current injection method and the FACTS damping controllers are realized using the residue method. Furthermore, programs for both steady-state study and dynamic study of large power systems embedded with FACTS devices are developed.

➤ **Optimal choice and allocation of FACTS devices**

FACTS devices can be used to control power flows. Provided that they are located at optimal locations, FACTS devices can be applied to achieve the optimal power flow without any constraint violation. Therefore, they can be used to achieve power system economic operation by means of increasing the utilization of the lowest cost generation. FACTS types and their locations should be chosen according to their contributions to the general objective of power system economic generation and dispatching. In this research, using genetic algorithms, the locations of the FACTS devices, their types and rated values are optimized simultaneously. The objective cost function, which consists of the investment costs for FACTS devices and the generation costs, is minimized using the proposed approach.

Besides to the above-mentioned economic criterion based allocation approach, the residue method based FACTS allocation approach is also applied to the power system dynamic analysis.

➤ **Adaptive FACTS transient controller design using ANFIS technology**

This objective deals with the development of adaptive FACTS transient stability controller using Adaptive Network based Fuzzy Inference System (ANFIS) technology. The approach adaptively activates the FACTS transient stability controller in large power systems during large disturbances. The design aspects and their implementation in form of fuzzy-adaptive switching controller are presented. Furthermore, ANFIS technology is employed for the parameter optimization of the proposed controller. This approach is realized in a large power system and it is proved to be an effective method for the adaptive transient control of FACTS devices.

➤ **Coordinated tuning of FACTS and conventional power system oscillation damping controllers**

This subject concerns the simultaneous coordinated tuning of the FACTS damping controller and the conventional PSS controllers in large power systems. Traditionally,

the controller parameters are determined sequentially and separately. These so determined parameters are not the global optimal settings. Moreover, the damping task is not properly allocated to each controller. A new method for the coordinated tuning of FACTS damping controller and the conventional PSS controllers has been developed based on non-linear optimization algorithm. Using this method, interactions among FACTS controller and PSS controllers are considered and their controller parameters are optimized simultaneously.

➤ **Robust FACTS loop-shaping POD (Power Oscillation Damping) controller design in large power systems**

This study deals with the FACTS robust loop-shaping POD controller design in large power systems. By applying the model reduction and modern robust loop-shaping control technique, the FACTS robust loop-shaping POD controller is realized. This controller exploits the advantages of both conventional loop-shaping and modern H_∞ robust control technique. Moreover, it is a decentralized approach and practical for FACTS controller design in real large power systems. The performance of the proposed control scheme has fulfilled the robust stability and robust performance criteria. Furthermore, non-linear simulation has proved that using the proposed controller, the power oscillation damping behavior is also satisfactory under large disturbances.

1.4 Outlines of the dissertation

This dissertation is organized as follows: following the Introduction, in Chapter 2, the FACTS modeling and controller design methods are discussed. Fuzzy coordinated control between two FACTS controllers is also introduced in this chapter.

In Chapter 3, a general economic criterion based algorithm for the optimal choice and allocation of FACTS devices in large power systems is discussed. Furthermore, the residue based FACTS allocation method is also introduced for the power system dynamic analysis.

In Chapter 4, the design of adaptive FACTS transient stability controller is introduced. The design aspects and their implementation in form of fuzzy adaptive

switching controller are presented. Furthermore, ANFIS technology is employed for the parameter optimization of the proposed controller.

In Chapter 5, the method for simultaneous coordinated tuning of the FACTS POD controller and the conventional PSS controllers is presented.

In Chapter 6, the robust loop-shaping control scheme for FACTS POD controller in large power systems is introduced.

Finally, in Chapter 7, the conclusions of this research work can be found. Moreover, some suggestions on the extensions to potential topics for future research are presented.

Chapter 2

FACTS Modeling and Controller Design

2.1 FACTS modeling

Incorporating FACTS into power system model

In order to investigate the impact of FACTS devices on power systems effectively, appropriate FACTS models are very important. In this section, the FACTS devices and their mathematical models will be introduced.

2.1.1 FACTS devices

In this thesis, four typical FACTS devices have been considered: TCSC, TCPST, UPFC, and SVC. As mentioned in Section 1.1, the reactance of the transmission line can be changed by TCSC. TCPST varies the phase angle between the two terminal voltages and SVC can be employed to achieve the reactive compensation. The UPFC is the most powerful and versatile FACTS device. The line impedance, terminal voltages, and the voltage angle can be controlled by it as well. The equivalent circuit diagrams of the four types of FACTS devices are shown in Figure 2.1.

The power flow P_{ij} through the transmission line $i-j$ is a function of line reactance X_{ij} , the voltage magnitude U_i , U_j and the phase angle between the sending and receiving end voltages $\delta_i - \delta_j$.

$$P_{ij} = 3 \cdot \frac{U_i U_j}{X_{ij}} \cdot \sin(\delta_i - \delta_j) \quad (2.1)$$

FACTS devices can be applied to control the power flow by adjusting the variables contained in Equation 2.1. Furthermore, since FACTS devices can regulate these variables in a very fast and effective way, they are also suitable for power system dynamic controls.

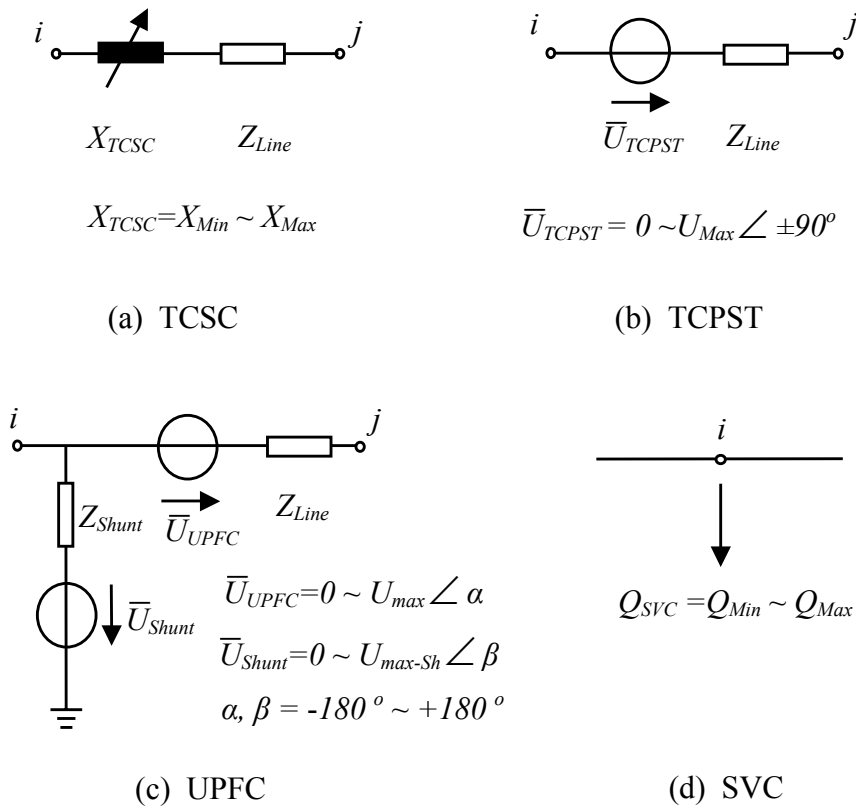


Figure 2.1 Equivalent circuit diagrams of the considered FACTS devices

2.1.2 Current injection model for FACTS devices

The mathematical models of the FACTS devices are developed as follows:

TCSC

The TCSC can serve as the capacitive or inductive compensation by modifying the reactance of the transmission line. In the power flow study, the reactance of TCSC, which is the control variable, can be considered in the admittance matrix directly. It is a function of the reactance of the transmission line where the TCSC is located:

$$X_{ij} = X_{Line} + X_{TCSC}, \quad X_{TCSC} = rtcsc \cdot X_{Line} \quad (2.2)$$

where X_{Line} is the reactance of the transmission line and $rtcsc$ is the coefficient which represents the compensation degree of TCSC.

To avoid overcompensation, the working range of the TCSC should be limited between $-0.7X_{Line}$ and $0.2 X_{Line}$ [9-10].

$$rtcsc_{\min} = -0.7, \quad rtcsc_{\max} = 0.2 \quad (2.3)$$

For the power system dynamic analysis, the X_{TCSC} will be changed continuously and this would result in changes in the factorized system admittance matrix. Therefore it is necessary to convert the change in X_{TCSC} into the injected currents:

$$\begin{aligned} \Delta \bar{I}_i &= \frac{\bar{U}_i^{(t)} - \bar{U}_j^{(t)}}{Z_{ij}^{(0)} (Z_{ij}^{(0)} + j\Delta X_{TCSC}^{(t)})} \cdot j\Delta X_{TCSC}^{(t)} = \frac{\bar{U}_i^{(t)} - \bar{U}_j^{(t)}}{Z_{ij}^{(0)} Z_{ij}^{(t)}} \cdot j\Delta X_{TCSC}^{(t)} \\ \Delta \bar{I}_j &= -\frac{\bar{U}_i^{(t)} - \bar{U}_j^{(t)}}{Z_{ij}^{(0)} (Z_{ij}^{(0)} + j\Delta X_{TCSC}^{(t)})} \cdot j\Delta X_{TCSC}^{(t)} = -\frac{\bar{U}_i^{(t)} - \bar{U}_j^{(t)}}{Z_{ij}^{(0)} Z_{ij}^{(t)}} \cdot j\Delta X_{TCSC}^{(t)} \end{aligned} \quad (2.4)$$

where

$Z_{ij}^{(0)} = Z_{Line} + jX_{TCSC}^{(0)}$ denotes the initial influence of TCSC on the transmission line.

$Z_{ij}^{(t)}$ denotes the influence of TCSC on the transmission line at the time t .

$X_{TCSC}^{(0)}$, $X_{TCSC}^{(t)}$ are the TCSC reactance at the initial operating point and at the time t .

$\Delta X_{TCSC}^{(t)} = X_{TCSC}^{(t)} - X_{TCSC}^{(0)}$ denotes the change of the TCSC reactance at the time t .

$\bar{U}_i^{(t)}, \bar{U}_j^{(t)}$ are the terminal voltages of TCSC at the time t .

TCSC mathematical model for dynamic analysis is shown in Figure 2.2.

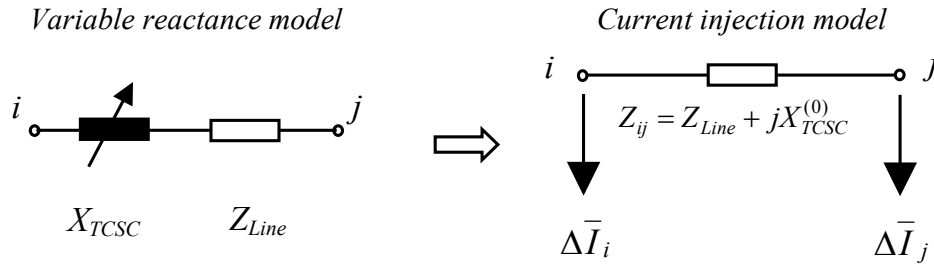


Figure 2.2 TCSC mathematical model for dynamic analysis

TCPST

TCPST regulates the voltage angle difference between the sending and receiving end of the transmission line. It is modeled as a series compensation voltage $\Delta \bar{U}_{FACTS} = \bar{U}_{TCPST}$, as shown in Figure 2.3, which is perpendicular to the sending bus voltage. The working range brought by the TCPST is between -5 degrees to +5 degrees.

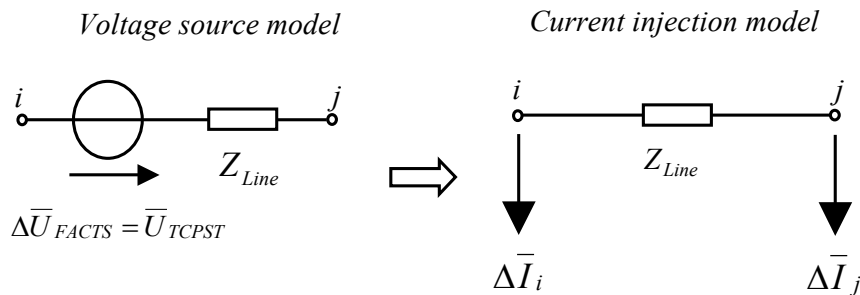


Figure 2.3 Mathematical model of TCPST

During the dynamic simulation, the injected voltage \bar{U}_{TCPST} , which is the controlled variable, is transformed into injected nodal currents according to Equation 2.5. For the steady-state power flow analysis, this model will also be applied.

$$\Delta \bar{I}_i = -\frac{\bar{U}_{TCPST}}{Z_{Line}}, \quad \Delta \bar{I}_j = \frac{\bar{U}_{TCPST}}{Z_{Line}} \quad (2.5)$$

SVC

The SVC can be operated at both inductive and capacitive compensation. In the steady-state and dynamic analysis, the injected power at bus i at the time t $\Delta Q_i = Q_{SVC}^{(t)}$, which is the controlled variable, can be transferred into injected current at bus i according to Equation 2.6, where $\bar{U}_i^{(t)}$ is the terminal voltage of SVC at the time t . The mathematic model of SVC is shown in Figure 2.4.

$$\Delta \bar{I}_i = \frac{Q_{SVC}^{(t)}}{\bar{U}_i^{(t)}} \quad (2.6)$$

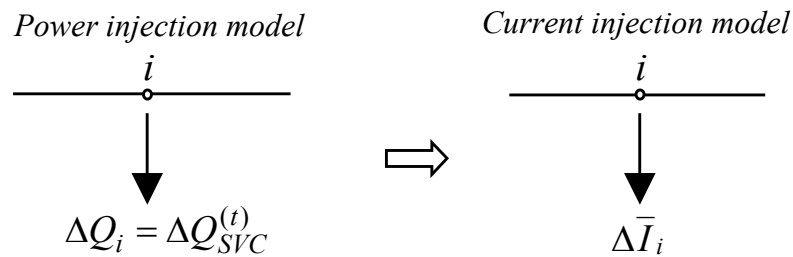


Figure 2.4 Mathematical model of SVC

UPFC

As shown in Figure 1.1, the UPFC has two voltage source inverters (VSI) sharing a common dc storage capacitor. It is connected to the system through two coupling transformers [11-13]. The UPFC is modeled using two voltage sources \bar{U}_{UPFC} and

\bar{U}_{Shunt} . During the steady-state and dynamic analysis, the control variables \bar{U}_{UPFC} and \bar{U}_{Shunt} are transformed into injected nodal currents according to Equation 2.7. The mathematical model of UPFC is shown in Figure 2.5.

$$\Delta \bar{I}_i = -\frac{\bar{U}_{UPFC}}{Z_{Line}} + \frac{\bar{U}_{Shunt}}{Z_{Shunt}}, \quad \Delta \bar{I}_j = \frac{\bar{U}_{UPFC}}{Z_{Line}} \quad (2.7)$$

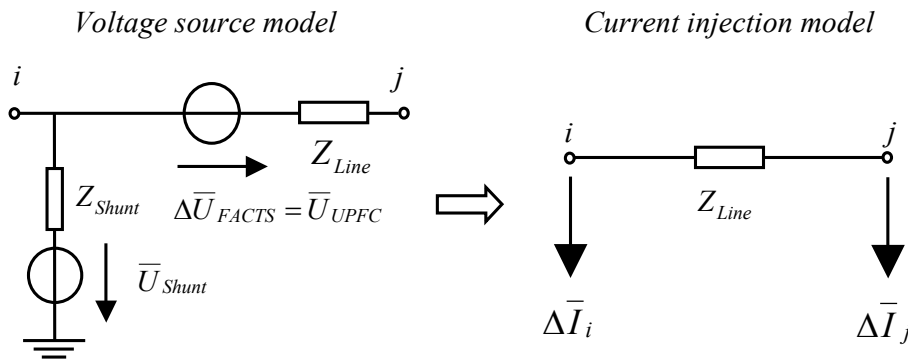


Figure 2.5 Mathematical model of UPFC

Practically, the outputs of FACTS devices must be restricted by the limits within their working conditions. This issue is also considered in the simulation programs.

2.2 FACTS controllers

Normally, the FACTS controllers consist of the following three main control schemes [15]:

- Steady-state power flow control
- Transient control for improving the first swing stability
- POD (Power Oscillation Damping) control to damp the power system oscillations

These control schemes will be introduced in detail in this section.

2.2.1 FACTS steady-state controller

The main function of the series FACTS steady-state controller is to control power flow. In general, the "constant line power" strategy will be applied [15]. The power flow control loop of series FACTS devices is shown in Figure 2.6.

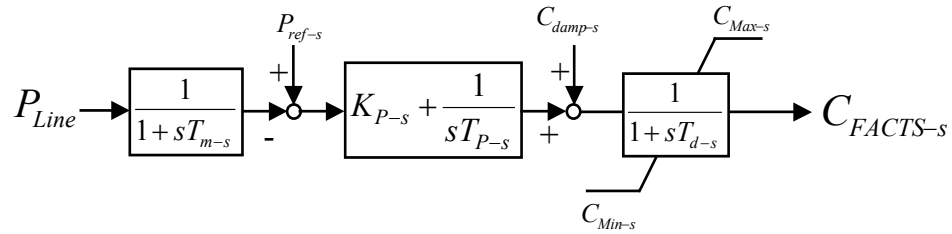


Figure 2.6 Series FACTS steady-state power flow controller

where P_{ref-s} and C_{damp-s} are reference values of the active power and the signal from series FACTS damping controller respectively. The controller input P_{Line} is the active power, which flows through the series FACTS devices. The output $C_{FACTS-s}$ represents the compensation value of the series FACTS devices. For instance, for TCSC, it is the value of the series compensation degree and for UPFC it is the series injected voltage.

T_{m-s} is the measurement time constant for the series FACTS devices. T_{d-s} approximates the delay due to the main circuit characteristics and control systems. K_{P-s} is the proportional part and T_{I-s} is the integral time constant of the series FACTS PI-controller respectively.

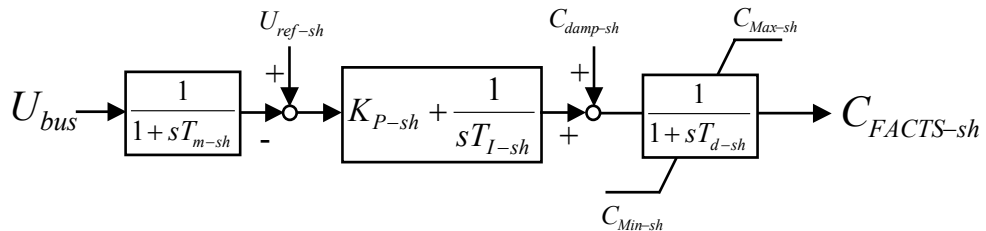


Figure 2.7 Shunt FACTS steady-state controller

For the shunt FACTS steady-state controller, its main function is to achieve the reactive compensation and bus voltage control. In general, as shown in Figure 2.7, PI-controller is always used to meet these objectives [15].

where U_{ref-sh} and $C_{damp-sh}$ are reference values of the bus voltage magnitude and the signal from shunt FACTS damping controller respectively. The controller input U_{bus} is the bus voltage magnitude. The output $C_{FACTS-sh}$ represents the compensation value of the shunt FACTS devices.

Similar to the series FACTS steady-state controller, T_{m-sh} is the measurement time constant for the shunt FACTS devices. T_{d-sh} approximates the delay due to the main circuit characteristics and control systems. K_{P-sh} and T_{I-sh} are the proportional part and integral time constant of the shunt FACTS PI-controller respectively.

2.2.2 FACTS transient stability controller

Following a large disturbance, the FACTS transient stability controller acts initially to give a maximum compensation for a pre-set time T_0 [15]. The function of the FACTS transient controller is shown in Figure 2.8, where $C_{Initial}$ and C_{Max} represent the initial compensation value and the maximum compensation value of FACTS devices respectively.

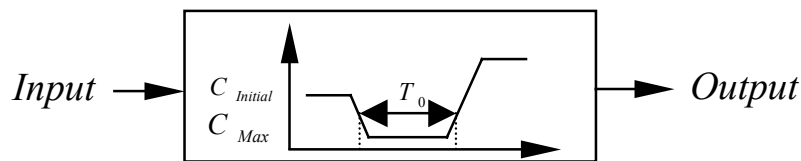


Figure 2.8 FACTS transient stability controller

The input to the FACTS transient stability controller is always the same as the FACTS steady-state controller. The output is a switch signal for activating the maximum compensation level required for transient stability support. After the pre-set time T_0 , the FACTS control will be transferred back to the damping control. This function will be discussed in detail in Chapter 4.

2.2.3 FACTS POD controller

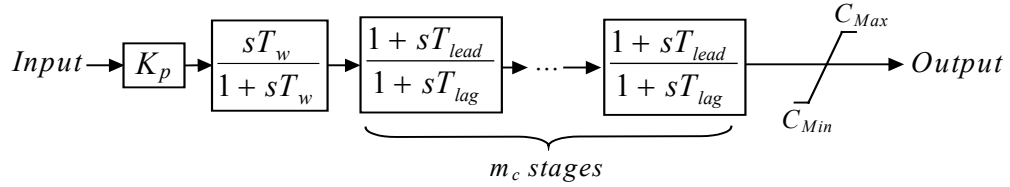


Figure 2.9 FACTS POD controller

Similar to the FACTS transient and steady-state controller, as shown in Figure 2.9, local signals are always employed as input to the POD controller, i.e. the active power flow through the FACTS device or the FACTS terminal voltages. The output represents the compensation value of FACTS devices. The structure and the design procedure of FACTS POD controller will be discussed in detail in Section 2.3.

2.3 Single FACTS POD controller design

In this section, two main methods for FACTS POD controller design, i.e. linear and non-linear approaches, will be discussed.

2.3.1 FACTS POD controller design – linear approach

Generally, there are two kinds of power oscillation damping controllers in power systems: PSS and FACTS POD controllers. PSS acts through the excitation system of generator to increase the damping of electromechanical oscillations by generating a component of electrical torque proportional to speed change.

Usually PSSs are designed for damping local electromechanical oscillations. However, in large power systems, these PSSs may not provide enough damping for inter-area modes. In this case, FACTS devices offer an effective strategy for inter-area modes damping control.

2.3.1.1 Modal analysis for power system

In this section some basics to modal analysis, which are necessary to understand the controller design methods, are introduced.

Power system is a typical dynamic system. By linearizing about an operating point, the total linearized system model including PSS and FACTS devices can be represented by the following equation:

$$\begin{aligned}\dot{\Delta \mathbf{x}} &= \mathbf{A}\Delta \mathbf{x} + \mathbf{B}\Delta \mathbf{u} \\ \Delta \mathbf{y} &= \mathbf{C}\Delta \mathbf{x} + \mathbf{D}\Delta \mathbf{u}\end{aligned}\quad (2.8)$$

where

$\Delta \mathbf{x}$ is the state vector of length equal to the number of states n

$\Delta \mathbf{y}$ is the output vector of length m

$\Delta \mathbf{u}$ is the input vector of length r

\mathbf{A} is the n by n state matrix

\mathbf{B} is the control or input matrix with dimensions n by the number of inputs r

\mathbf{C} is the output matrix of size m by n

\mathbf{D} is the feed forward matrix of dimensions m by r

By taking the Laplace transform of the above equations, the state equations in the frequency domain can be obtained:

$$\begin{aligned}s\Delta \mathbf{x}(s) - \Delta \mathbf{x}(0) &= \mathbf{A}\Delta \mathbf{x}(s) + \mathbf{B}\Delta \mathbf{u}(s) \\ \Delta \mathbf{y}(s) &= \mathbf{C}\Delta \mathbf{x}(s) + \mathbf{D}\Delta \mathbf{u}(s)\end{aligned}\quad (2.9)$$

A formal solution of the state equations results in:

$$\Delta \mathbf{y}(s) = \mathbf{C}(s\mathbf{I} - \mathbf{A})^{-1}[\Delta \mathbf{x}(0) + \mathbf{B}\Delta \mathbf{u}(s)] + \mathbf{D}\Delta \mathbf{u}(s) \quad (2.10)$$

where \mathbf{I} represents the identity matrix.

The equation

$$\det(s\mathbf{I} - \mathbf{A}) = 0 \quad (2.11)$$

is referred to as the characteristic equation of matrix \mathbf{A} and the values of s which satisfy the characteristic equation are the eigenvalues of matrix \mathbf{A} .

The natural modes of system response are related to the eigenvalues. Analysis of the eigenproperties of \mathbf{A} provides valuable information regarding the stability characteristics of the system [16].

Because power systems are physical systems, thus \mathbf{A} is a n by n matrix and it has n solutions of eigenvalues:

$$\lambda = \lambda_1, \lambda_2, \dots, \lambda_n \quad (2.12)$$

For any eigenvalue λ_i , the n -column vector $\boldsymbol{\phi}_i$, which satisfies Equation 2.13, is called the right eigenvector of \mathbf{A} associated with the eigenvalue λ_i [16].

$$\mathbf{A} \cdot \boldsymbol{\phi}_i = \lambda_i \cdot \boldsymbol{\phi}_i \quad (2.13)$$

Similarly, the n -row vector $\boldsymbol{\psi}_i$, which satisfies

$$\boldsymbol{\psi}_i \cdot \mathbf{A} = \lambda_i \cdot \boldsymbol{\psi}_i \quad (2.14)$$

is called the left eigenvector associated with the eigenvalue λ_i .

Physically, the right eigenvector describes how each mode of oscillation is distributed among the systems states and it is called mode shape. The left eigenvector, together with the input coefficient matrix and the disturbance determines the amplitude of the mode in time domain solution for a particular case [16].

In order to express the eigenproperties of \mathbf{A} succinctly, the modal matrices are also introduced:

$$\Phi = [\phi_1 \phi_2 \dots \phi_n] \quad (2.15)$$

$$\Psi = [\psi_1^T \psi_2^T \dots \psi_n^T]^T \quad (2.16)$$

Eigenvalue sensitivity

Eigenvalue sensitivity is applied to determine the sensitivity of eigenvalues to changes in the elements of the state matrix \mathbf{A} . The sensitivity of the eigenvalue λ_i to the element a_{kj} of the state matrix is equal to the product of the left eigenvector element ψ_{ik} and the right eigenvector element ϕ_{ji} :

$$\frac{\partial \lambda_i}{\partial a_{kj}} = \psi_{ik} \phi_{ji} \quad (2.17)$$

Participation matrix

Participation matrix \mathbf{P} , which combines the right and left eigenvectors as a measure of the association between the state variables and the modes, denotes the eigenvalue sensitivity with respect to the diagonal element of the state matrix:

$$\mathbf{P} = [\mathbf{p}_1 \quad \mathbf{p}_2 \quad \dots \quad \mathbf{p}_n] \quad (2.18)$$

with

$$\mathbf{p}_i = \begin{bmatrix} p_{1i} \\ p_{2i} \\ \dots \\ p_{ni} \end{bmatrix} = \begin{bmatrix} \frac{\partial \lambda_1}{\partial a_{ii}} \\ \frac{\partial \lambda_2}{\partial a_{ii}} \\ \dots \\ \frac{\partial \lambda_n}{\partial a_{ii}} \end{bmatrix} = \begin{bmatrix} \phi_{1i} \psi_{i1} \\ \phi_{2i} \psi_{i2} \\ \dots \\ \phi_{ni} \psi_{in} \end{bmatrix} \quad (i = 1 \sim n) \quad (2.19)$$

where

ϕ_{ki} is the element on the k^{th} row and i^{th} column of the modal matrix Φ ($i \leq n, k \leq n$).

ψ_{ik} is the element on the i^{th} row and k^{th} column of the modal matrix Ψ .

$p_{ki} = \phi_{ki}\psi_{ik}$ is the participation factor. It is a measure of the relative participation of the k^{th} state variable in the i^{th} mode, and vice versa [16].

Controllability and observability

In order to modify a mode of oscillation by feedback, the chosen input must excite the mode and it must also be visible in the chosen output. The measures of these two properties are controllability and observability respectively [5].

The system is said to be controllable if for any initial state $\Delta \mathbf{x}(t_0) = \mathbf{x}_0$ and any final state $\Delta \mathbf{x}(t_1) = \mathbf{x}_1$, there exists an input that transfers \mathbf{x}_0 to \mathbf{x}_1 in a finite time. Otherwise, the system is said to be uncontrollable.

The system is said to be observable if for any unknown initial state $\Delta \mathbf{x}(t_0) = \mathbf{x}_0$, there exists a finite $t_1 > 0$ such that the knowledge of the input \mathbf{u} and output \mathbf{y} over $[0, t_1]$ suffices to determine uniquely the initial state \mathbf{x}_0 . Otherwise, the system is said to be unobservable.

The modal controllability and modal observability matrices are defined as follows:

$$\tilde{\mathbf{B}} = \Phi^{-1} \cdot \mathbf{B} \quad (2.20)$$

$$\tilde{\mathbf{C}} = \mathbf{C} \cdot \Phi \quad (2.21)$$

The $n \times r$ matrix $\tilde{\mathbf{B}}$ is referred to as the modal controllability matrix, and the $m \times n$ matrix $\tilde{\mathbf{C}}$ as modal observability matrix [16].

A mode must be both controllable by the chosen input and observable in the chosen output for a feedback control to have any effect on the mode. Therefore, the

determination of suitable feedback variables is an important objective in FACTS damping controller design procedure.

Residues

The above-mentioned state-space representation is concerned not only with input and output properties of the system but also with its complete internal behavior. In contrast, the transfer function representation specifies only the input-output behavior [16].

Considering Equation 2.8 with single input and single output (SISO) and assuming $\mathbf{d}=0$:

$$\begin{aligned}\Delta \dot{\mathbf{x}} &= \mathbf{A}\Delta \mathbf{x} + \mathbf{b}\Delta u \\ \Delta y &= \mathbf{c}\Delta \mathbf{x}\end{aligned}\quad (2.22)$$

the transfer function of this SISO system can be obtained as:

$$G(s) = \frac{\Delta y(s)}{\Delta u(s)} = \mathbf{c}(s\mathbf{I} - \mathbf{A})^{-1} \mathbf{b} \quad (2.23)$$

$G(s)$ has the general form and can be factored:

$$G(s) = K \frac{(s - z_1)(s - z_2)\dots(s - z_l)}{(s - p_1)(s - p_2)\dots(s - p_n)} \quad (2.24)$$

where p_1, p_2, \dots, p_n are the poles of $G(s)$ and the eigenvalues of the system. z_1, z_2, \dots, z_n are the zeros of $G(s)$.

$G(s)$ can also be expanded in partial fractions as:

$$G(s) = \frac{R_1}{(s - p_1)} + \frac{R_2}{(s - p_2)} + \dots + \frac{R_n}{(s - p_n)} = \sum_{i=1}^n \frac{R_i}{(s - p_i)} = \sum_{i=1}^n \frac{R_i}{(s - \lambda_i)} \quad (2.25)$$

where R_i is the residue of $G(s)$ at pole p_i and it can be expressed as [16]:

$$R_i = \mathbf{c} \boldsymbol{\phi}_i \boldsymbol{\psi}_i \mathbf{b} \quad (2.26)$$

Residues give the sensitivity of the corresponding eigenvalue to feedback of the transfer function output to its input. They are useful in finding the feedback signal, which gives the largest influence on the researched mode.

2.3.1.2 FACTS POD controller design

Generally, the damping function of FACTS devices is performed mainly through the changes of the power delivered along the transmission line. With appropriate lead-lag compensation, the damping torque provided by FACTS damping control is proportional to the gain of the controller.

Since FACTS devices are located in transmission systems, local input signals are always preferable. Residue method is an appropriate approach in finding the most proper local feedback signal in the controller design procedure. Moreover, it is also a simple and practical approach for designing of FACTS POD controllers. Therefore, in this research, residue method is applied and the linear FACTS POD controller design procedure is shown as follows:

- Selection of the proper feedback signal
- Design of the controller using the residue method
- Test the controller under wide range of operation conditions

Introduction to the residue method

Considering the close loop system shown in Figure 2.10, where $G(s)$ represents the transfer function of the original power system and $H(s)$ is the transfer function of the FACTS POD controller. Assuming the FACTS location is determined, therefore the input signal $u(s)$ is available. The output signal $y(s)$ can be chosen based on the maximum residue provided by the selected outputs.

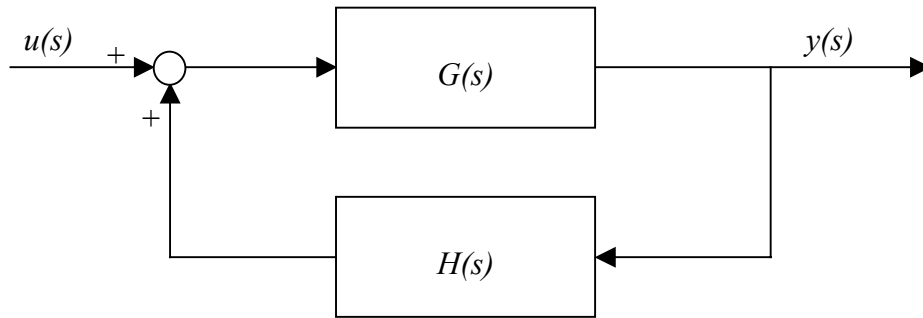


Figure 2.10 Power system with FACTS POD controller

As illustrated in Figure 2.9, FACTS POD controller involves a transfer function consisting of an amplification block, a wash-out block and m_c stages of lead-lag blocks (usually $m_c=2$) [5,15]. Therefore, the transfer function of the FACTS POD controller is:

$$H(s) = K_P \frac{sT_w}{1 + sT_w} \left[\frac{1 + sT_{lead}}{1 + sT_{lag}} \right]^{m_c} = K_P H_1(s) \quad (2.27)$$

where K_P is a positive constant gain and $H_1(s)$ is the transfer function for the wash-out and lead-lag blocks. T_w is the washout time constant. T_{lead} and T_{lag} are the lead and lag time constant respectively.

For the system closed with the feedback transfer function $H(s)$, the eigenvalue sensitivity to the feedback gain K_P is given by the following equation (proof is given Appendix 1.1) [18-19]:

$$\frac{\partial \lambda_i}{\partial K_P} = R_i \frac{\partial H(\lambda_i)}{\partial K_P} = R_i \frac{\partial [K_P H_1(\lambda_i)]}{\partial K_P} = R_i H_1(\lambda_i) \quad (2.28)$$

where

R_i is the open loop residue corresponding to eigenvalue λ_i

λ_i denotes the mode that should be influenced by the FACTS damping controller

At the initial operating point, which is usually the open loop system, small changes of eigenvalue λ_i can be described as:

$$\Delta\lambda_i = R_i \Delta K_P H_1(\lambda_i) \quad (2.29)$$

The objective of the FACTS damping controller is to improve the damping ratio of the selected oscillation mode i . Therefore, $\Delta\lambda_i$ must be a real negative value to move the real part of the eigenvalue λ_i direct to the negative region without changing its frequency. Figure 2.11 shows the displacement of the eigenvalue after the FACTS damping controller action [18].

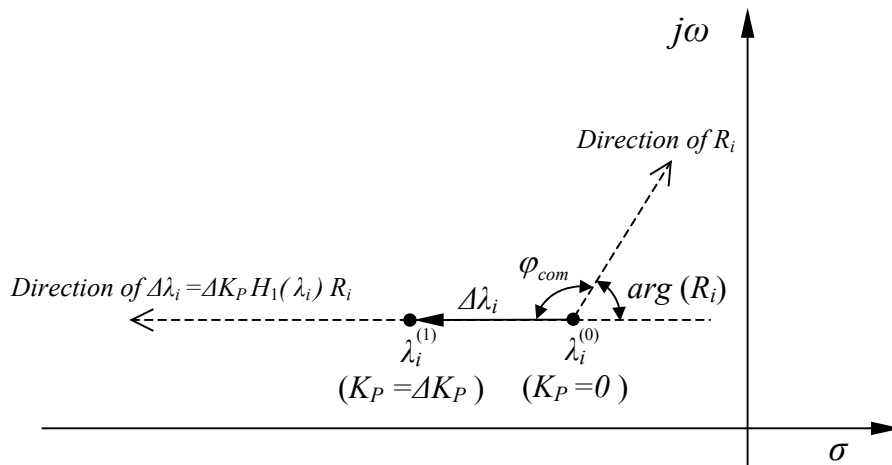


Figure 2.11 Eigenvalue displacement after FACTS POD control action

Determination of the feedback signal and suitable location for FACTS controller

As mentioned above, there are many possible local signals of FACTS devices, such as line active power flow or terminal voltages, that can be employed as the feedback signal. From Equation 2.29, it is clear that with the same gain of the feedback loop, a larger residue will result in a larger change in the corresponding oscillation mode. Therefore the best feedback signal of the FACTS damping controller is that, which results in the largest residue for the considered mode of oscillation. The residue method is the most proper approach in finding the suitable feedback signal.

Determination of the lead-lag parameters

After the selection of the feedback signal, in order to control the direction of the eigenvalue displacement, the lead-lag parameters will be determined.

As shown in Figure 2.11, the phase angle φ_{com} shows the compensation angle which is needed to drive the change of eigenvalue direct to the negative region. This angle will be achieved by the lead-lag function and the parameters T_{lead} and T_{lag} can be determined using the following equations [18]:

$$\begin{aligned}\varphi_{com} &= 180^\circ - \arg(R_i) \\ \alpha_c &= \frac{T_{lag}}{T_{lead}} = \frac{1 - \sin\left(\frac{\varphi_{com}}{m_c}\right)}{1 + \sin\left(\frac{\varphi_{com}}{m_c}\right)} \\ T_{lead} &= \frac{1}{\omega_i \sqrt{\alpha_c}}, \quad T_{lag} = \alpha_c T_{lead}\end{aligned}\tag{2.30}$$

where

- $\arg(R_i)$ denotes phase angle of the residue R_i
- ω_i is the frequency of the researched mode of oscillation in *rad/sec*
- m_c is the number of compensation stages (usually $m_c=2$). The angle compensated by each block should be 30° - 50° .

Determination of the K_p

Providing proper lead-lag compensation, the effectiveness of FACTS POD controller is proportional to the controller gain K_p . However, with the variation of K_p , all modes of oscillation will be influenced. Therefore, in order to optimize the damping of all modes of oscillations, the most proper value of K_p is always determined by the root-locus method.

With the increase of K_p , as shown in Figure 2.11, the eigenvalue $\lambda_i^{(0)}$ of the original operating point will move to $\lambda_i^{(1)}$. This operating point results in a new residue, which would, according to Equation 2.29, require an adjustment of parameters in the controller transfer function $H_1(s)$. However, in practical applications, the controller design can be carried out based on the open loop eigenvalue sensitivities, because the change of the residue angle with small increasing of K_p is negligible.

The above-mentioned residue based design approach will be used in the example shown in Chapter 3.

2.3.2 FACTS POD controller design–non-linear approach

As discussed in Section 2.3.1, the residue method is a linear approach and it requires the linearized system model at a particular operating point. Therefore, this so designed FACTS controller may provide desired damping on certain modes of oscillations. The controller parameters may be required to be tuned again at another operating point to ensure a satisfactory performance. Therefore, due to the inherent non-linear nature, non-linear design methods are useful for improving the performance of power system under severe disturbances [20].

In this section, the parameters of the FACTS POD controller are optimized using non-linear programming algorithm. Series FACTS device is applied in this simulation.

2.3.2.1 Non-linear parameter optimization for FACTS controller

The objective of this section is to find the optimal parameter settings for the FACTS POD controller so as to minimize the power angle difference between two areas after large disturbances. This objective can be formulated as the minimization of a non-linear programming problem expressed as follows:

$$\begin{aligned}
 &\min. && f_1(\mathbf{x}) \\
 &s.t. && \mathbf{A}_0(\mathbf{x}) = 0 \\
 &&& \mathbf{B}_0(\mathbf{x}) \geq 0
 \end{aligned} \tag{2.31}$$

where

$f_1(\mathbf{x})$ is the objective function

\mathbf{x} is a vector that consists the parameters of the FACTS POD controller

$\mathbf{A}_0(\mathbf{x})$ represents the equality constrains

$\mathbf{B}_0(\mathbf{x})$ represents the inequality constrains

$\mathbf{B}_0(\mathbf{x})$ indicate the restrictions of the POD parameter, i.e. the restrictions of lead-lag parameters and wash-out parameter. In this simulation, only the parameter constrains for \mathbf{x} are necessary.

The objective function is extremely important for the parameter optimization. In this research, the objective function is defined as follows:

$$f_1(\mathbf{x}) = \sum \int_0^{t_1} |\delta_{Area1-2}(t, \mathbf{x}) - \delta_{Area1-2}(0, \mathbf{x})| dt = \sum \int_0^{t_1} \Delta\delta(t, \mathbf{x}) dt \quad (2.32)$$

where

$\delta_{Area1-2}(t, \mathbf{x})$ is the power angle difference between the two researched areas at time t

$\delta_{Area1-2}(0, \mathbf{x})$ is the original power angle difference between the two areas

$\Delta\delta(t, \mathbf{x})$ denotes the power angle difference form the original operating point

t_1 is the time range of the simulation

Σ the summary of power angle differences for all researched disturbances

With the variation of the controller parameters \mathbf{x} , the $\Delta\delta(t, \mathbf{x})$ will also be changed. In this research, the power system simulation program PSD (Power System Dynamic) is employed to evaluate the influence of the FACTS POD controller [22]. Moreover, as shown in the objective function, many large disturbances can be simulated for ensuring the robustness of the result.

Equation 2.31 illustrates a general parameter-constrained non-linear optimization problem and can be solved successfully. In this simulation, the *Matlab Optimization Toolbox* is used [12]. Figure 2.12 shows the flow chart of the parameter optimization. The optimization starts with the pre-selected initial values of the FACTS POD

controller. Then the non-linear algorithm is used to iteratively adjust the parameters, until the objective function $f_1(\mathbf{x})$ is minimized. These so determined parameters are the optimal settings of the FACTS POD controller.

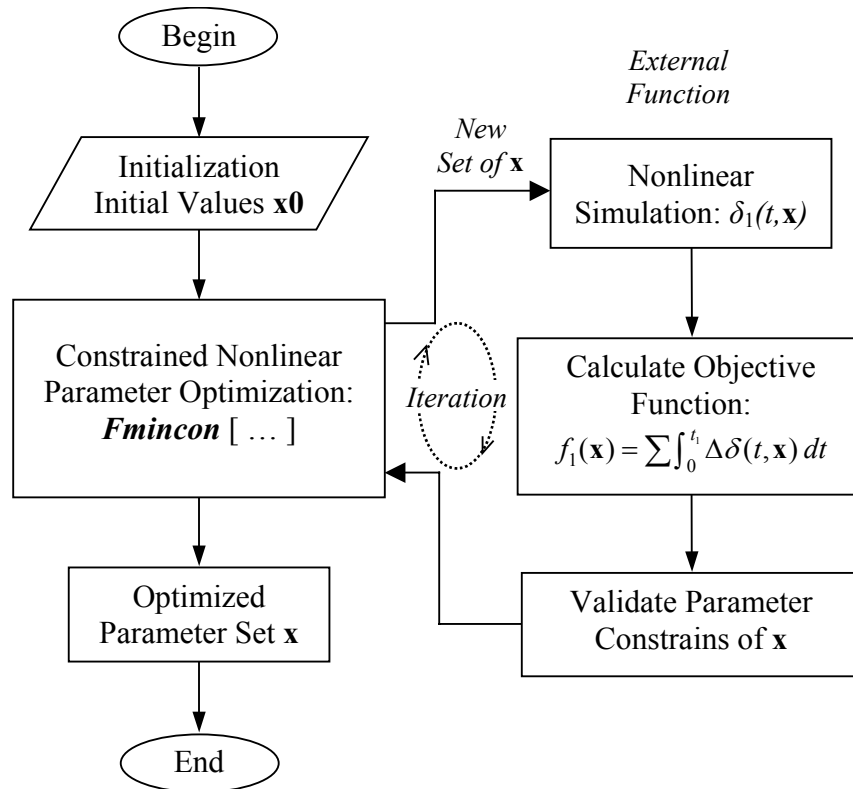


Figure 2.12 Flow chart of the parametric optimization

2.3.2.2 Simulation result

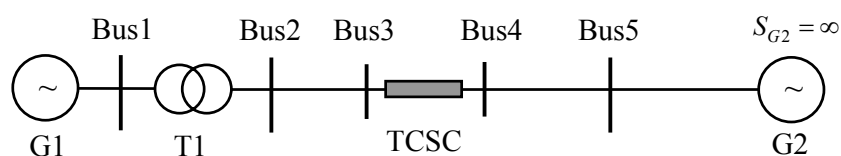


Figure 2.13 Single machine infinite bus power system model

For simplicity, the non-linear parameter optimization is simulated in a single machine infinite bus system shown in Figure 2.13, where a TCSC is applied on the tie-line. In practice, if the FACTS device is located on the tie line between two areas of a large

power system, the corresponding center of power angles (which will be discussed in detail in Section 4.4.3) of each area can be applied for the research.

Figure 2.14 demonstrates the improvement in damping of power system oscillation. It is obvious that the damping behavior of the system is quite improved. The initial and optimized parameters of the FACTS POD controller are given in Appendix 1.2.

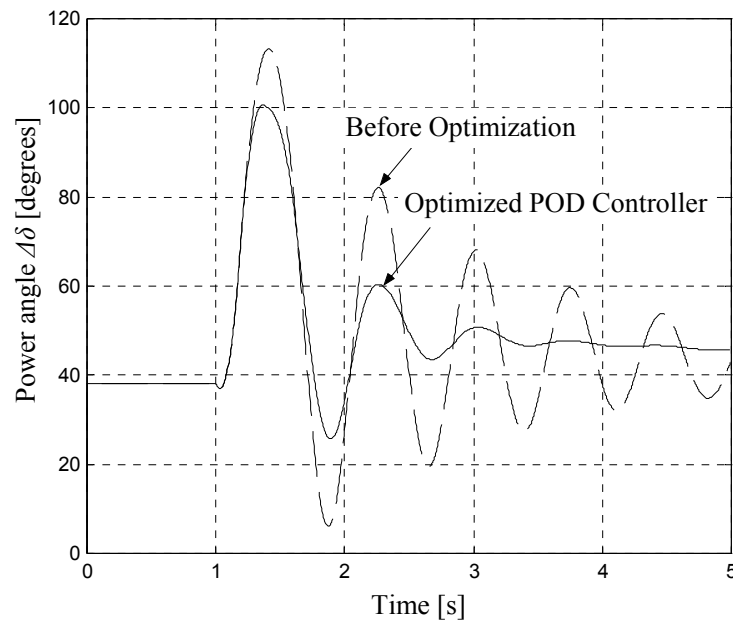


Figure 2.14 Non-linear simulation results

2.4 Multi-FACTS coordinated POD controller design

In this section, the coordinated control between two FACTS POD controllers will be considered.

2.4.1 Traditional sequential design

In order to minimize the adverse interactions among FACTS controllers, they are designed sequentially and separately. Traditionally, the linear design method given in Section 2.3 is always applied.

The linear design method considers only one particular operating point. Once the system operation point is varied, the controller parameters must be adjusted. Particularly in recent years, with the deregulation of the electricity market, the operating point of power system may be varied frequently to meet the needs according to power purchase contract. Therefore, the FACTS controllers must also be capable of being modified to incorporate with the new operating point.

Furthermore, besides the change of operating point, power system parameters (i.e. reactance of the transmission line) can also be changed due to the operation of FACTS devices. Together with the non-linearities of power systems, the parametric uncertainties and various operating points make the FACTS controllers coordination more complicated. In order to handle the uncertainties of fault sequences and different operating conditions, fuzzy-logic controller is employed in this research.

2.4.2 Fuzzy-logic based coordinated controller design

Fuzzy-logic is one of the most practically successful approaches for utilizing the qualitative knowledge of a system to design a controller [23,58]. Furthermore, fuzzy-logic controllers do not require the mathematical model of a system. They can cover a wider range of operating conditions and they are robust [24,55,58]. In addition, by using the fuzzy-logic coordination controller, the advantages of the traditional FACTS POD controllers are still maintained.

A three-machine interconnected power system equipped with two series FACTS devices is simulated in this study. Here G1~G3 represent three areas. The UPFCs are located on the transmission line between Bus 2 and Bus 3 and, between Bus 6 and Bus 7. The power system diagram is shown in Figure 2.15 and the system parameters are given in Appendix 1.3.

This power system is simulated only to verify the dynamic coordination performance of the FACTS damping controllers. Though all types of series FACTS devices can be used in this system, only two UPFCs are considered in this study. In practical application, UPFC is mainly used to control power flow. However, in this study, only the power oscillation damping functions of the UPFCs are considered.

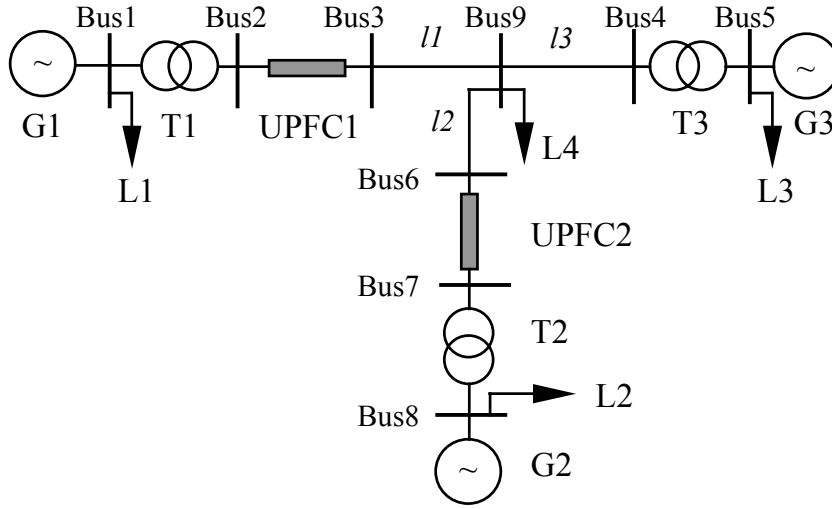


Figure 2.15 Three-area power system model

As mentioned in Section 2.1, the UPFCs are simulated using current injection model. For the damping control, only the series voltage source control of UPFC is necessary [14,40]. The active power flow through UPFC is employed as the input signal to the POD controller. The output of the POD controller can be expressed as follows:

$$\bar{U}_{UPFC} = U_{UPFC} \angle(\alpha) = U_{UPFC} \angle[-90^\circ + \arg(\bar{I}_{UPFC})] \quad (2.33)$$

where

α denotes the angle of the UPFC series voltage source

$\arg(\bar{I}_{UPFC})$ denotes the angle of the current flow through the UPFC

\bar{U}_{UPFC} is the damping control signal provided by the UPFC POD controller. If UPFC operates in power oscillation damping mode, the series injected voltage provided by UPFC is perpendicular to the current flow through UPFC [40].

The structure of the proposed fuzzy coordinated damping control scheme is shown in Figure 2.16, where the inputs P_{UPFC1} and P_{UPFC2} are the active power flow (per unit value) through the UPFC1 and UPFC2.

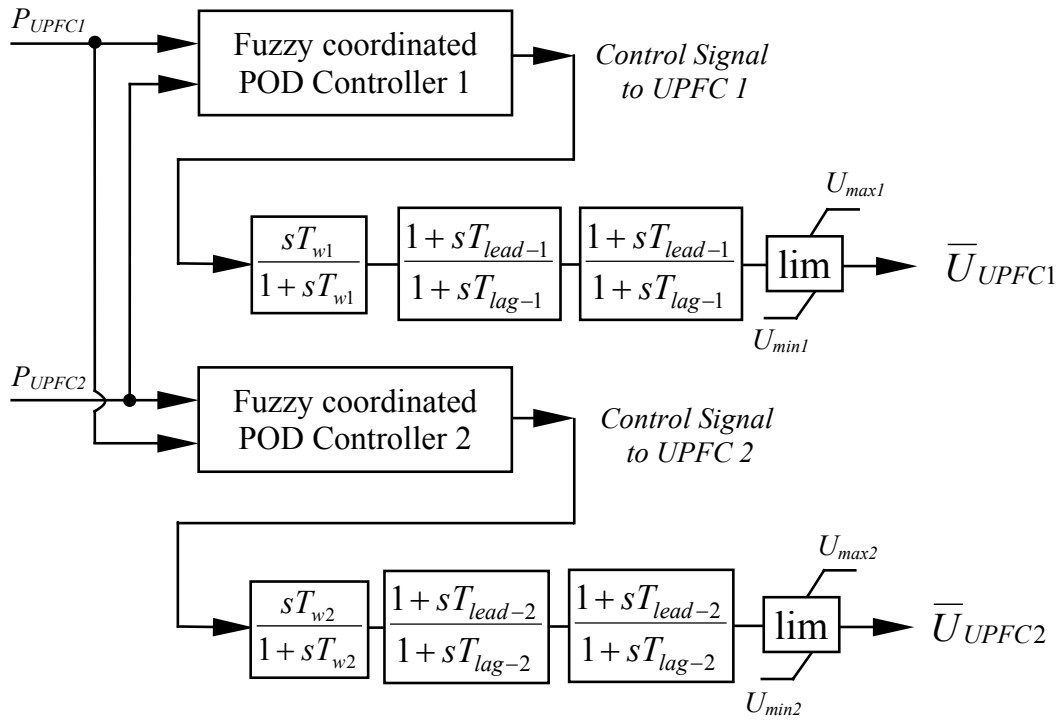


Figure 2.16 Fuzzy coordinated POD controllers

As shown in Figure 2.16, the output of the fuzzy coordinated POD controllers are the amplification signals adjusted to the UPFC POD controllers. In this way, the conventional POD controllers are coordinated dynamically by means of fuzzy-logic.

2.4.2.1 Fuzzy approach for coordination of POD controllers

The fuzzy-logic was first introduced in 1960 by Professor Lofti Zadeh and it handles the natural linguistic variables. The fuzzy-logic controllers are rule-based controllers in which a set of rules represents a control decision mechanism to adjust the effect of certain cases coming from power system.

Similar to the standard fuzzy-logic controller, this fuzzy coordinated control scheme involves three different and sequential processes: fuzzification, fuzzy inference system (FIS) and defuzzification. The block diagram of the fuzzy coordinated controller is shown in Figure 2.17.

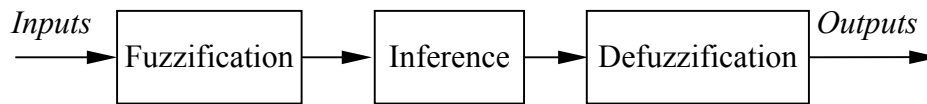


Figure 2.17 Block diagram of the fuzzy coordinated controller

Fuzzification

Fuzzification is a process whereby the input variables are mapped onto fuzzy variables (linguistic variables). In other words, fuzzification converts crisp numerical values into the degrees of membership in fuzzy sets. A fuzzy set is a set without a crisp, clearly defined boundary and it can contain elements with only a partial degree of membership [25].

Fuzzy sets are represented in fuzzy-logic systems by fuzzy membership functions (MF). A membership function is a curve that defines how each point in the input space is mapped onto a membership value (or degree of membership). The degree of membership returned by a membership function is always in the range $[0, 1]$. A value will have a membership degree of 0 if it is wholly outside of the fuzzy set, 1 if it is completely within the fuzzy set, or any value in between [25].

There are different types of membership functions. The function itself can be an arbitrary curve whose shape can be defined as a function that suits the simplicity, convenience, speedy, and efficiency [25].

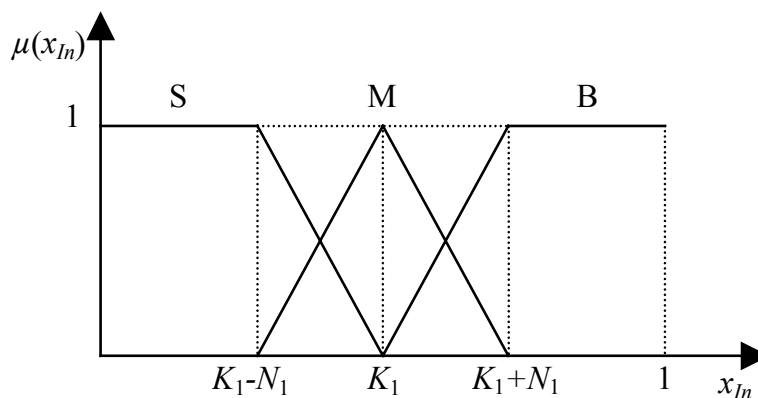


Figure 2.18 Membership function

The simplest membership functions are formed using straight lines. These straight line membership functions have the advantage of simplicity and are adequate for the accuracy of power system analysis. The trapezoidal and triangle membership functions are used in this simulation, as shown in Figure 2.18.

The fuzzified linguistic variables represent: B (big), M (medium) and S (small):

The membership function of the small set is:

$$\mu_S(x_{In}) = \begin{cases} 1 & x_{In} < K_1 - N_1 \\ \frac{-x_{In} + K_1}{N_1} & K_1 - N_1 \leq x_{In} \leq K_1 \\ 0 & x_{In} > K_1 \end{cases} \quad (2.34)$$

where x_{In} , namely P_{UPFC1} or P_{UPFC2} , is the input to the fuzzy coordinated controller.

Similarly, the big set membership function is:

$$\mu_B(x_{In}) = \begin{cases} 0 & x_{In} < K_1 \\ \frac{x_{In} - K_1}{N_1} & K_1 \leq x_{In} \leq K_1 + N_1 \\ 1 & x_{In} > K_1 + N_1 \end{cases} \quad (2.35)$$

The medium set membership function is:

$$\mu_M(x_{In}) = \begin{cases} 0 & x_{In} < K_1 - N_1 \\ \frac{x_{In} + N_1 - K_1}{N_1} & K_1 - N_1 \leq x_{In} \leq K_1 \\ \frac{-x_{In} + N_1 + K_1}{N_1} & K_1 \leq x_{In} \leq K_1 + N_1 \\ 1 & x_{In} > K_1 + N_1 \end{cases} \quad (2.36)$$

The parameters K_1 and N_1 , as given in Appendix 1.4, are determined basing upon the operating range of UPFCs by trial and error. These parameters can also be optimized by using of ANFIS (Adaptive Network based Fuzzy Inference System) technology.

Inference system

Once the inputs have been fuzzified, control decisions can be made based on these fuzzified variables. Fuzzy inference is the process of formulating the mapping from a given input to an output using fuzzy-logic [25]. This inference system involves rules for determining output decisions. These rules can be obtained from the system operation and the knowledge of the operator. Moreover, the fuzzy inference system also assigns degrees of membership to the output linguistic variables.

Since each input is fuzzified into three fuzzy variables, the fuzzy coordinated controller has nine rules. The inference tables are shown in Table 2.1 and Table 2.2. Both of the two UPFC fuzzy coordinated controllers use the same inference system and only their inputs are exchanged (as shown in Figure 2.16).

Table 2.1 Fuzzy inference table for fuzzy coordinated POD controller 1

P_{UPFC1} \ P_{UPFC2}	B	M	S
B	B	M	S
M	B	M	S
S	M	S	S

Table 2.2 Fuzzy inference table for fuzzy coordinated POD controller 2

P_{UPFC2} \ P_{UPFC1}	B	M	S
B	B	M	S
M	B	M	S
S	M	S	S

In this simulation, the Mamdani (Min-Max) type of fuzzy inference system is applied [25]. The inference tables shown in Table 2.1 and 2.2 are obtained by trial and error.

Defuzzification

After evaluating inputs and applying them to the rule base, a control signal will be generated by the fuzzy-logic controller. The output variables of the inference system are linguistic variables. They will be evaluated for the derivation of the output control signal. This process is the defuzzification.

The defuzzification is achieved using the centroid method and the output of the fuzzy coordinated controller is

$$v_{Fuzzy} = \frac{\sum_{i=1}^9 \mu_i \cdot v_i}{\sum_{i=1}^9 \mu_i} \quad (2.37)$$

where v_i corresponds to the value of control output for which the membership values in the output sets are equal to unity.

2.4.2.2 Simulation results

Using the multi-machine power system shown in Figure 2.15, different disturbances and different system parameters are simulated. The performance of the fuzzy coordinated control scheme in damping power system oscillations is examined. In this research, machine G3 is taken as the reference machine. δ_{13} and δ_{23} denote the power angle difference between generators G1-G3 and G2-G3 respectively.

Case 1: Three-phase fault at Bus 2

A three-phase fault of 100 ms duration is simulated at Bus 2. The pre-fault operating condition (in p.u.) is: $P_{G1}=0.105$, $P_{G2}=0.185$. Figure 2.19 presents the results of the examined power system with fuzzy coordinated controllers. It can be seen that with the

proposed control scheme, the dynamic performance of the power system is quite improved.

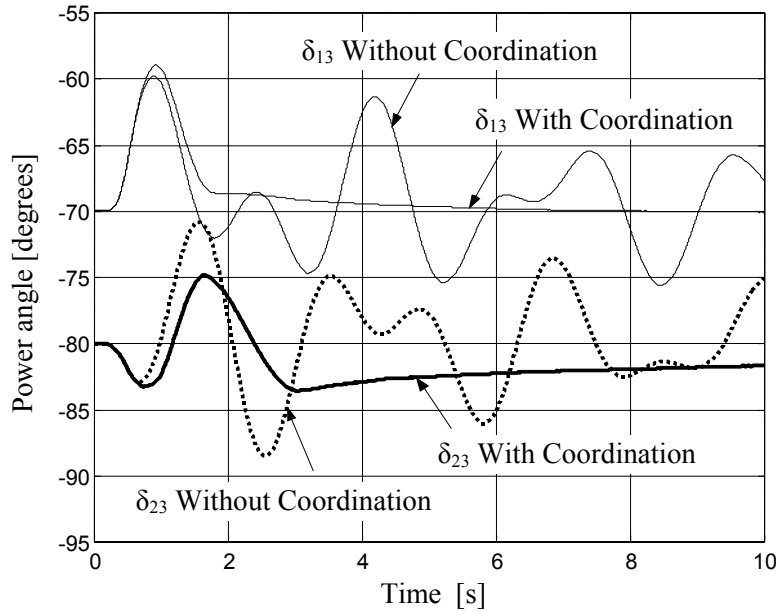


Figure 2.19 Simulation result - case 1

Case 2: *Changing of operation conditions (Three-phase fault at Bus 3)*

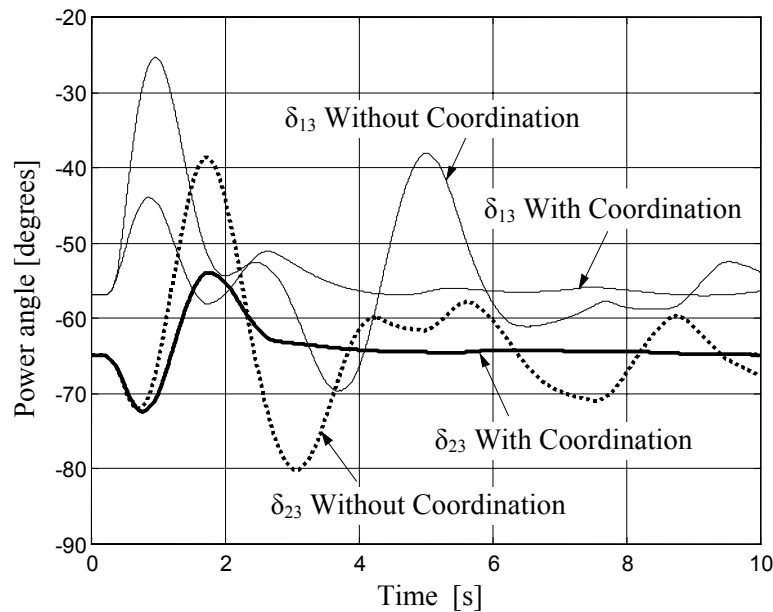


Figure 2.20 Simulation result - case 2

To validate the robustness of fuzzy coordinated control scheme, the pre-fault operating conditions of the power network is changed to $P_{G1}=0.195$, $P_{G2}=0.28$. Moreover the fault type is also different: a three-phase fault of 110 ms duration is simulated at Bus 3. Figure 2.20 shows the results of the simulation. The proposed control scheme acts pretty well with the variation of operation condition.

Case 3: Changing of network parameters (Three-phase fault at Bus 9)

In order to verify the performance of the fuzzy coordinated control scheme for the changing of system parameters, the reactance of transformers T1 and T2 are increased by 20%. A three-phase fault of 100 ms is simulated at Bus 9. The simulation results, as shown in Figure 2.21, illustrate that the proposed control scheme is robust in parametric change. In this case, the pre-fault operating condition (in p.u.) is: $P_{G1}=0.10$, $P_{G2}=0.120$.

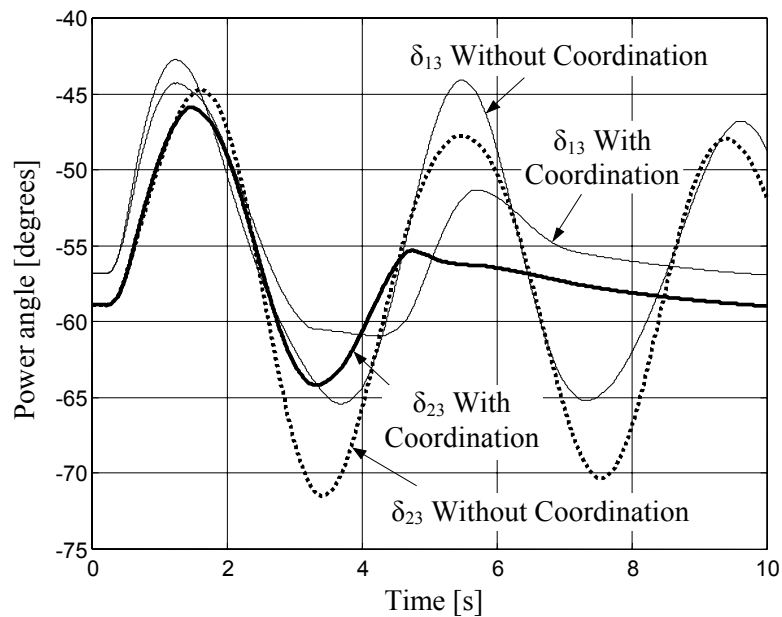


Figure 2.21 Simulation result - case 3

2.4.2.3 Conclusion of fuzzy coordinated control scheme

As presented in this section, the fuzzy coordinated control scheme is an appropriate method for coordination of POD controllers in power systems. This scheme exploits the

advantages of the conventional FACTS POD controller and it is not only robust but also simple and easy to be implemented in real power systems.

2.5 Comments on the FACTS damping controller design

In this chapter, two main methods for designing FACTS POD controllers are introduced: linear method and non-linear parameter optimization method.

The non-linear optimization design method captures the complex dynamics of the power system, especially during critical faults. Thus the non-linear design method is suitable to improve the performance of power system under severe disturbances. However, in large power systems, non-linear optimization needs much more time than the linear methods. Therefore, in practical applications, the linear methods are preferred.

The residue controller design method is a typical linear approach. It requires the linearized system model at a particular operating point. Therefore, this so designed FACTS POD controller can provide desired damping for certain modes of oscillations at the selected operating point. However, the controller parameters may be required to tune again at another operating point to ensure a satisfactory performance.

In practical applications, the following FACTS POD controller design procedure is suggested:

- Considering the time-domain simulation speed, non-linear method may be applied only to simple power systems. In the future, with the development of computer technology, non-linear method may also be applicable in large power systems.
- In large power systems, the linear method is preferred since it has the advantages of simple and fast. In practical applications, many possible operating points can also be evaluated quickly to ensure a satisfactory performance.
- For the coordinated control of FACTS POD controllers, fuzzy coordinated approach is suitable for multi possible operating points of power system and it is robust in comparison with the conventional sequential designed controllers. It is also a simple method that can be easily implemented in real power systems.

Chapter 3

Selection of the Proper Locations for FACTS Devices

3.1 Introduction

Many researches were made on optimal site selections for placement of FACTS devices in power systems by considering different criteria [9,33,51-52]. In this chapter, three criteria will be considered for FACTS optimal allocations: available transfer capability (ATC) criterion, steady-state stability criterion and economic criterion. Since the major profits brought by FACTS devices are the economic and power oscillation damping control effects, the economic criterion and steady-state stability criterion will be further investigated in detail.

3.2 ATC criterion

ATC is composed of total transfer capability (TTC), existing transmission commitment, transmission reliability margin (TRM) and capacity benefit margin (CBM) [50,52,57].

TTC is the amount of power that can be transferred over the interconnected transmission network in a reliable manner while meeting a specific set of pre- and post-contingency system conditions. TTC can be considered as the maximum power that can be transferred through the network from one node (usually the power supplier node) to another node (usually the power consumer node).

TRM is the amount of transmission transfer capability needed to ensure that the interconnected transmission network is secure under a reasonable range of uncertainties in system conditions.

CBM is the amount of transmission transfer capability reserved by load serving entities to ensure access to generation from interconnected systems to meet generation reliability requirements.

Mathematically, ATC is given by:

$$ATC = TTC - TRM - CBM - \text{existing transmission commitments}$$

In other words, ATC is the measure of the transfer capability remaining in the physical transmission network for further commercial activity, over and above already committed uses.

FACTS devices, capable for the flexible power flow controls, have great impacts on the enhancement of ATC. Therefore, the optimal allocation of FACTS devices can be determined using the ATC criterion. Many researches were made in this direction so as to enhance the competitiveness of the power market [33,51,57].

For this criterion, only the technical benefits of the FACTS controllers, in terms of ATC, are considered. However, the economic criterion, which considers both the investment costs for FACTS devices and the generation costs, is not addressed. Therefore power system economic planning and operation need to be considered.

Further, the steady-state stability criterion needs also be taken into account in the dynamic investigations of power systems.

3.3 Steady-state stability criterion

FACTS devices are recognized as an effective approach for damping of power system inter-area oscillations. As discussed in Chapter 2, the FACTS damping behavior is mainly influenced by their locations and their controller parameters. Using the residue method, the optimal locations of FACTS devices can be determined. This allocation criterion is said to be steady-state stability criterion.

The simplified New England Power System with 16-machine and 68-bus, as shown in Figure 3.1, is considered in this study [5]. TCSC is used in this simulation and it is modeled using current injection model. The bus voltages are applied as inputs to the TCSC controller, and impacts of these input signals on the critical eigenvalue of the power system will be analyzed using the residue method.

By means of the participation factor and rotor mode shape analysis, the researched system can be divided into five coherent areas. The main critical inter-area oscillation is between area 3 and area 4 due to the relative weak tie-line connection between them. Figure 3.2 shows the dominant eigenvalues of this system. It can be seen that the damping ratio of the inter-area mode 2, which corresponds to the inter-area oscillation between area 3 and area 4, is not satisfactory.

To find the best location for TCSC, the following tie-lines have been investigated: 41-42, 42-52, 50-51 and 46-49. Residues associated with the inter-area mode 2 are shown in Table 3.1. The residues are calculated using the transfer function between the TCSC terminal voltages and TCSC inputs (TCSC reactance).

As can be seen from Table 3.1, Bus 50 has the highest residue on the inter-area oscillation mode 2. Based on the residue method, the TCSC should be installed on the transmission line 50-51 (tie-line between area 3 and area 4), as shown in Figure 3.1. The voltage of Bus 50 is the selected feedback signal.

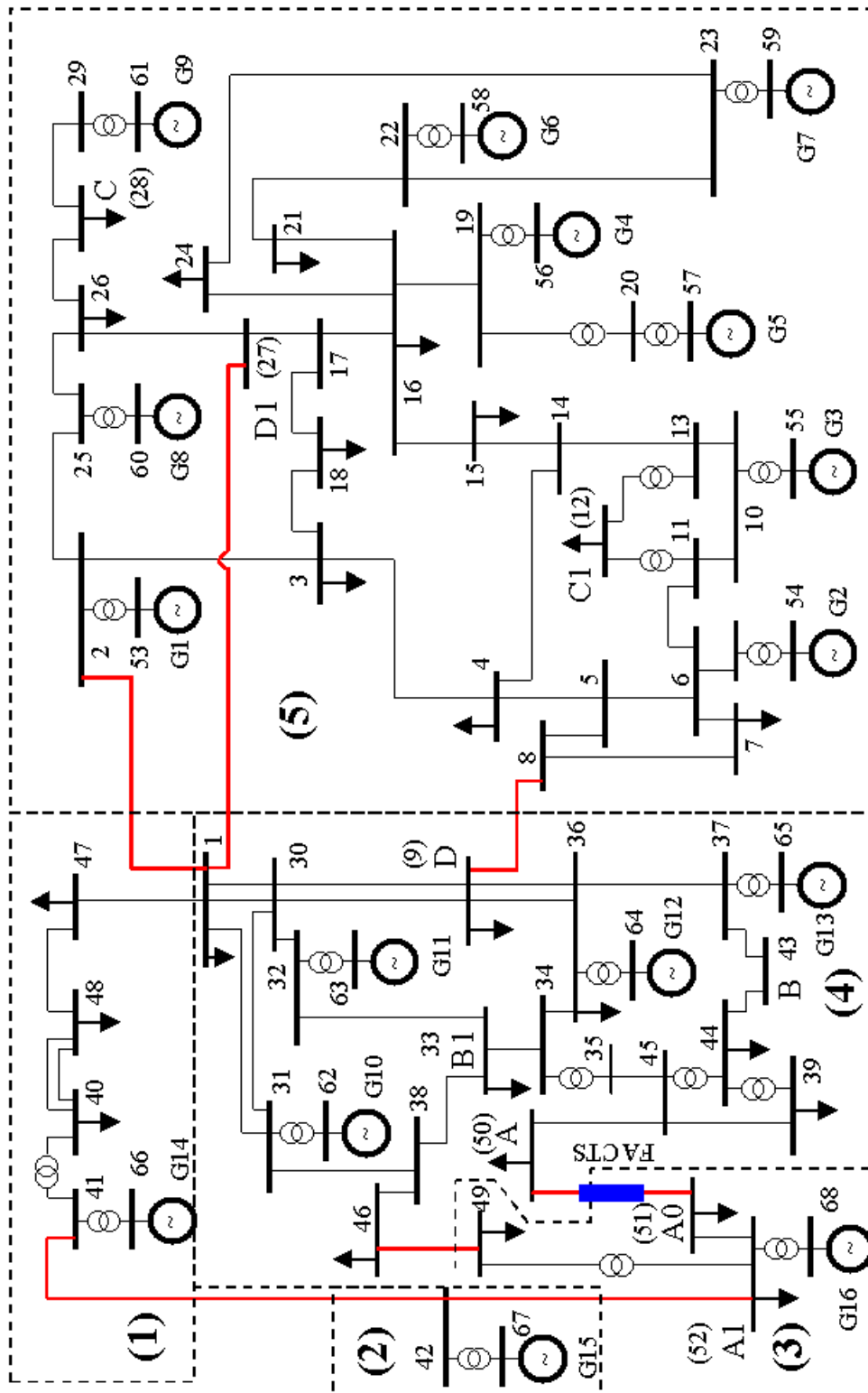


Figure 3.1 Simplified New England Power System

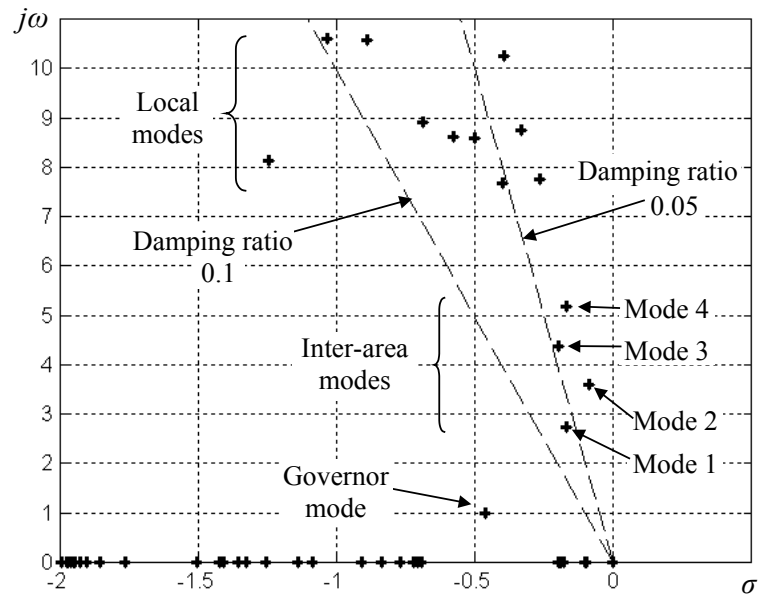


Figure 3.2 Dominant eigenvalues of the power system

Table 3.1 The residues associated with the inter-are mode 2

		Absolute Value of Residues ($\times 10^{-4}$)			
Bus Voltage as Feedback Signal	TCSC Location Line	41-42	42-52	50-51	46-49
	Bus 41		0.0060	0.1390	0.0281
Bus 42		0.0721	0.1662	0.3359	0.2274
Bus 46		0.0612	0.1412	0.2855	0.2358
Bus 49		0.1046	0.2412	0.4676	0.4022
Bus 50 (A)		0.1744	0.4021	0.8129	0.6714
Bus 51 (A0)		0.1363	0.3144	0.6355	0.5249
Bus 52		0.1420	0.3275	0.6620	0.5462

As stated in Chapter 2, using the residue method, parameters of the FACTS POD controller can also be determined. The angle of the residue associated with Bus 50 voltage and inter-area mode 2 is 79.628° . Thus the lead-lag parameters of the FACTS POD controller can be obtained (using negative feedback):

$$H_{TCSC}(s) = -K_P H_1(s) = -K_P \cdot 100 \cdot \frac{5.0s}{1 + 5.0s} \cdot \left[\frac{1 + 0.1s}{1 + 0.5s} \right]^2 \quad (3.1)$$

The bode diagram of the $H_1(s)$ is shown in Figure 3.3. The controller has a phase lag of 79.6° at the inter-area mode frequency.

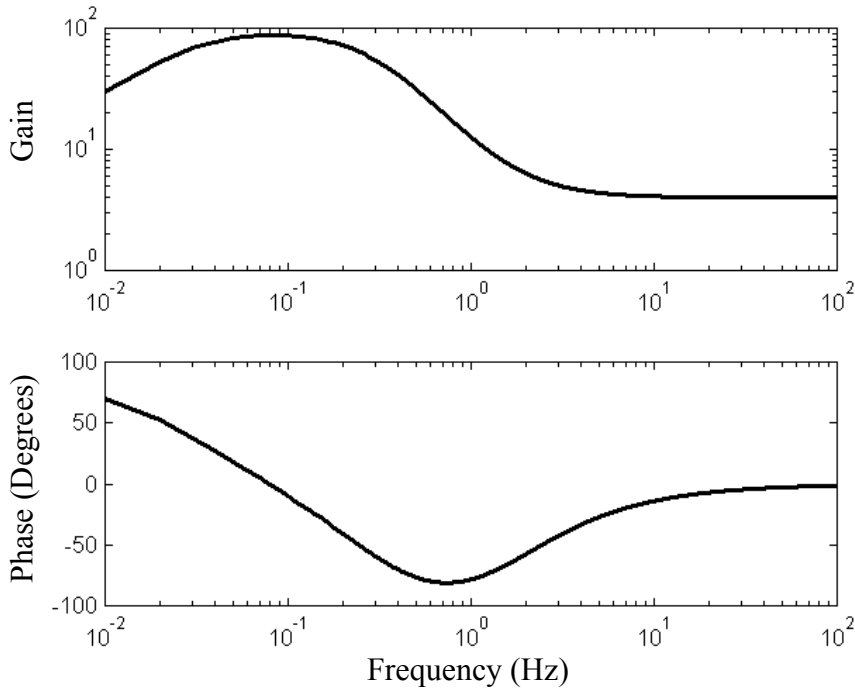


Figure 3.3 Bode plot of the FACTS POD controller

The root-locus, when the gain of TCSC controller K_P varies from 0 to 200, is shown in Figure 3.4. It is clear that the FACTS POD controller has little influence on the local modes. It is also obvious that with the increase of K_P , the root-locus of the inter-area mode 2 goes directly toward the negative region. Thus, the lead-lag parameters are optimal settings for damping of power system oscillation. Furthermore, considering root-locus of all modes of oscillations, the optimal K_P can be determined.

However, as can be seen from Figure 3.4, some other inter-area modes and local modes are not satisfactory. Therefore, the coordinated tuning of the FACTS POD

controller together with the PSS controllers is further required. The latter will be discussed in detail in Chapter 5.

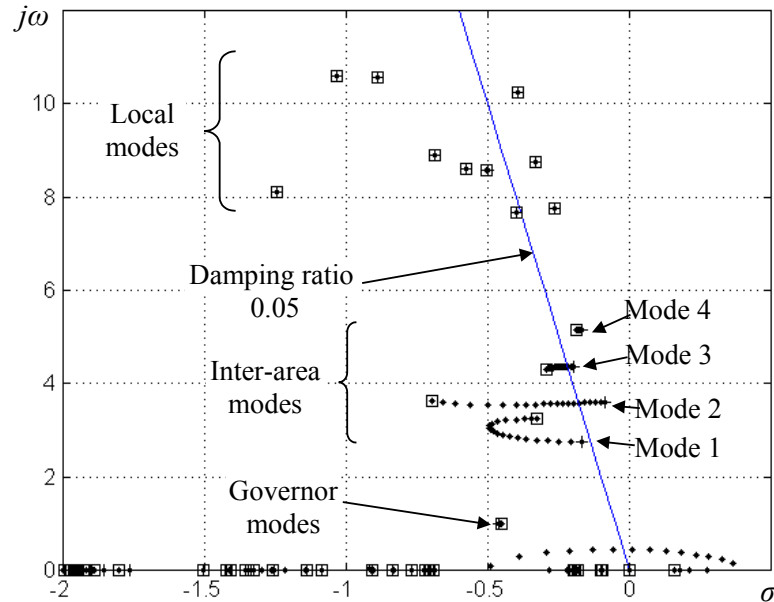


Figure 3.4 Root-locus of the FACTS POD controller

- Root-locus when K_P varies from 0 (+) to 200 (□).

As stated above, the steady-state stability criterion is based on the power system dynamic analysis. However, the investments of the FACTS devices and the optimal power system operation are not considered. Therefore power system economic planning and operation need to be investigated.

3.4 Economic criterion

Optimal choice and allocation of FACTS devices using genetic algorithm

The primary function of FACTS devices in power systems is to control power flows. Provided that if they are located in optimal locations, FACTS devices can be used to achieve the optimal power flow without any constraint violations and with this

they can increase the utilization of the lowest cost generation in power systems. Therefore, FACTS types and their locations can be chosen according to their contributions to the general objective of power system economic generation and dispatch. This criterion is said to be economic criterion and it will be discussed in detail in this section.

The purpose of this section is to develop a general algorithm to find the most suitable FACTS devices and choose the best locations for them. By re-dispatching of the load flows in power systems, the total generation costs can be minimized by optimal FACTS allocation. Therefore, the objective is to minimize the overall cost function, which includes the generation costs of power plants and the investment costs of FACTS devices. Consequently, the FACTS investment and its impact on the total power generation costs are considered together.

Different kinds of FACTS devices and their different locations have different advantages. In realizing the proposed objective, the suitable types of FACTS devices, their locations and their rated values must be determined simultaneously. This combinatorial optimization problem is solved using genetic algorithm (GA).

3.4.1 Cost functions

The overall cost function consists of generation costs and FACTS devices investment costs. For minimizing the generation costs in power systems, algorithms are well developed and being used for unit commitment and economic operation. In this work, a modified version of power simulation software: *Matpower* 2.0 is employed [26]. For the intended research, *Matpower* has been extended by incorporating the mathematical models of FACTS devices. Furthermore, FACTS investment cost functions are also incorporated.

3.4.1.1 Generation cost function

The generation cost function is represented by a quadratic polynomial as follows:

$$c_2(P_G) = \alpha_0 + \alpha_1 P_G + \alpha_2 P_G^2 \quad (3.2)$$

where P_G is the output of the generator (MW), and α_0 , α_1 and α_2 are constant coefficients. The detailed parameters of the generation cost functions are given in Appendix 2.1.

3.4.1.2 Cost functions for FACTS devices

Based on the Siemens AG Database [27], the cost functions for SVC, TCSC and UPFC are developed:

The cost function for UPFC in $US\$/kVar$ is:

$$c_{1UPFC} = 0.0003s_{FACTS}^2 - 0.2691s_{FACTS} + 188.22 \quad (3.3)$$

For TCSC in $US\$/kVar$ is:

$$c_{1TCSC} = 0.0015s_{FACTS}^2 - 0.7130s_{FACTS} + 153.75 \quad (3.4)$$

For SVC in $US\$/kVar$ is:

$$c_{1SVC} = 0.0003s_{FACTS}^2 - 0.3051s_{FACTS} + 127.38 \quad (3.5)$$

where s_{FACTS} is the operating range of the FACTS devices in $MVar$.

The cost functions for SVC, TCSC and UPFC are shown in Figure 3.5.

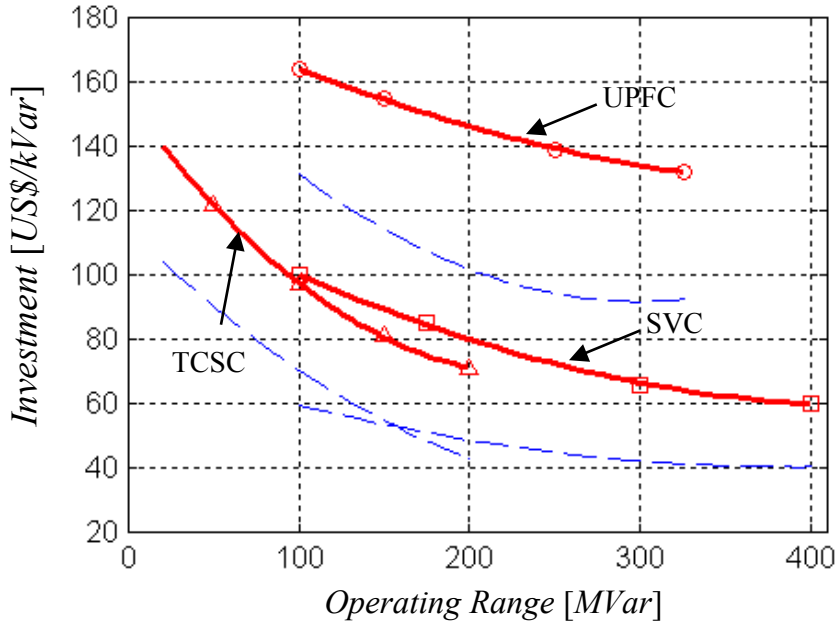


Figure 3.5 Cost functions of the FACTS devices: SVC, TCSC and UPFC

- : Upper limit (Total investment costs)
- - - : Lower limit (Equipment costs)
- : UPFC. —△— : TCSC. —□— : SVC.

The cost of a TCPST is more related to the operating voltage and the current rating of the considered transmission line. Thus, the cost function can be expressed as follows [10,28-29]:

$$C_{TCPST} = d_{TCPST} \cdot P_{\max} + IC \quad (3.6)$$

where d_{TCPST} is a positive constant representing the capital cost coefficient. IC is the installation cost of the TCPST, and P_{\max} corresponds to the thermal limit of the transmission line where TCPST is installed.

3.4.2 Optimal FACTS allocation

The formulation of the optimal allocation of FACTS devices can be expressed as follows:

$$\begin{aligned}
\min. \quad & c_{\text{Total}} = c_1(\mathbf{f}) + c_2(\mathbf{P}_G) \\
s.t. \quad & \mathbf{E}_1(\mathbf{f}, \mathbf{g}) = 0 \\
& \mathbf{B}_1(\mathbf{f}) \geq 0, \quad \mathbf{B}_2(\mathbf{g}) \geq 0
\end{aligned} \tag{3.7}$$

where

- c_{Total} : the overall cost objective function which includes the average investment costs of FACTS devices $c_1(\mathbf{f})$ and the generation cost $c_2(\mathbf{P}_G)$
- $\mathbf{E}_1(\mathbf{f}, \mathbf{g})$: represents the conventional power flow equations
- $\mathbf{B}_1(\mathbf{f}), \mathbf{B}_2(\mathbf{g})$: are the inequality constrains for FACTS devices and the optimal power flow respectively
- \mathbf{f}, \mathbf{P}_G : are vectors that represent the variables of FACTS devices and the active power outputs of the generators
- \mathbf{g} : represents the operating state of the power system

The unit for generation cost is *US\$/Hour* and for the investment costs of FACTS devices are *US\$*. They must be unified into *US\$/Hour*. Normally, the FACTS devices will be in service for many years [1-2,13,30]. However, only a part of its lifetime will be employed to regulate the power flow. In this research, three years is applied to evaluate the average cost function for all the four kinds of FACTS devices. This value has been applied only to unify the unit and has no influence on the global optimization. Therefore the average value of the investment costs are calculated using the following equation:

$$c_1(\mathbf{f}) = \frac{c(\mathbf{f})}{8760 \times 3} (\text{US} \$ / \text{Hour}) \tag{3.8}$$

where $c(\mathbf{f})$ is the total investment costs of FACTS devices.

As mentioned in Chapter 2, power system parameters can be regulated using FACTS devices. Different parameters derive different results on the objective function in Equation 3.7. Also, the variation of FACTS locations and FACTS types has also influences on the objective function. Therefore, using the conventional optimization methods, it is not easy to find the optimal location of FACTS devices, their types and their rated values simultaneously. To solve this problem, the genetic algorithm is employed.

3.4.3 Genetic algorithm

Based on the mechanisms of natural selection and genetics, genetic algorithms are global search techniques. They can search several possible solutions simultaneously and they do not require any prior knowledge or special properties of the objective function [9,31]. Moreover, they always produce high quality solutions and, therefore, they are excellent methods for searching optimal solution in a complex problem.

Particularly in this research, the problem has a very large range of combinations of solutions so that it is unfeasible to search exhaustively. Furthermore, the objection function given in Equation 3.7 contains both discrete variables (FACTS types and locations) and continuous variables (FACTS rated values). GAs are proper algorithm for solving this kind of problem.

Commonly, GAs start with random generation of initial population which represent possible solutions of the problem. Then the fitness of each individual is evaluated and new populations are generated by genetic operators (Reproduction, Crossover and Mutation) until the maximal number of generation is reached.

3.4.3.1 Encoding

The objective is to find the optimal locations for the FACTS devices within the equality and inequality constrains. Therefore, the configuration of FACTS devices is encoded by three parameters: their locations, their types and rated values [9]. Each

individual is represented by n_{FACTS} number of strings, as shown in Figure 3.6, where n_{FACTS} is the number of FACTS devices needed to be analyzed in the power systems.

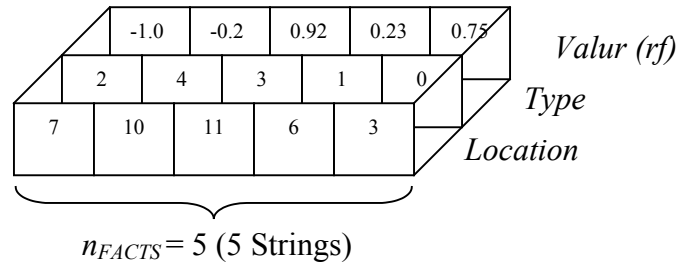


Figure 3.6 Individual configuration of FACTS devices

As shown in Figure 3.6, the first value of each string corresponds to the location information. It is the number of the transmission line where the FACTS is to be located. Each string has a different value of location [9]. In other words, it must be ensured that on one transmission line there is only one FACTS device. Moreover, SVC is installed only at one node of the transmission line and the sending node is selected in this simulation.

The second value represents the types of FACTS devices [9]. The values assigned to FACTS devices are: 1 for TCSC; 2 for TCPST; 3 for UPFC, 4 for SVC and 0 for no FACTS situation. Particularly, if there is no FACTS device needed on the transmission line, the value 0 will be employed.

The last value rf represents the rated value of each FACTS device. This value varies continuously between -1 and $+1$. The real rated value of each FACTS device can be obtained according to the different FACTS model under the following criteria:

TCSC

As discussed in Chapter 2, TCSC has a working range between $-0.7X_{Line}$ and $+0.2X_{Line}$ [33], where X_{Line} is the reactance of the transmission line where the TCSC installed. Therefore rf is converted into the real compensation degree $rtcsc$ using the following equation:

$$rtcsc = rf \times 0.45 - 0.25 \quad (3.9)$$

UPFC

\bar{U}_{UPFC} , which is the inserted voltage of UPFC, has a maximum magnitude of $10\%U_m$, where U_m is the rated voltage of the transmission line where the UPFC is installed. The angle of \bar{U}_{UPFC} can be varied from -180° to $+180^\circ$. Therefore rf is converted into the working angle $rupfc$ using the following equation:

$$rupfc = rf \times 180 \text{ (degrees)} \quad (3.10)$$

TCPST

The working range of TCPST is between -5° and $+5^\circ$. Then rf is converted into the real phase shift value $rtcpst$ using the following equation:

$$rtcpst = rf \times 5 \text{ (degrees)} \quad (3.11)$$

SVC

The working range of SVC is between -100 MVar and $+100$ MVar. Then rf is converted into the real compensation value using:

$$rsvc = rf \times 100 \text{ (MVar)} \quad (3.12)$$

3.4.3.2 Initial population

The initial population is generated by the following parameters [9]:

- n_{FACTS} : the number of FACTS devices to be located
- n_{Type} : FACTS types
- $n_{Location}$: the possible locations for FACTS devices
- n_{Ind} : the number of individuals in a population

First, as shown in Figure 3.7, a set of n_{FACTS} numbers of strings are produced. For each string, the first value is randomly chosen from the possible locations $n_{Location}$.

The second value, which represents the types of FACTS devices, is obtained by randomly drawing numbers among the selected devices [9]. Particularly, after the optimization, if there is no FACTS device necessary on the transmission line, the second value will be set to zero.

The third value of each string, which contains the rated values of the FACTS devices, is randomly selected between -1 and $+1$.

To obtain the entire initial population, the above operations are repeated n_{Ind} times. Figure 3.7 shows the calculation of the entire population.

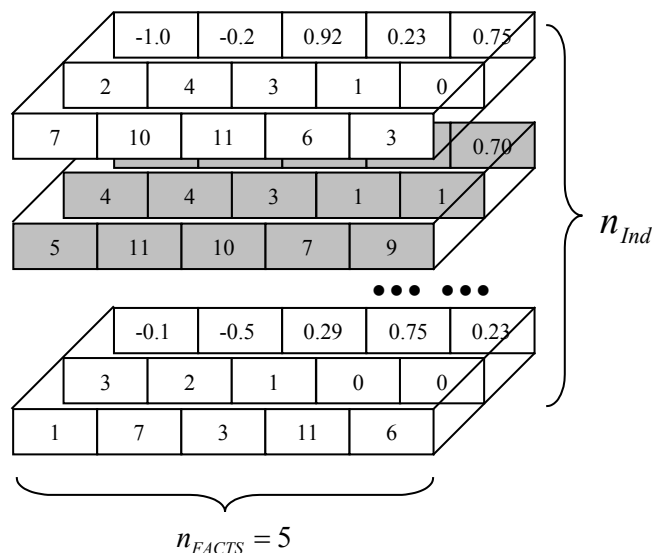


Figure 3.7 Calculation of the entire population

3.4.3.3 Fitness calculation

After encoding, the objective function (fitness) will be evaluated for each individual of the population. The fitness is a measure of quality, which is used to compare different solutions [9,31]. In this work, the fitness is defined as follows:

$$Fitness = c_{max} - c_{Total} \quad (3.13)$$

Because the GAs can only find the maximum positive value of the objective function, a large positive constant c_{max} is selected to convert the objective function into a maximum one.

Then reproduction, crossover and mutation are applied successively to generate the offspring.

3.4.3.4 Reproduction

Reproduction is a process where the individual is selected to move to a new generation according to its fitness [9,31].

In the reproduction process, the fittest individual will be selected. In other words, the individual with a larger fitness has the higher probability of contribution to one or more offspring in the next generation. In this research, the roulette wheel selection method is employed.

Each individual in the population has its interval. The size of each interval corresponds to the fitness of the individual and can be defined as [34]:

$$p_r = \frac{Fitness_r}{\sum_{i=1}^{n_{ind}} Fitness_i} = \frac{Fitness_r}{Fitness_{sum}} \quad (3.14)$$

where

- n_{Ind} : the number of individuals in the population
- $Fitness_r$: the fitness of the r^{th} individual
- p_r : the proportion of the r^{th} individual on the roulette wheel
- $Fitness_{sum}$: the sum of fitness of the population

To select an individual, a random number is generated in the interval $[0, 1]$ and the individual whose segment spans the random number is selected [34]. The probability of an individual's reproduction is proportional to its fitness.

A five individual example is shown in Figure 3.8. Individual 5 is the fittest individual and occupies the largest part in the roulette wheel. Therefore, it has higher probability of contribution to offspring in the next generation.

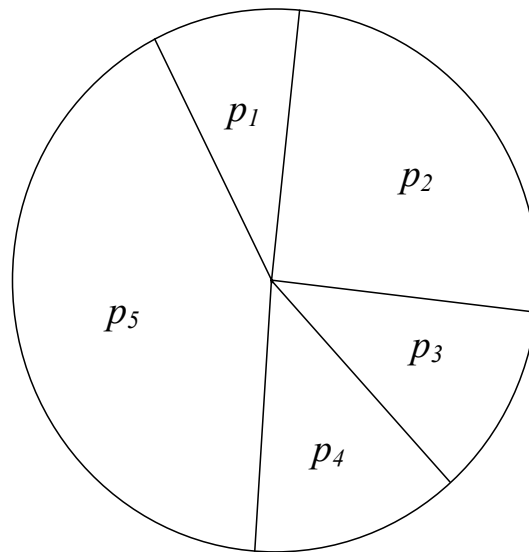


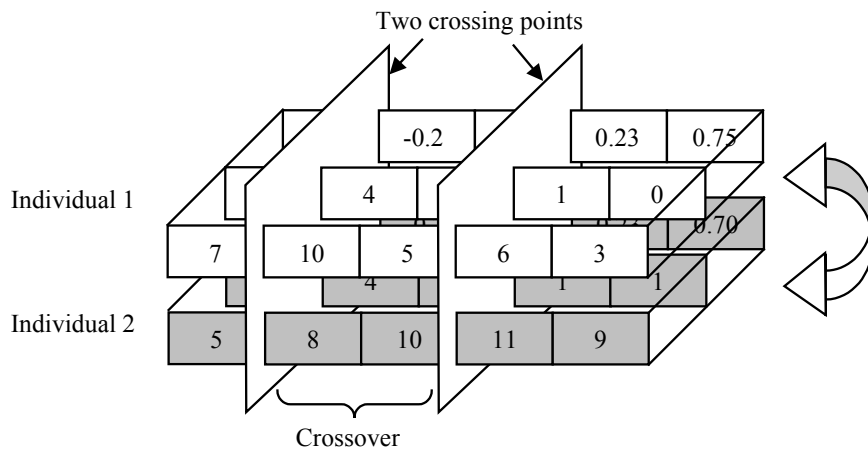
Figure 3.8 Roulette wheel selection

3.4.3.5 Crossover

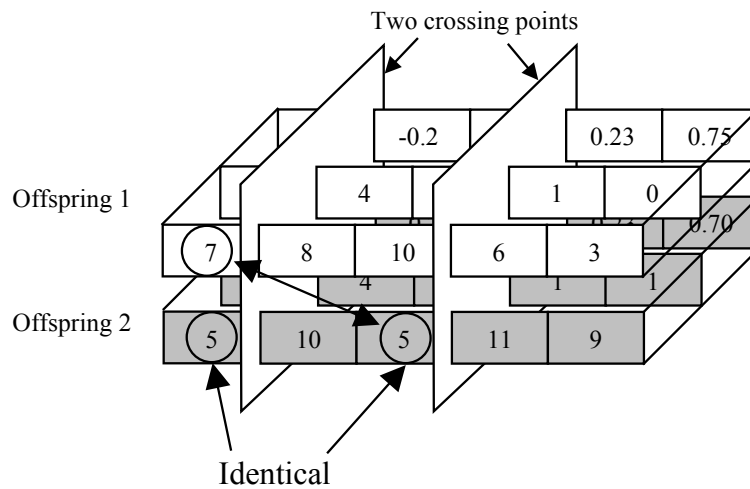
After the process of reproduction, crossover is applied. The main objective of crossover is to reorganize the information of two different individuals and produce a

new one [9,31]. This operator promotes the exploration of new regions in the search space.

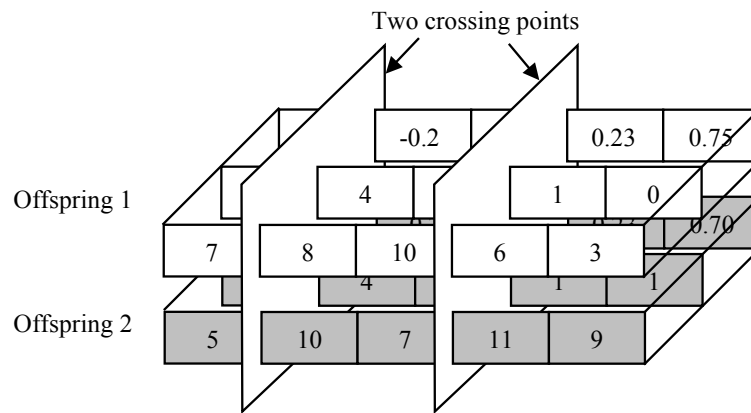
As shown in Figure 3.9 (a), a two-points crossover [9,31] is applied and the probability of the crossover p_c is selected as 0.95. First, two crossing points are selected uniformly at random along the individuals. Elements outside these two points are kept to be part of the offspring. Then, from the first position of crossover to the second one, elements of the three strings of both individuals are exchanged. After crossover, the two individuals are shown in Figure 3.9 (b).



(a) Individuals



(b) Offspring before correction



(c) Offspring after correction

Figure 3.9 Two points crossover

As mentioned above, only one FACTS device can be located on a transmission line. After crossover, if there are two devices allocated on one transmission line, the "arrangement of the FACTS locations" process has to be applied. In the case where an element of the first string already occupies a position in the kept part of the parent, it is replaced by the element corresponding to the same position in the other parent. This algorithm is repeated until an element not already present in the string is reached [9].

As shown in Figure 3.9 (b), after crossover operation, individual 2 contains two strings that have the identical first part. This means there is already a FACTS device located on the line "5". Therefore, the line "5" at the third position is replaced by the first element of individual 1, which corresponds to the line "7". After this arrangement, the two individuals are shown in Figure 3.9 (c).

3.4.3.6 Mutation

Mutation is used to introduce some sort of artificial diversification in the population to avoid premature convergence to local optimum [6,31]. Non-uniform mutation,

which has proved to be successful in a number of studies [31], is employed in this research.

For a given parent $X_{par} = x_1 x_2 \dots x_k \dots x_l$, if the gene x_k is selected for mutation and the range of x_k is $[U_{Min}^k, U_{Max}^k]$, then the result x_k' is:

$$x_k' = \begin{cases} x_k + \Delta(t, U_{Max}^k - x_k) & \text{if } \text{random}(0,1) = 0 \\ x_k - \Delta(t, x_k - U_{Min}^k) & \text{if } \text{random}(0,1) = 1 \end{cases} \quad (3.15)$$

where

$$\Delta(t_{gen}, y_{mu}) = y_{mu} \cdot \left(1 - r_{gen} \left(1 - \frac{t_{gen}}{T_{gen}} \right)^{b_{gen}} \right) \quad (3.16)$$

$\Delta(t_{gen}, y_{mu})$ (y_{mu} represents $x_k - U_{Min}^k$ and $U_{Max}^k - x_k$) returns a value in the range $[0, y_{mu}]$. Its probability being close to 0 and increases as t_{gen} increases (t_{gen} is the current generation number and T_{gen} is the total generation number). This property enables the operator to search the space uniformly at initial stages (when t_{gen} is small), and very locally at later stages (when t_{gen} is large). In Equation 3.16, r_{gen} is a random value in the range of $[0,1]$ and b_{gen} is a parameter determining the degree of non-uniformity. In this simulation, $b=2$ is applied.

The above-mentioned operations of selection, crossover and mutation will be repeated until the maximal number of generation is reached.

The proposed optimization strategy is summarized in Figure 3.10. In order to ensure that there is only one FACTS device on each transmission line, the process of "Arrangement of the FACTS locations" is necessary.

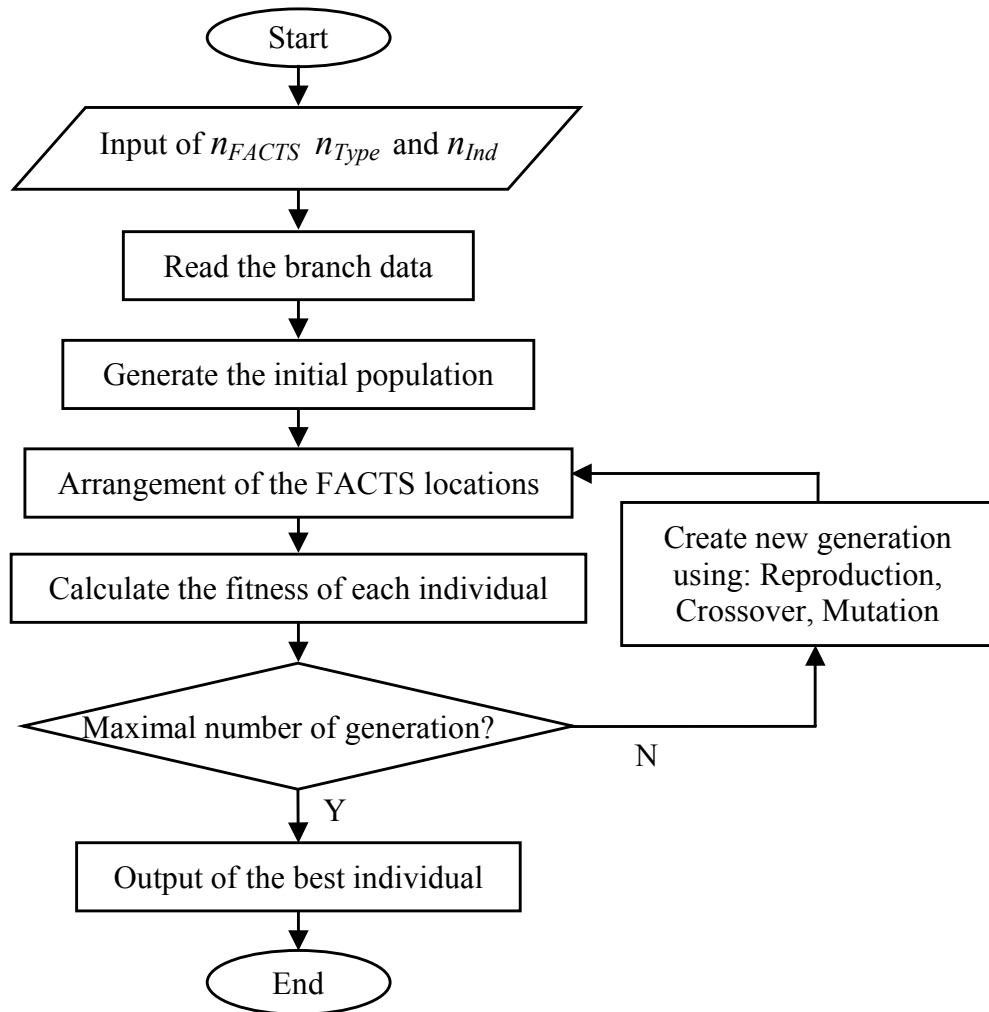


Figure 3.10 Flow chart of the GA optimization

3.4.4 Case study

In order to verify the effectiveness of the proposed method, a modified IEEE 14-bus test system, as shown in Figure 3.11, is considered. The generation cost functions are given in Appendix 2.1. Different operating conditions are simulated for the determination of the optimal FACTS locations.

The initial value of n_{FACTS} , which indicates the number of FACTS devices to be simulated, is considered as five. The total number of generation is 200 and there are 20 individuals in each generation.

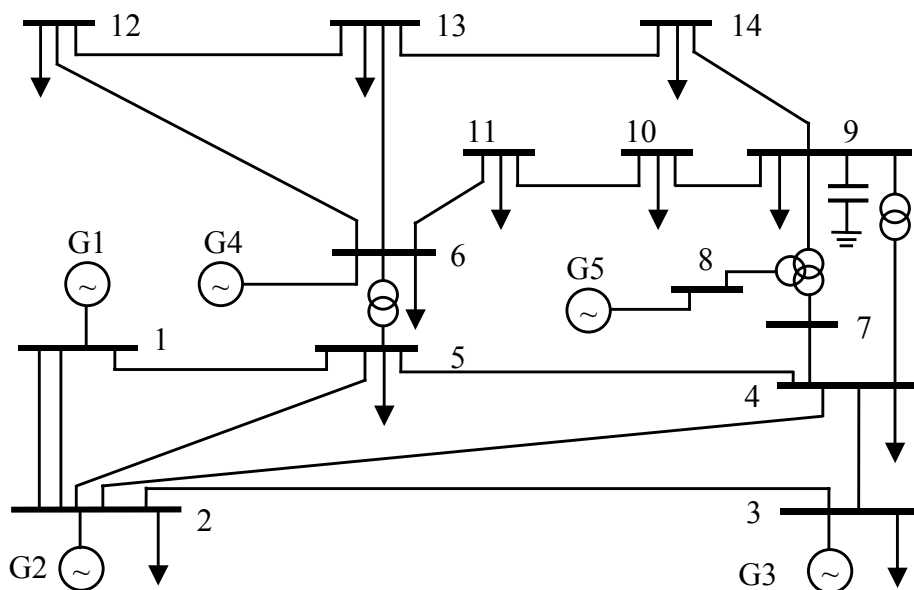


Figure 3.11 Modified IEEE 14-bus test system

3.4.4.1 Case 1 — Voltage congestion at bus 2

In this case, all generators are in service and there is only voltage congestion at bus 2. The simulated result is shown in Figure 3.12. After the optimization, for the considered power system only a SVC at bus 5 is necessary. The optimized settings of SVC are given in Appendix 2.2.

3.4.4.2 Case 2 — Active power flow congestion on the transmission line between bus 1 and bus 5

In this case, only generators 1 and 3 are in service and there is a power flow congestion on the transmission line between bus 1 and bus 5. The simulation result is also shown in Figure 3.12. After the optimization, a TCSC needs to be installed between bus 2 and bus 5. The optimized settings of TCSC are given in Appendix 2.2.

Simulation results indicated that for the considered power system, the TCSC and SVC are the appropriate FACTS devices in terms of economic criterion. Moreover,

SVC is the most favorable choice for the voltage congestion management. Even though UPFC is the most powerful FACTS device, it has not been used in operation due to its extremely high investment cost.

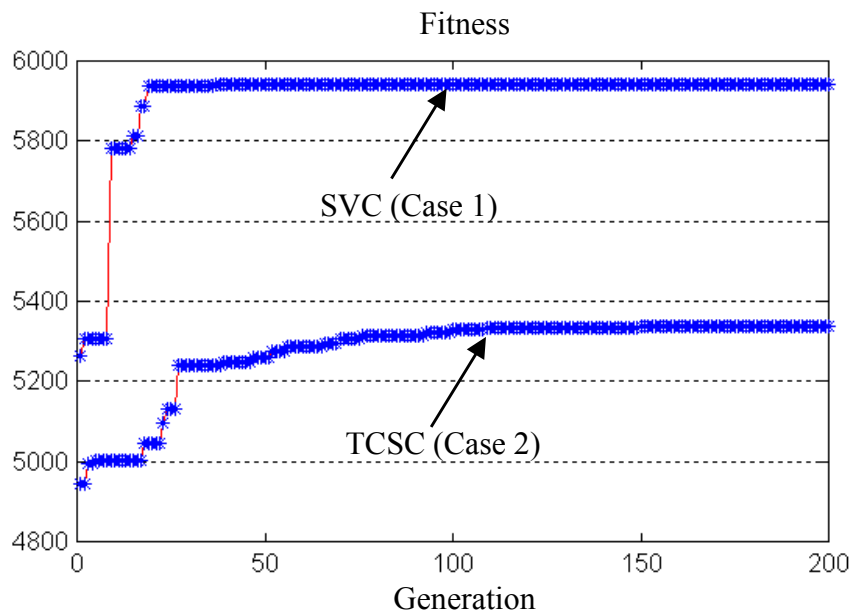


Figure 3.12 Simulation results

3.4.5 Conclusions of GA optimization method

Simultaneous optimization of the locations of the FACTS devices, their types and rated values is a very complicated optimization problem in large power systems. The algorithm proposed in this section is a general optimization method, which is suitable to solve such combinatorial problems. It always gives the best solutions and it is faster than the classical optimization methods. Furthermore, since the total cost function, which includes the generation costs and the FACTS investment costs, is minimized, the FACTS investment costs can be provided by sparing of the generation costs. This algorithm is practical and easy to be implemented into the large power system analysis.

3.5 Comments on the allocation of FACTS devices

In large power systems, the selection of proper location and type for FACTS devices is the first and important step in designing FACTS controllers. Based on the FACTS locations, the design and coordination of their controllers can be carried out.

As discussed in last sections, FACTS devices are capable of changing the system parameters in a fast and effective way. Therefore it is obvious that the benefit brought by FACTS devices includes improvement of system stability, enhancement of system reliability and reduction of operation and transmission investment cost. Various criteria can be applied for the allocation of FACTS devices.

In practical operation, the main concern for the allocation of FACTS devices is the economic effect. For instance, to increase the power transfer capability and to reduce the generation costs. Power oscillation damping effects are the additional FACTS benefits. The proposed GA method is based on the economic criterion and it is a general method for allocating and selection of proper types of FACTS devices in large power systems.

In large power systems, poorly damped oscillations usually occur because of the relative weak tie-lines between interconnected areas. Transferring of bulk powers, both for economic and technical reasons, through tie-lines will be feasible when these tie-lines are equipped with FACTS devices. This further, based on the residue criterion, affirmed that these tie-lines are also the possible FACTS locations for damping of inter-area oscillations. Hence, in practice, the residue method can be applied to find the most suitable locations among these tie-lines.

Chapter 4

Adaptive FACTS Transient Controller Design using ANFIS Technology

4.1 Introduction

This chapter deals with the development of adaptive FACTS transient controller using Adaptive Network based Fuzzy Inference System (ANFIS) technology. The approach adaptively switches between the transient stability controller and POD controller for series FACTS devices in large power systems. The designed controller using ANFIS technology adaptively activates the transient stability controller for series FACTS devices during large disturbances.

Traditionally, the switching mechanism between FACTS transient controller and POD controller is achieved using a pre-set fixed switching time [15]. However, the optimal switching time is varied with different disturbances and different operating conditions. Moreover, the switching time cannot be automatically adjusted to different situations.

In this study, the switching mechanism is controlled automatically by means of the fuzzy-logic approach. The 16-machine system described in Chapter 3 is considered to illustrate the approach. The series FACTS device is located between bus A and bus A0

(on the tie-line between area 3 and area 4) and its location is determined using the residue algorithm (as discussed in Chapter 3) for damping of inter-area oscillations.

4.2 Switching strategy for FACTS transient controller

FACTS controller, as discussed in Chapter 2, focuses mainly on the following three control objectives [15]: steady-state power flow control, transient stability control for improving the first swing stability, and power oscillation damping control to damp the power system oscillations. The comprehensive control scheme is shown in Figure 4.1, i.e. the combination of control schemes shown in Figure 2.6, Figure 2.8 and Figure 2.9 [15]. In this study, the active power flow through the FACTS device is used as an input for the comprehensive control scheme.

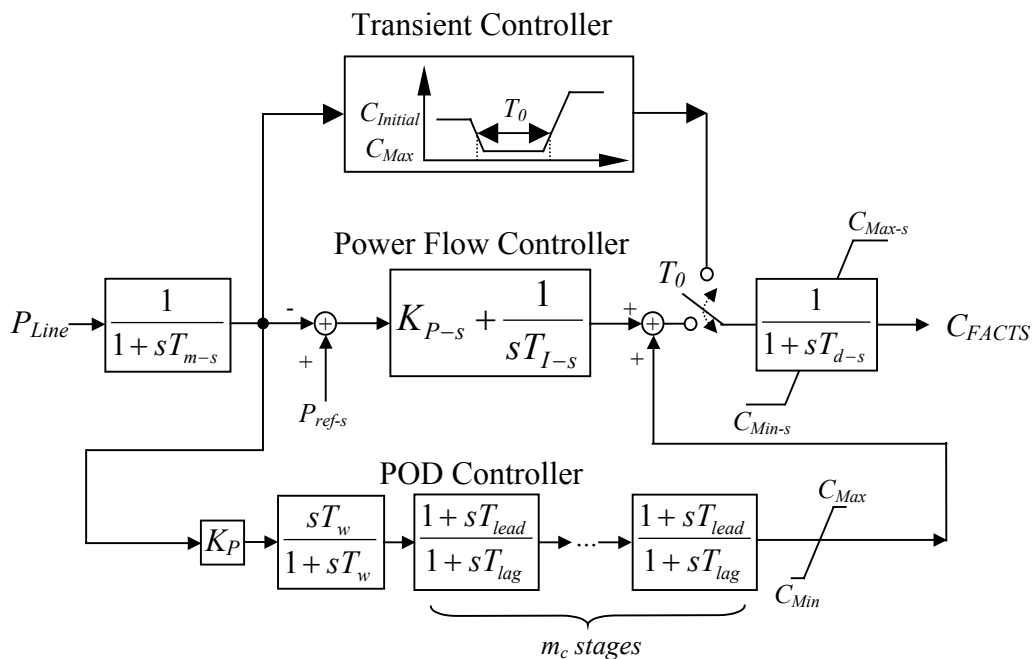


Figure 4.1 FACTS comprehensive control scheme

The FACTS transient controller and POD controller achieve different control objectives in different situations. Conventionally, in order to enhance transient stability

and damp the subsequent oscillations, a switching control strategy is always used between these two different controllers [15]. The switching control strategy is as follows:

- Following a large disturbance, the transient controller acts first to maintain the transient stability of power systems.
- After the pre-set switching time period T_0 , the control is then transferred to the power flow and POD controller. During the post-fault oscillations, due to the large integral time constant of T_{I-s} , the POD controller has the most influence.

The pre-set switching time T_0 should be reasonably chosen within the transient period. Practically, the exact switching time is determined by trial and error using transient simulation results. This so determined switching time is physically fixed according to one particular fault sequence. However, power systems may have different disturbances and different operating conditions and therefore this pre-set switching time T_0 may not be suitable for all those situations.

4.3 Fuzzy adaptive switching controller

In this study, the fuzzy-logic approach is used to switch the FACTS transient stability controller adaptively under different operating situations and fault sequences. The fuzzy adaptive switching controller design procedure involves the following steps:

- 1 Determination of the structure of fuzzy adaptive switching controller
- 2 Use ANFIS for training of the fuzzy adaptive switching controller
- 3 Non-linear simulation for verifying the performance of the proposed controller

4.3.1 Structure of the fuzzy adaptive switching controller

As stated in Chapter 2, the reason for choosing fuzzy-logic controller is that fuzzy-logic is one of the most successful approaches for utilizing the qualitative knowledge of

a system to design a controller. Particularly, in this study, in order to handle the uncertainties of fault sequences and different operating conditions, fuzzy-logic controller is an appropriate approach for the non-linear adaptive control of FACTS transient controller [55,58].

As stated above, the objective is to achieve a good transient behavior and damping performance for the considered system. Therefore, the switching controller must have the following functions:

- Using only local signals, the controller must switch adaptively, i.e. as a time-variant switch, between the FACTS transient controller and POD controller.
- Moreover, the controller must also react robustly under different situations without knowing fault sequences in the system.

Therefore, in this work, two control loops are used in the fuzzy adaptive switching controller, as shown in Figure 4.2, the controller consists of fuzzy-logic loop and protection loop.

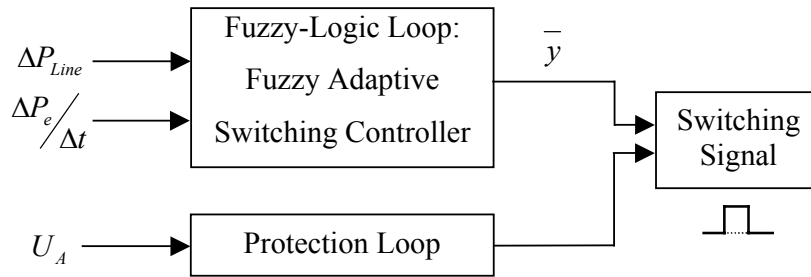


Figure 4.2 Fuzzy adaptive switching controller

The three inputs to the fuzzy adaptive switching controller are: ΔP_{Line} , $\frac{\Delta P_e}{\Delta t}$ and U_A . Here U_A is the FACTS terminal voltage magnitude. ΔP_{Line} and $\frac{\Delta P_e}{\Delta t}$ are defined as follows:

$$\begin{aligned} \Delta P_{Line} &= P_{Line}^{(ns+1)} - P_{Line}^{(0)} \\ \frac{\Delta P_e}{\Delta t} &= \frac{P_{Line}^{(ns+1)} - P_{Line}^{(ns)}}{\Delta t} \end{aligned} \quad (4.1)$$

where

ΔP_{Line} Active power difference flow through FACTS device

$P_{Line}^{(0)}$ The initial (pre-fault) active power transferred through the FACTS device

$P_{Line}^{(ns)}, P_{Line}^{(ns+1)}$ The active power transferred through the FACTS device at the sample time ns and $ns+1$

Δt : The time step between two sample points

The output \bar{y} is the switching signal for the adaptive switching between FACTS transient controller and POD controller. The statement of the function is as follows:

If $\bar{y}=1$, then FACTS transient controller should be employed. Otherwise, if $\bar{y}=0$, then FACTS POD controller should be employed.

4.3.2 Fuzzy-logic loop

Similar to the conventional fuzzy-logic controller discussed in Chapter 2, this fuzzy-logic loop also involves fuzzification, inference and defuzzification.

4.3.2.1 Fuzzification

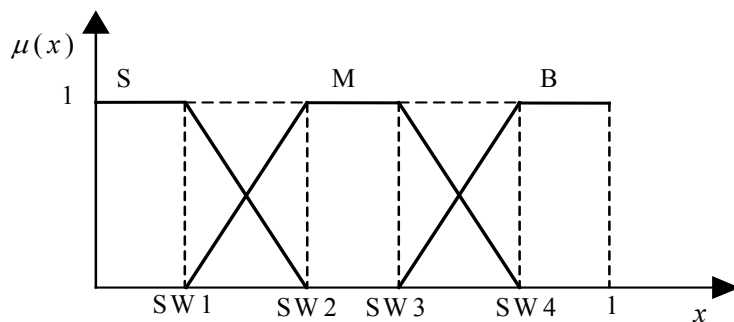


Figure 4.3 Membership functions

As stated in Chapter 2, fuzzification is a process whereby the input variables are mapped onto fuzzy variables (linguistic variables). Each fuzzified variable has a certain membership function. The inputs are fuzzified using three fuzzy sets: B (big), M (medium) and S (small), as shown in Figure 4.3.

4.3.2.2 Inference

Fuzzy inference system involves fuzzy rules for determining output decisions. The fuzzified input variables are mapped onto the output variables using these fuzzy rules.

In this work, the Sugeno fuzzy inference system is employed, because it is able to combine transparency of the rules and the accuracy of the predictions concomitantly [25,35]. The outputs of the inference system are linear membership functions and the first order Sugeno fuzzy model is given as:

$$\text{if } x \text{ is } A_1 \text{ and } y \text{ is } A_2 \text{ then } f_i = p_{ci}x + q_{ci}y + r_{ci} \quad (4.2)$$

where x and y represent the ΔP_{Line} and the $\frac{\Delta P_e}{\Delta t}$ defined in Equation 4.1 respectively. A_1 and A_2 are fuzzy sets in the antecedent, while p_{ci} , q_{ci} and r_{ci} are the consequent parameters $S2$ [35]. Conventionally, the fuzzy inference system is always obtained from the system operation and operator knowledge. Here in this study, in order to achieve high accuracy, the fuzzy inference system is trained using the ANFIS technology.

4.3.2.3 Defuzzification

As stated in Chapter 2, the defuzzification process transforms the fuzzy results of the inference into a crisp output. In this work, the weighted average method is employed. Since the output of each rule is a linear combination of input variables, the final output is the weighted average of each rule's output [35]:

$$\bar{y} = \frac{\sum_{i=1}^9 \beta_i f_i}{\sum_{i=1}^9 \beta_i} = \frac{\sum_{i=1}^9 \beta_i (p_{ci}x + q_{ci}y + r_{ci})}{\sum_{i=1}^9 \beta_i} \quad (4.3)$$

where β_i represents the firing strength of the i^{th} rule expressed as Equation 4.4 in the following section.

4.3.3 Protection loop

The function of the protection loop is to protect the FACTS devices under large disturbances. Its input is the FACTS terminal voltage magnitude U_A at bus A (as shown in Figure 3.1). For instance, under large disturbances, if U_A has a large difference (more than $\pm 15\%$) with the nominal voltage, the FACTS devices must be blocked from being damaged.

4.4 ANFIS training

ANFIS serves as a basis for constructing a set of fuzzy *if-then* rules with appropriate membership functions to generate the stipulated input-output pairs. In this section, the ANFIS structure and the procedure for training will be discussed in detail. Furthermore, using ANFIS technology, both the membership functions and the inference system will be optimized.

4.4.1 ANFIS structure

ANFIS consists of an adaptive network, which contains nodes and directional links. The nodes are connected through the directional links. Moreover, part or all of the nodes are adaptive, which means each output of these nodes depends on the parameters pertaining to this node, and the learning rule specifies how these parameters should be changed to minimize a prescribed error measure [35].

Commonly, as shown in Figure 4.4, the ANFIS has five layers. In layer 1, each node generates membership grades of a linguistic label [24,35]. In this research, as shown in Figure 4.3, the trapezoid functions are selected. The parameters in this layer are referred to as premise parameters SI and they can be trained using the ANFIS learning algorithm.

Every node in layer 2 is a fixed node and calculates the firing strength (the weight) of each rule via multiplication of the incoming signals:

$$\beta_i = \mu_{A_j}(x) \times \mu_{B_j}(y) \quad (4.4)$$

where μ_{A_j} and μ_{B_j} ($j=1\sim3$) represent the fuzzified rules and β_i ($i=1\sim9$) is the firing strength.

Nodes in layer 3 compute the normalized firing strength of each rule. The i^{th} node calculates the ratio of the i^{th} rule's firing strength to the sum of all rules' firing strengths:

$$\bar{\beta}_i = \beta_i \cdot \left(\sum_{i=1}^9 \beta_i \right)^{-1} \quad (4.5)$$

The nodes in layer 4 are adaptive nodes and the i^{th} node has the following output:

$$f_i = \bar{\beta}_i \cdot (p_{ci}x + q_{ci}y + r_{ci}) \quad (4.6)$$

where

$\bar{\beta}_i$ is the output of layer 3.

p_{ci} , q_{ci} and r_{ci} are referred to as the consequent parameter set $S2$. They can also be trained using ANFIS learning algorithm.

The node in layer 5 sums up all the incoming signals and its output is given by Equation 4.7.

$$\bar{y} = \sum_{i=1}^9 \bar{\beta}_i \cdot (p_{ci}x + q_{ci}y + r_{ci}) \quad (4.7)$$

The detailed ANFIS structure is shown in Figure 4.4.

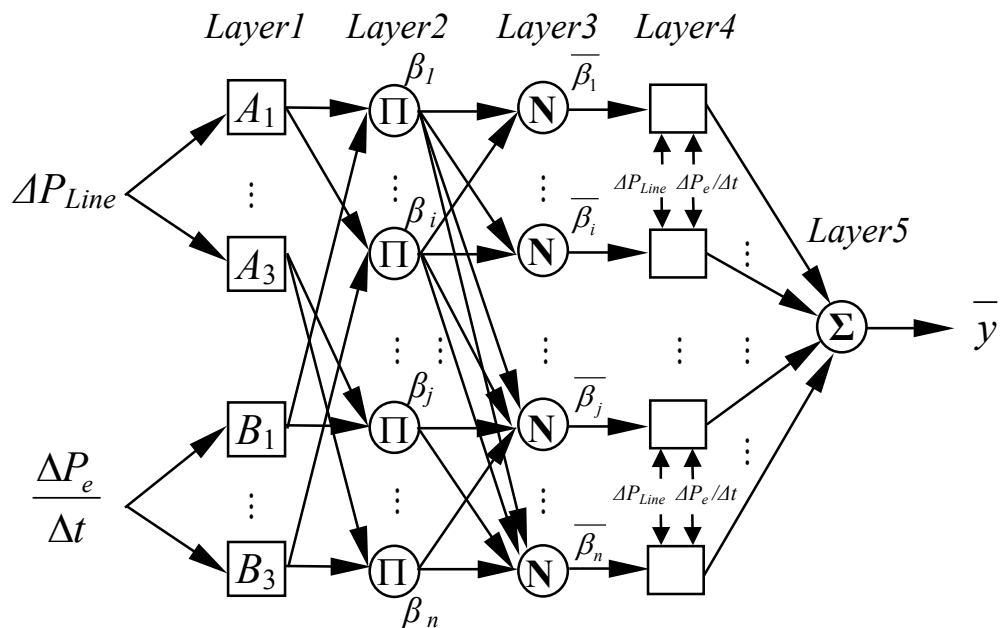


Figure 4.4 ANFIS structure

Given the initial values of premise parameters $S1$, the overall output can be expressed as a linear combinations of the consequent parameters $S2$. Therefore the hybrid learning algorithm, which consists of forward pass and backward pass, can be applied for the training [24,35]. In the forward pass, functional signals go forward till layer 4 and the consequent parameters $S2$ are identified by the least squares estimate (LSE). In the backward pass, the error rates propagate backward and the premise parameters are updated by the gradient descent.

4.4.2 ANFIS training

The objective of ANFIS training is to train the fuzzy-logic controller so as to switch the FACTS transient controller adaptively in presence of uncertainties. The training procedure, i.e. the tuning of the fuzzy-logic controller, is achieved based on the batch learning technique using input–output training data set. Considering the computational

complexity and the resulting performance, parameters are trained using the above-mentioned gradient descent and the LSE methods (hybrid learning rule) [24].

4.4.2.1 Fine-tuning of the membership functions

The human-determined membership functions are subject to the differences from person to person and from time to time, and therefore they are rarely optimal in terms of reproducing desired outputs [35]. In this simulation, due to the size of the input-output data set, the fine-tuning of membership functions is employed in the learning mechanisms.

4.4.2.2 Training of the fuzzy inference system

Using Equation 4.7 and the premise parameters, the overall system output can be expressed as a linear combination of the consequent parameters [24]:

$$\bar{y} = \sum_{i=1}^9 \bar{\beta}_i \cdot (p_{ci}x + q_{ci}y + r_{ci}) = \mathbf{F}_c \mathbf{z}_c \quad (4.8)$$

where

\mathbf{z}_c is the vector which contains consequent parameters

\mathbf{F}_c is the matrix of coefficients

As mentioned in the previous sections, in the forward training pass, using the initial values of SI , functional signals are transferred to layer 4 and then the vector \mathbf{z}_c will be identified by means of the LSE. In the backward pass, the error rates propagate backward and the premise parameters SI are updated by the gradient descent [35].

4.4.3 Training data

The training data must cover a wide range of operation and disturbance conditions. Furthermore, they must also contain as much information as possible about the

examined power systems. Therefore, power system with different fault sequences is simulated to obtain the training data.

Input data for the training

The two input data for the training: ΔP_{Line} and $\Delta P_e / \Delta t$ can be obtained by means of the non-linear simulation.

The output data for training

Since the series FACTS device is installed to damp the power oscillations between area 3 and area 4, the output data for training can be determined by the difference of power angle between the these two areas. In this simulation, the corresponding center of power angles (COA) of each area (area 3: δ_{Area3} ; area 4: δ_{Area4}) are employed for the investigation [36]:

$$\delta_{Area3}(t) = \frac{\sum_{k \in Area3} S_k H_k \delta_k(t)}{\sum_{k \in Area3} S_k H_k}, \quad \delta_{Area4}(t) = \frac{\sum_{k \in Area4} S_k H_k \delta_k(t)}{\sum_{k \in Area4} S_k H_k} \quad (4.9)$$

where

H_k is the inertia constant of the k^{th} generator

S_k is the base power of the k^{th} generator

The first swing characteristic can be determined using δ_{Area3} and δ_{Area4} :

$$\delta(t) = \delta_{Area3}(t) - \delta_{Area4}(t) \quad (4.10)$$

The ideal switching time from transient controller to POD controller is determined at the time when the derivative of Equation 4.10 vanished, i.e. $\frac{d\delta(t)}{dt} = 0$. However, this signal is employed only for the training procedure.

The complete training data set

The complete data for the training procedure are obtained from the following four events: three-phase short circuits at bus A (Local bus), B (Middle bus), C (Remote bus) and the load shedding at bus D (Load).

Each disturbance is simulated for one second. Therefore, there are discontinuities between the four parts. Figure 4.5 depicts the complete training data events.

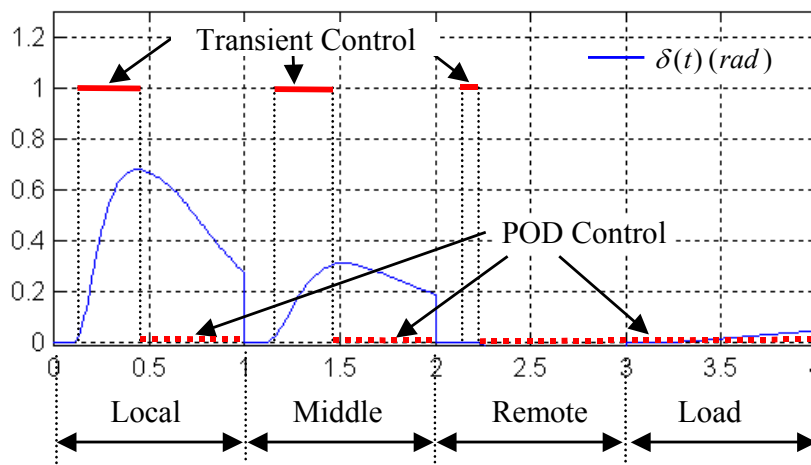


Figure 4.5 Training data

— : Time range for transient controller

⋯ : Time range for POD controller

Using the training data, the membership functions and the inference system can be optimized.

4.4.4 Training results

In this simulation, ANFIS is trained using 100 epochs and an initial step size of 10^{-4} .

4.4.4.1 Membership functions

The initial membership functions are equally spaced with enough overlap within the input range as shown in Figure 4.3. These are typical membership functions to start with the ANFIS learning.

In order to fit the output of the training data, as given in Appendix 3.1, the initial membership functions of $\Delta P_e/\Delta t$ and ΔP_{Line} are changed completely. Figure 4.6 shows the optimized membership functions of ΔP_{Line} .

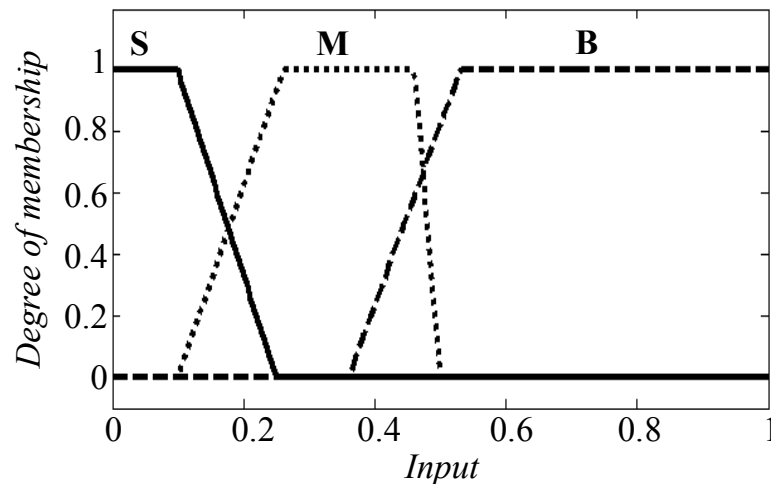


Figure 4.6 Optimized membership functions of ΔP_{Line}

4.4.4.2 Fuzzy inference system

Using the training data, the Sugeno fuzzy inference system is optimized by comparing its output with the objective output data.

Figure 4.7 shows the behavior of the trained fuzzy adaptive switching controller under the most critical training condition: a short circuit of 100 ms duration on the line between bus A0 and a supplementary bus. The near end (supplementary bus) and the remote end (bus A0) of the line are cleared at $t=0.2$ s and $t=0.3$ s respectively.

The difference between the output of the fuzzy adaptive switching controller and the objective between $t=0.2$ s and $t=0.3$ s is due to the remote end clearance time, where there is an impulse in active power flow through FACTS devices. Other training results (middle bus, remote bus and loss of load) match pretty well the objective. The detail membership functions and the first-order Sugeno fuzzy model are given in Appendix 3.2.

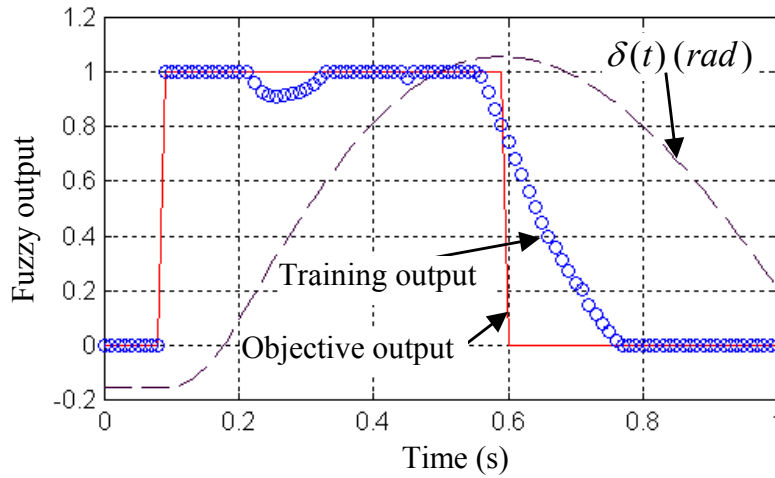
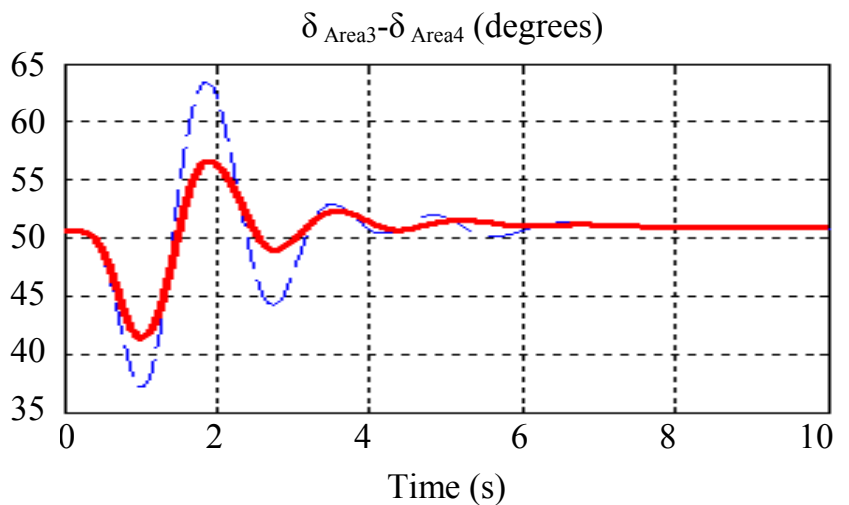


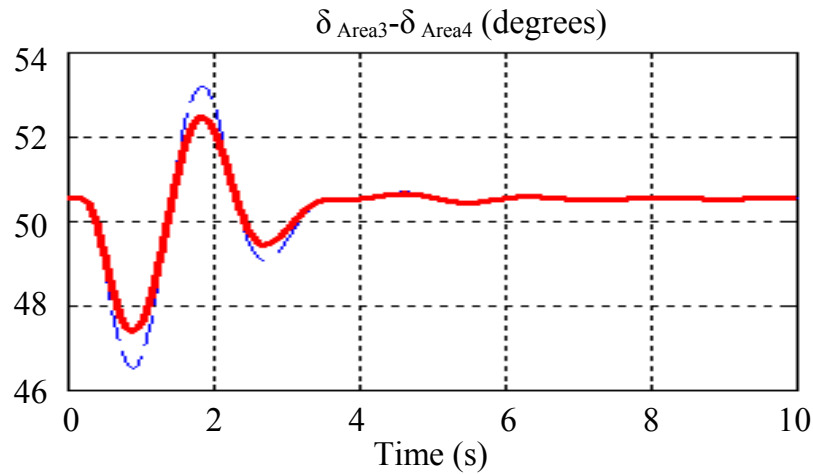
Figure 4.7 Training result

4.5 Simulation results

To verify the performance of the proposed controller, two disturbances are considered in the system, i.e. three-phase short circuits at the bus B1 (area 4, local bus) and at the bus C1 (area 5, remote bus) with duration of 100 ms and 150 ms respectively. Figure 4.8 demonstrates the rotor angle difference between area 3 and area 4 in case of using the conventional fix-time-switching controller and the fuzzy adaptive switching controller.



(a) Three-phase short circuit at bus B1



(b) Three-phase short circuit at bus C1

Figure 4.8 Simulation results

- — : Conventional fix-time-switching controller
- : Fuzzy adaptive switching controller

In comparison with the conventional fix-time-switching controller, the power system performs better with the proposed fuzzy adaptive switching controller and the dynamic performance is also improved. Particularly, as shown in Figure 4.8 (a), the proposed control scheme leads to significantly better transient behavior under the local bus disturbance.

4.6 Conclusion

This chapter presents a new fuzzy adaptive FACTS transient controller design method using ANFIS technology. The approach adaptively activates transient stability controller for series FACTS devices during large disturbances.

Using the training data set, which is obtained by simulating over a wide range of operating situations and disturbance conditions, the parameters of the proposed controller are optimized using the ANFIS technology. The performance of the proposed controller is verified for the large power system under different disturbances.

Simulation results validate the effectiveness of the proposed control strategy. Moreover, the approach is easy to realize and implement in real power systems.

Chapter 5

Simultaneous Coordinated Tuning of FACTS POD and PSS Controllers for Damping of Power System Oscillations

5.1 Introduction

In large power systems, damping of power oscillations between interconnected areas is important for the system secure operation. However, using only conventional PSS may not provide sufficient damping for the inter-area oscillations. As discussed in the previous chapters, FACTS POD controllers can provide effective damping for the inter-area modes.

However, uncoordinated local control of FACTS devices and PSSs may cause unwanted interactions that further result in the system destabilization. To improve overall system performance, many researches were made on the coordination among PSS and FACTS POD controllers [14,20,37-39]. Some of these methods are based on the complex non-linear simulation [14,20], the others are linear approaches [37-39].

In this chapter, since power system non-linear simulations require much more time than the linear approaches, the modal analysis based tuning algorithm is proposed to coordinate the multiple damping controllers simultaneously. The overall power system

performance is optimized by means of sequential quadratic programming algorithm. By minimizing the objective function, in which the influences of PSSs and FACTS POD controllers are taken into account, interactions among these damping controllers are improved.

The 16-machine system discussed in Chapter 3 is used in this study. The series FACTS device is also employed for damping of inter-area oscillations. It is located on the tie-line between area 3 and area 4, i.e. between bus A and bus A0.

5.2 PSS and FACTS POD controller

5.2.1 PSS controller

In this study, all generators are equipped with PSSs. As mentioned in Chapter 3, PSS acts through the excitation system to import a component of additional damping torque proportional to speed change of the generator [56]. It involves a transfer function consisting of an amplification block, a wash-out block and two lead-lag blocks [5,56]. The lead-lag blocks provide the appropriate phase-lead characteristic to compensate the phase lag between the exciter input and the generator electrical torque. The structure of the PSS controller is shown in Figure 5.1.

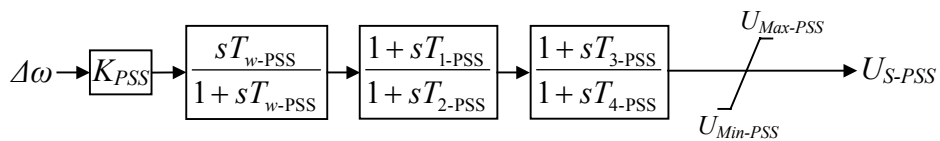


Figure 5.1 PSS controller

5.2.2 FACTS POD controller

As discussed in Chapter 2, the structure of series FACTS POD controller, which is shown in Figure 5.2, is similar to that of the PSS controllers. Commonly, local signals of FACTS devices are applied for the damping control. In this study, the active power

flow through the series FACTS device P_{Line} is employed. The output C_{FACTS} represents the controlled variable of the series FACTS devices. For example, for TCSC it is the value of the series capacitance [15] and for UPFC it is the series injected voltage, which is perpendicular to the line current [40-41].

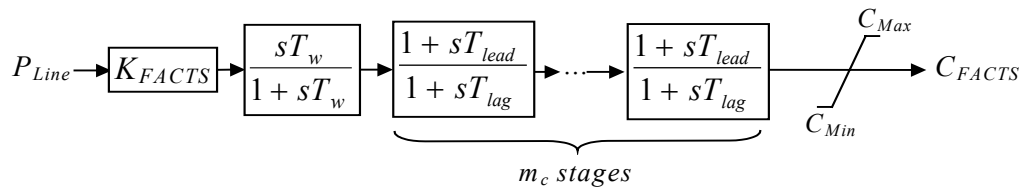


Figure 5.2 FACTS POD controller

5.2.3 Conventional approach for allocation and parameter tuning of PSS and FACTS POD controllers

Originally, the aim of tuning FACTS POD controller was to damp power system oscillations on the tie-lines where the FACTS devices are installed. Based on the participation factor analysis, the PSS controllers are designed to damp the critical modes of oscillations that can be influenced by them. Well-designed PSS and FACTS POD controllers can provide enough damping ratio over a wide range of system operating conditions. Based on modern control theory, the design and tuning methods for PSS and FACTS controllers are well developed for single-machine systems. However, the tuning of damping controllers in large power systems is much more complicate than that in single machine system. The conventional tuning methods are always based on the modal analysis and the procedure is given as follows [42]:

- 1 The locations of PSS and FACTS controllers are determined using participation factor and residue method respectively.
- 2 Then, FACTS and PSS controllers are designed based on their selected locations. For this design, different methods can be used [14,15,20].

- 3 Finally, the controller settings will be verified under various operating conditions.

Conventional design approaches, like the decoupled and sequential loop closure, cannot adequately handle interactions among controls. Properly coordinated designs can mitigate possible adverse interactions among controls [59]. In this research, an optimization based tuning algorithm is proposed to coordinate among multiple controllers simultaneously.

5.3 Simultaneous coordinated tuning method

Many researches were made on the parameter tuning [14,20]. In [20], non-linear optimization based global tuning procedures are introduced for minimizing the interactions among the FACTS and PSS controllers. The non-linear optimization based tuning method considers complex dynamics of power systems, especially during critical faults. However, the non-linear simulation of large power system requires much more time than linear approaches [14]. Therefore, in practice, due to computational simplicity, modal analysis based methods are more preferable.

In this section, an optimization based linear method for simultaneous tuning of the FACTS and PSS controllers is introduced. The objective of the simultaneous parameter tuning is to globally optimize the overall system damping performance. This requires the simultaneous optimization and coordination of the parameter settings of the FACTS and PSS controllers to maximize the damping of all modes of oscillations: for instance local modes, inter-area modes, exciter modes and other controller modes.

In this study, the parameters of each PSS and FACTS POD controller are determined simultaneously using non-linear programming technique. The main procedure is give as follows:

- 1 System linearization for analyzing the dominant oscillation modes of the power system.
- 2 Allocation of PSS and FACTS POD controllers by means of the participation factor and the residue method.

- 3 Using the linearized system model and parameter-constrained non-linear optimization technique to optimize the global system behavior.

Nowadays, by means of the modified ARNOLDI method, there is no problem in the system linearization mentioned in Step 1 and Step 2. This section focuses on the last step concerning the optimization based parameter tuning. Furthermore, in order to cope with the non-linear nature of the power system, a particular range of system operating conditions are also considered to verify the performance of the optimized controller settings.

5.3.1 Linearized system model

Once the optimal locations of the controllers are chosen, as discussed in Section 2.3, the total linearized system model extended by PSS and FACTS controllers can be determined. Thus, the eigenvalues $\lambda_i = \sigma_i \pm j\omega_i$ ($i=1\sim n$) of the entire system can be evaluated, where n is the total number of the eigenvalues which include the inter-area modes, local modes, exciter modes and other controller modes, as shown in Figure 5.3. The proposed method is to search the best parameter set for the controllers, so as to achieve the minimal Comprehensive Damping Index (*CDI*) which is given by Equation 5.1.

$$CDI = \sum_{i=1}^n (1 - \zeta_i) \quad (5.1)$$

where $\zeta_i = \frac{-\sigma_i}{\sqrt{\sigma_i^2 + \omega_i^2}}$ is the damping ratio and the *CDI* index function depends on

the parameters of both FACTS POD controller and PSS controllers.

Among the dominant eigenvalues, only those, which have an insufficient damping ratio, are considered in the optimization. In this study, only eigenvalues with less than 10% damping ratio have been taken into account. The objective of the optimization is to move the total considered eigenvalues to left hand side of the *s*-plane, and thus to maximize the damping ratio as much as possible. The movements of eigenvalues based on this optimization approach are shown in Figure 5.3.

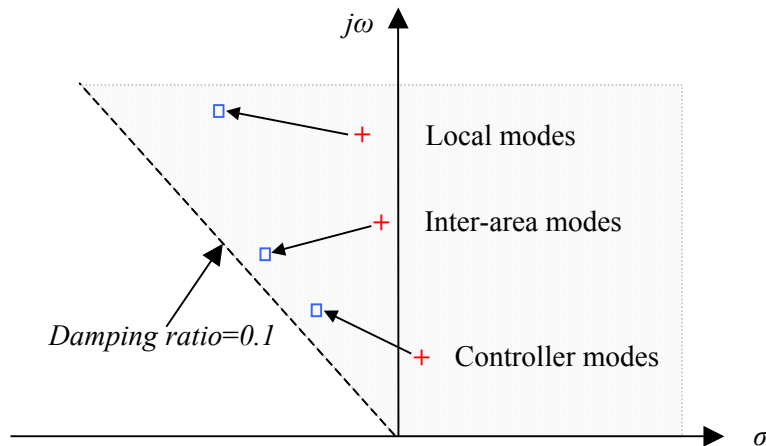


Figure 5.3 Movements of eigenvalues

+ : Eigenvalues before the optimization

□ : Eigenvalues after the optimization

5.3.2 Non-Linear optimization technique

In order to minimize the objection function given in Equation 5.1, non-linear optimization technique is employed in this study.

The objective of the parameter optimization can be formulated as a non-linear programming problem expressed as follows:

$$\begin{aligned}
 \min. \quad & f(\mathbf{z}) = CDI = \sum_{i=1}^n (1 - \zeta_i) \\
 \text{s.t.} \quad & \mathbf{E}_0(\mathbf{z}) = 0 \\
 & \mathbf{F}(\mathbf{z}) \geq 0
 \end{aligned} \tag{5.2}$$

where $f(\mathbf{z})$ is the objective function defined as in Equation 5.1 and \mathbf{z} is a vector, which consists of the parameters of the PSSs and FACTS POD controllers. In this study, \mathbf{z} contains the gain of the FACTS POD controller (K_{FACTS}) and those of all PSS controllers (K_{PSS}). The lead-lag parameters of the PSS controllers are optimized based on the approach given in [16]. The lead-lag parameters of the FACTS POD controller are optimized using the residue method.

$\mathbf{E}_0(\mathbf{z})$ are the equality constrains and $\mathbf{F}(\mathbf{z})$ are the inequality constrains respectively. For the proposed method, only the inequality constrains \mathbf{z} , which represent the parameter constrains of the damping controllers, are necessary.

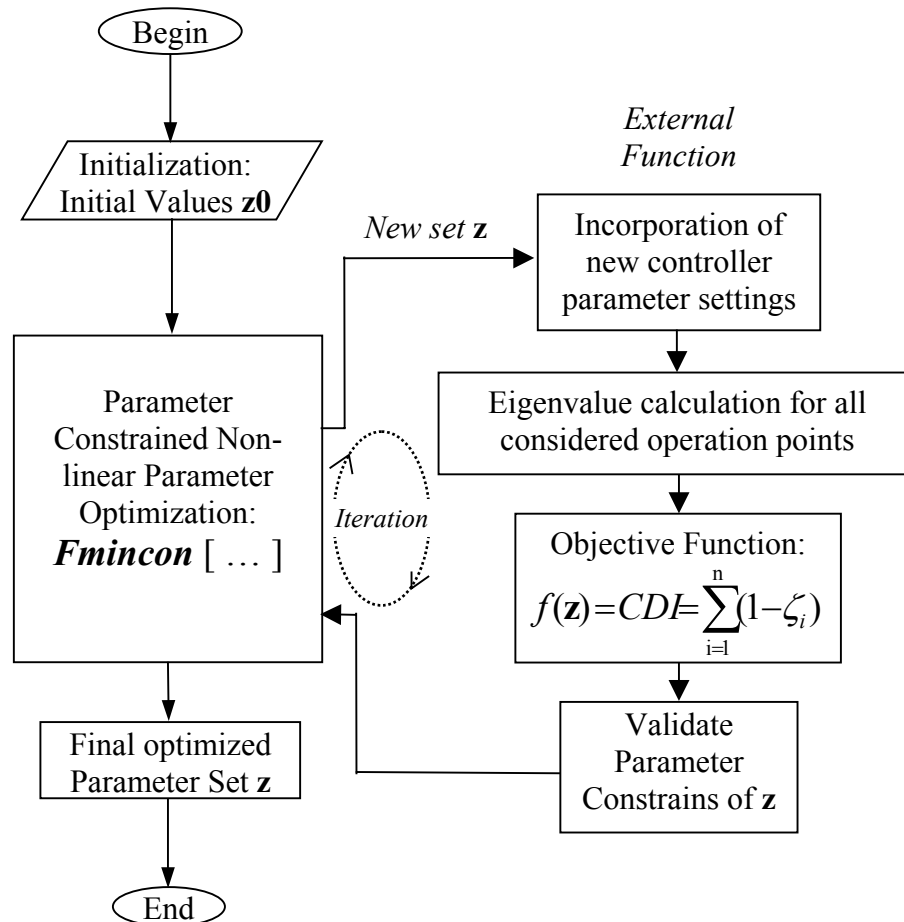


Figure 5.4 Flow chart of optimization based coordinated tuning method

In this study, in order to solve the above-mentioned parameter-constrained non-linear optimization problem, the SQP (Sequential Quadratic Programming) algorithm provided by the *Matlab Optimization Toolbox* is applied [21]. The flow chart of the optimization based coordinated tuning algorithm is shown in Figure 5.4.

The optimization starts with the pre-selected initial values of the controllers: \mathbf{z}_0 . Then the non-linear algorithm is employed to adjust the parameters iteratively, until the objective function, i.e. Equation 5.1, is minimized. These so determined parameters are the optimal settings for the FACTS POD controller and PSS controllers.

5.3.3 Practical application

Practically, the optimized PSS and FACTS controllers should produce an adequate damping torque over a wide range of operation conditions. Thus, it is necessary to optimize the controller settings under different possible operating conditions. The proposed method in the previous sections allows simultaneously considering several operating conditions of the power systems. In other words, the *CDI* of each operating condition can be calculated successively and then added to a global *CDI* for the optimization algorithm. Therefore, this parameter tuning method will provide optimal controller setting for all considered operating conditions.

In comparison with the approaches given in [14,20], this algorithm optimizes the damping ratios more rapidly for every state of the researched system. It is an effective method for tuning of controllers in large power systems.

5.4 Simulation results

To illustrate the performance of the proposed tuning method, the modified New England Power System discussed in Chapter 3 is considered. In this simulation, all the 16 machines are equipped with static exciters and PSSs.

5.4.1 Dominant eigenvalues

The dominant eigenvalues of the test system without FACTS and PSS controllers are shown in Figure 5.5 and it is clear that the system is unstable.

The test system can be stabilized by sequentially designing of PSS and FACTS controllers without any coordinated tuning. For this case, the eigenvalues of the test system are also shown in Figure 5.5. However, the damping ratios of some local modes and some inter-area modes (inter-area mode 2, 3 and 4) are not satisfactory.

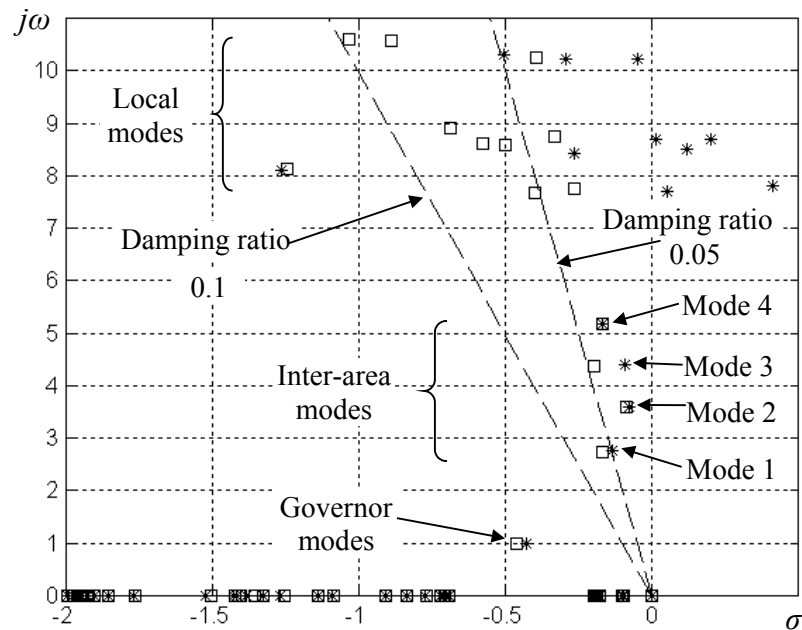


Figure 5.5 Results of the conventional controller tuning

* : Eigenvalues of the power system without any controller

\square : Eigenvalues of the power system with PSS and FACTS controllers

5.4.2 Root-locus

The root-locus, when the gain of series FACTS controller K_{FACTS} varies from 0 to 100, is shown in Figure 5.6. It is obvious that the FACTS POD controller has little influence on the local modes whereas it has significant influence on the inter-area modes of oscillations. It is also clear that a gain of 100 sufficiently increases the damping of the inter-area mode 1. However, when K_{FACTS} is beyond 70, the damping ratio of the inter-area mode 2 and inter-area mode 3 will be slightly reduced again. Furthermore, with the increase of the gain of FACTS controller, the damping ratio of exciter mode is reduced significantly and will be unstable.

Therefore, the simultaneous coordinated tuning among FACTS POD controller and PSS controllers is necessary.

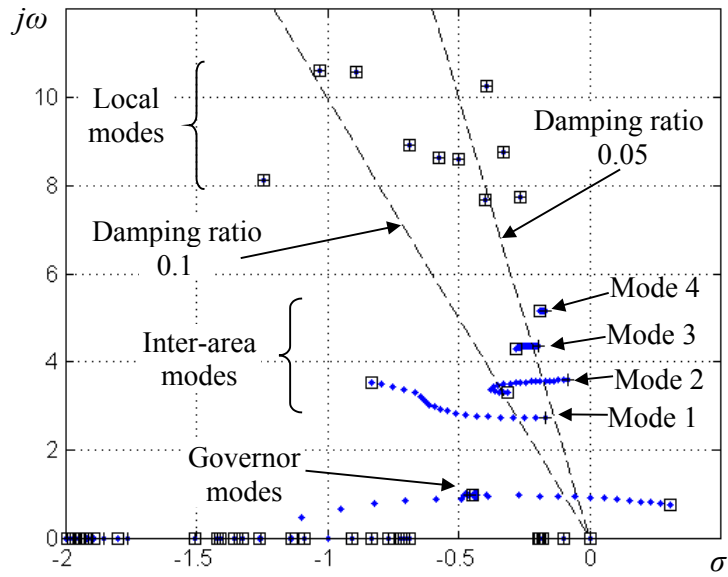


Figure 5.6 Root-locus of the FACTS POD controller

◆ Root-locus when K_{FACTS} vary from 0 (+) to 100 (□)

5.4.3 Optimized system performance

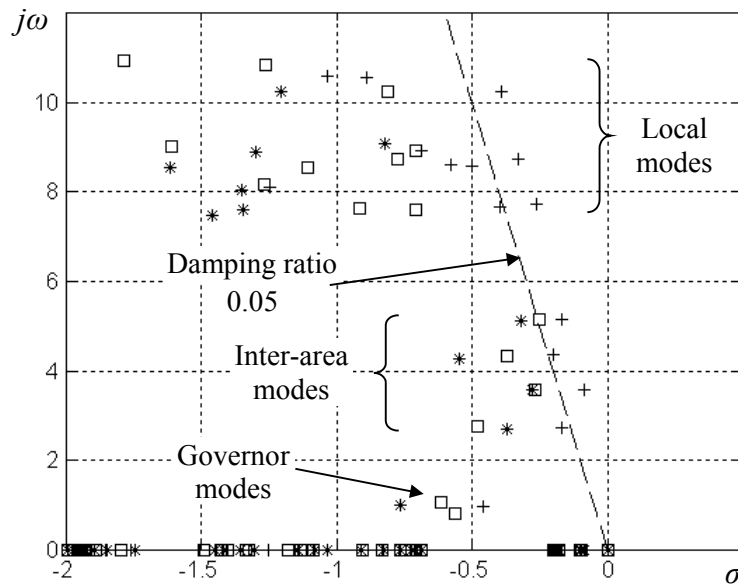


Figure 5.7 Optimization based coordinated tuning results

+ : Eigenvalues before optimization * : Eigenvalues after optimization
 □ : Eigenvalues when the two tie-lines between area 4 and area 5 disconnected

After the coordinated tuning of FACTS and PSS controllers, local modes, inter-area modes and the exciter modes of oscillations are well damped. The dominant eigenvalues are shown in Figure 5.7 and all the damping ratios are more than 5%. The results show the improvement in damping of overall power oscillations in the system. The detailed controller parameters are given in Appendix 4.1 and the final dominant modes, damping ratios and frequencies are also given in Appendix 4.2.

5.4.4 System performance under different operating condition

In practice, in order to achieve the robustness of the coordinated tuning, the controller settings should be optimized under different possible operation conditions.

In this study, two tie-lines (line 1-2, line D-8) between area 4 and area 5 are disconnected to verify the performance of the optimized controller setting. The eigenvalues for this condition are also shown in Figure 5.7. In the new operating point, the damping ratio of inter-area mode 1 is improved but the damping ratios of the other three modes of inter-area oscillations are reduced. Although the eigenvalue of inter-area mode 4 moves to the right side significantly, its damping ratio still remains in a sufficient range (>5%). Even if some local modes are also changed, their damping ratios are also favorable.

5.4.5 Non-linear simulation results

In order to illustrate the performance of the coordinated tuning result, a three-phase short circuit of 100 ms duration is simulated at bus A in area 4 in the test system.

For evaluation of the system damping behavior, the corresponding center of power angles (COA) of each area, i.e. δ_{Area3} and δ_{Area4} , as discussed in Chapter 4, are employed.

The simulation results are shown in Figure 5.8 and the results validate the proposed tuning method under large disturbance. Furthermore, it can be seen that the damping behavior is improved significantly.

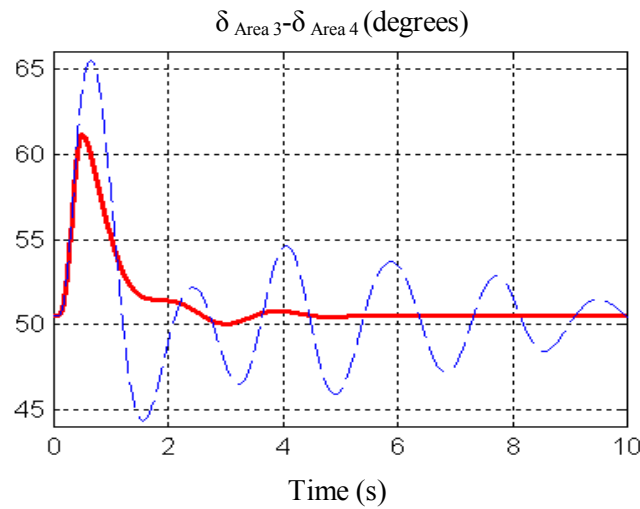


Figure 5.8 Non-linear simulation results

- System behavior before the coordinated tuning
- System behavior after the coordinated tuning

5.5 Conclusion

This chapter presents a method for the simultaneous coordinated tuning of the series FACTS POD controller and PSS controllers in large power systems. This approach is based on the modal analysis and parameter-constrained non-linear optimization technique. Using this approach, the overall system performance is optimized. Simulation results have proved that with the optimized controller settings, the system becomes stable and power system oscillations are well damped. Also, non-linear simulations validate the controller setting under large system disturbance. Moreover, this tuning method is simple and easy to be realized in practical large power systems.

Although only series FACTS device is simulated, the proposed simultaneous coordinated tuning method is a general approach and applicable to other types of FACTS devices.

Chapter 6

Robust FACTS Loop-shaping POD Controller Design in Large Power Systems

6.1 Introduction

This chapter mainly deals with the robust FACTS POD controller design in large power systems. The influence of conventional damping controllers is also considered on the overall system performance. The requirement for the power system damping controllers is to ensure that the oscillations have enough damping ratio under all possible operating conditions. In practice, it is required that the FACTS damping controller should have the ability to perform satisfactorily under a wide range of operating conditions, and in the presence of uncertainties, i.e. disturbances and errors due to monitoring instruments [43].

In this chapter, the robust loop-shaping FACTS damping controller design in large power systems will be discussed in detail. This approach provides a robust controller that performs satisfactorily for a wide range of operating conditions and under certain degree of uncertainties.

6.2 System model and performance criteria

This section presents the fundamental analysis of the feedback control system. In doing so, the feedback control system performance criteria for power system analysis are also characterized.

6.2.1 General concepts of feedback control system

6.2.1.1 General model

For the simplicity of the analysis, feedback controller design concepts and techniques are always developed based on single input single output (SISO) system [5,43]. A block diagram of general SISO feedback control system model is shown in Figure 6.1. In this chapter, all Laplace variables s have been dropped to simplify the notation.

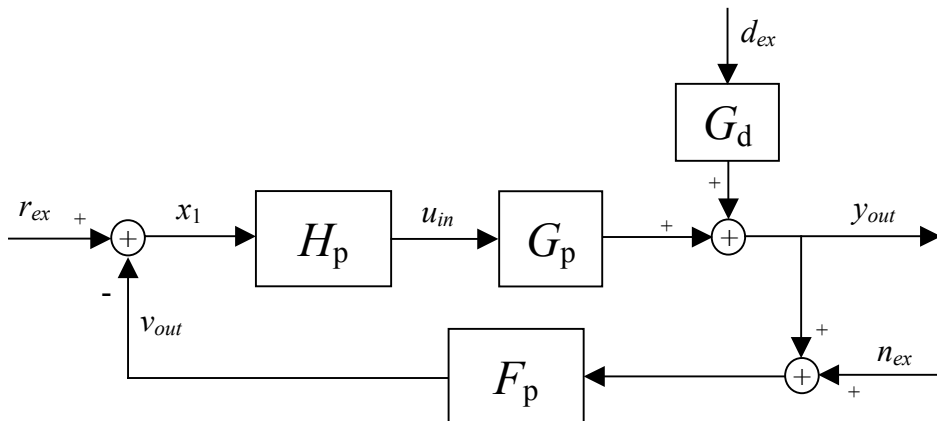


Figure 6.1 General SISO feedback control system model

where

- G_p transfer function of the plant
- H_p transfer function of the feedback controller
- F_p transfer function of the sensor (is concerned as unity in this study)

G_d	transfer function of the output disturbance (is concerned as unity in this study)
u_{in}	actuating signal, plant input
r_{ex}	reference or command input
d_{ex}	external disturbance
n_{ex}	sensor noise
x_1	tracking error
v_{out}	sensor output
y_{out}	plant output and measured signal

Generally, the performance objectives of the feedback controller H_p can be summarized as follows:

- To enable the output y_{out} to track the input r_{ex} following some pre-specified functions
- To minimize the effect of the disturbance d_{ex} , the noise n_{ex} and the plant uncertainty on the outputs y_{out}

6.2.1.2 Loop transfer function and sensitivities

According to the feedback control system model shown in Figure 6.1, the loop transfer function is defined as ($F_p = G_d = 1$):

$$L_p = G_p H_p \quad (6.1)$$

The transfer function from reference input r_{ex} to tracking error x_1 is defined as the sensitivity function:

$$S_s = \frac{1}{1 + L_p} = \frac{1}{1 + G_p H_p} \quad (6.2)$$

The complementary sensitivity function is defined as:

$$T_s = 1 - S_s = \frac{G_p H_p}{1 + G_p H_p} \quad (6.3)$$

6.2.1.3 Loop-shaping

According to the system model shown in Figure 6.1, the objective of the feedback controller H_p is to ensure that the control error e remains small in spite of disturbances d_{ex} and n_{ex} . The control error e is defined as follows [45]:

$$\begin{aligned} e &= y_{out} - r_{ex} \\ &= (1 + L_p)^{-1} \cdot d_{ex} - (1 + L_p)^{-1} \cdot r_{ex} - (1 + L_p)^{-1} L_p \cdot n_{ex} \\ &= S_s \cdot d_{ex} - S_s \cdot r_{ex} - T_s \cdot n_{ex} \end{aligned} \quad (6.4)$$

The control objective is to make $e \approx 0$ and the ideal controller H_p should achieve:

$$e \approx 0 \cdot d_{ex} - 0 \cdot r_{ex} - 0 \cdot n_{ex} \quad (6.5)$$

The first two parts in Equation 6.5 are referred to as disturbance rejection and command tracking and they can be achieved ideally with $S_s \approx 0$, or equivalently $T_s \approx 1$. According to Equation 6.1 and 6.2, this requires that the loop transfer function must be large in magnitude: $L_p \approx \infty$.

The third part of Equation 6.5 represents zero noise transmission and requires that $T_s \approx 0$. This requires that the loop transfer function must be small in magnitude: $L_p \approx 0$.

The above-mentioned two requirements are conflicting and it can be solved using the classical approach in which the magnitude of the loop transfer function, L_p , is shaped [45]. Usually no optimization is involved and the designer aims to obtain $|L_p|$ with desired bandwidth, slopes etc. However, classical loop shaping is difficult to be applied in complex systems. Therefore, in this study, the robust loop-shaping technique will be employed and this issue will be discussed in detail in Section 6.3.

6.2.2 Robust performance criteria

In this section, some basic concepts and criteria for the evaluation of the feedback control system will be considered. The inputs and outputs normalization and power system performance criteria will be discussed in detail.

The main objective of this study is to develop a robust loop-shaping FACTS POD controller to damp power system oscillations. At the same time, other power system controllers, which have influences on the power oscillation damping behavior are also considered. Therefore, in this section, the normalization and system performance criteria are discussed based on the multi-variable feedback control system model.

6.2.2.1 Normalization of inputs and outputs

Before proceeding the robust controller design procedure, the power system inputs and outputs must be normalized. The purpose of this procedure is to normalize the physical inputs and outputs to the range zero to one. In this study, the bus voltages, generator field voltages, generator frequencies, and load modulations are normalized according to the following criteria:

- The change in bus voltage and generator field voltage of $\pm 5\%$ around the nominal voltage will be converted into the range of $[0,1]$.
- The change in generator frequency of ± 0.05 Hz around 50Hz will be normalized to the range of $[0,1]$.
- The system load modulation of ± 5 MW will be converted into the range of $[0,1]$.

6.2.2.2 Power system performance under uncertainties

Power system robust stability and robust performance are defined in terms of a plant model with the controller and a model of the uncertainties placed in additional loops around the plant [5,44]. The general power system feedback control model with uncertainty is shown in Figure 6.2.

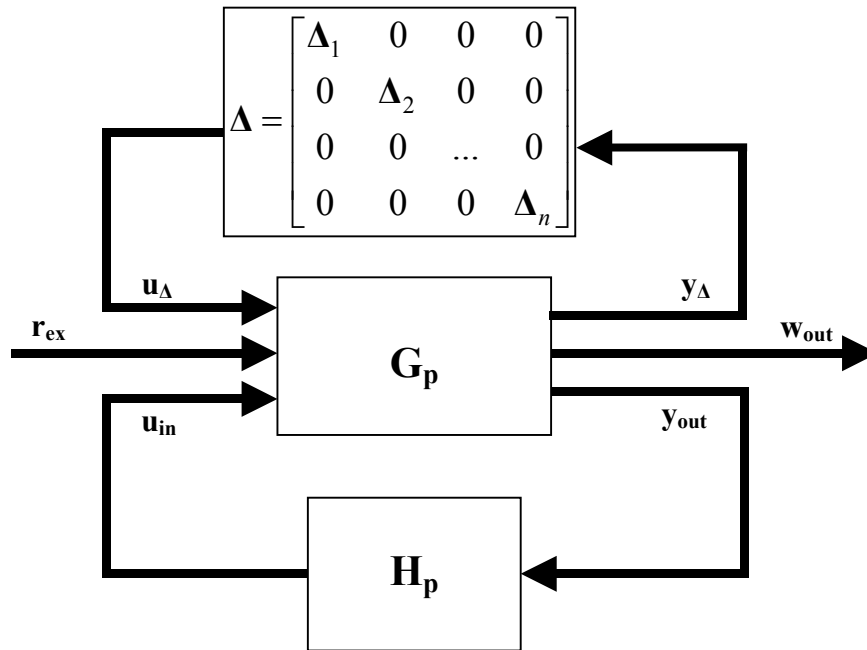


Figure 6.2 General feedback control system with uncertainty

where

\mathbf{G}_p : Plant transfer functions

\mathbf{H}_p : Controller transfer functions

Δ : Disturbance transfer functions

\mathbf{y}_{out} : Outputs from the plant to the controller

\mathbf{w}_{out} : Normalized outputs which may be used to specify system performance

\mathbf{u}_{in} : Inputs from the controller to the plant

\mathbf{r}_{ex} : Normalized reference inputs

\mathbf{u}_{Δ} : Inputs to the system from uncertainties

\mathbf{y}_{Δ} : Outputs of the system, which drive the uncertainty dynamics

In this study, the \mathbf{H}_p consists of FACTS POD controller and exciters and Δ represents the disturbance transfer functions that define the uncertainties in the power system. Particularly, only the structured uncertainty, which means the uncertainty transfer function is structured with a block-diagonal structure, is considered in this study [49]. The structured uncertainty transfer function of Δ is also illustrated in Figure 6.2.

The plant transfer function \mathbf{G}_p is partitioned and can be expressed as follows [5,45]:

$$\begin{bmatrix} \mathbf{y}_\Delta \\ \mathbf{w}_{out} \\ \mathbf{y}_{out} \end{bmatrix} = \begin{bmatrix} \mathbf{G}_{p11} & \mathbf{G}_{p12} & \mathbf{G}_{p13} \\ \mathbf{G}_{p21} & \mathbf{G}_{p22} & \mathbf{G}_{p23} \\ \mathbf{G}_{p31} & \mathbf{G}_{p32} & \mathbf{G}_{p33} \end{bmatrix} \cdot \begin{bmatrix} \mathbf{u}_\Delta \\ \mathbf{r}_{ex} \\ \mathbf{u}_{in} \end{bmatrix} = \mathbf{G}_p \cdot \begin{bmatrix} \mathbf{u}_\Delta \\ \mathbf{r}_{ex} \\ \mathbf{u}_{in} \end{bmatrix} \quad (6.6)$$

By eliminating \mathbf{y}_{out} and \mathbf{u}_{in} through using $\mathbf{u}_{in} = \mathbf{H}_p \cdot \mathbf{y}_{out}$ [5]:

$$\begin{bmatrix} \mathbf{y}_\Delta \\ \mathbf{w}_{out} \end{bmatrix} = \begin{bmatrix} \mathbf{N}_{11} & \mathbf{N}_{12} \\ \mathbf{N}_{21} & \mathbf{N}_{22} \end{bmatrix} \cdot \begin{bmatrix} \mathbf{u}_\Delta \\ \mathbf{r}_{ex} \end{bmatrix} = \mathbf{N}_c \cdot \begin{bmatrix} \mathbf{u}_\Delta \\ \mathbf{r}_{ex} \end{bmatrix} \quad (6.7)$$

where

$$\begin{aligned} \mathbf{N}_c &= \begin{bmatrix} \mathbf{N}_{11} & \mathbf{N}_{12} \\ \mathbf{N}_{21} & \mathbf{N}_{22} \end{bmatrix} \\ &= \begin{bmatrix} \mathbf{G}_{p11} & \mathbf{G}_{p12} \\ \mathbf{G}_{p21} & \mathbf{G}_{p22} \end{bmatrix} + \begin{bmatrix} \mathbf{G}_{p13} \\ \mathbf{G}_{p23} \end{bmatrix} \cdot (\mathbf{H}_p \cdot (\mathbf{I} - \mathbf{G}_{p33} \mathbf{H}_p)^{-1}) \cdot [\mathbf{G}_{p31} \quad \mathbf{G}_{p32}] \end{aligned} \quad (6.8)$$

The controlled plant with uncertainty loop is shown in Figure 6.3.

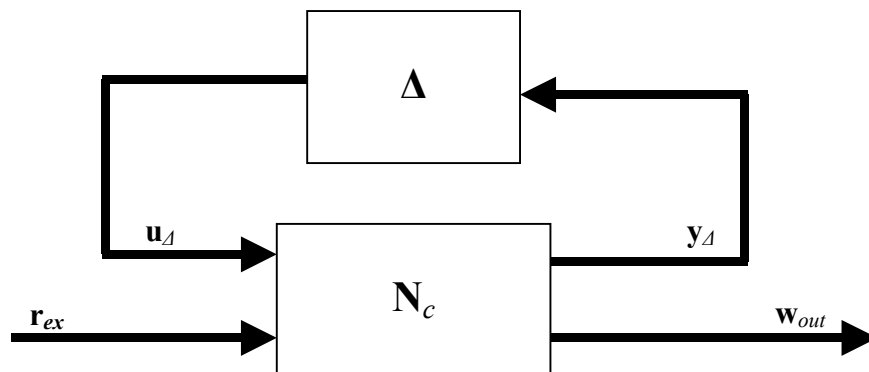


Figure 6.3 Controlled plant with uncertainty loop

By eliminating \mathbf{u}_d and \mathbf{y}_d through using $\mathbf{u}_d = \Delta \cdot \mathbf{y}_d$, the relationship between \mathbf{r}_{ex} and \mathbf{w}_{out} can be expressed as [5]:

$$\mathbf{w}_{out} = \left[\mathbf{N}_{22} + \mathbf{N}_{21} \cdot \Delta \cdot (\mathbf{I} - \mathbf{N}_{11} \Delta)^{-1} \cdot \mathbf{N}_{12} \right] \cdot \mathbf{r}_{ex} = \mathbf{F}_w \cdot \mathbf{r}_{ex} \quad (6.9)$$

where

\mathbf{N}_{11} is the transfer function for the system closed with uncertainties

\mathbf{N}_{22} is the transfer function between \mathbf{r}_{ex} and \mathbf{w}_{out} when $\Delta = 0$

\mathbf{F}_w is the transfer function between \mathbf{r}_{ex} and \mathbf{w}_{out} (system closed with uncertainties and controllers)

\mathbf{I} represents the identity matrix

In this study, the following criteria are employed to characterize the performance of the power system: nominal stability, nominal performance, robust stability and robust performance.

Nominal stability criterion:

The nominal stability criterion requires the stability of \mathbf{N}_c . As defined in Equation 6.8, \mathbf{N}_c is the transfer function of the controlled plant.

In power system analysis, this criterion means that the system with nominal controls, i.e. exciters, governors, PSSs and the conventional FACTS POD controller, has eigenvalues with only negative real parts and it should be stable.

Nominal performance criterion:

This criterion requires nominal stability together with:

$$\|\mathbf{N}_{22}\|_{\infty} < 1 \quad (6.10)$$

where $\|\cdot\|_{\infty}$ represents the H_{∞} norm of the transfer function. This norm is calculated using the maximum singular value of the transfer function over all researched frequencies [43,45].

In general, in power system analysis, nominal performance can be measured by the following three criteria [5]:

- 1 Its ability to recover from specified design faults and other large disturbances
- 2 Its ability to maintain an acceptable voltage profile under load changes
- 3 Its ability to maintain an acceptable system frequency under load changes

The first requirement is based on the non-linear transient characteristics of the power system and therefore, it cannot be considered in the linear system analysis discussed in this chapter. The second requirement concerns the generator automatic voltage control and the third is related to the effectiveness of generator speed governors [5].

In this study, the 16-machine system discussed in Chapter 3 is simulated and the last two issues are considered. An active load modulation at Bus 50 is simulated to verify the nominal performance criteria. The block diagram for the evaluation of nominal performance is shown in Figure 6.4.

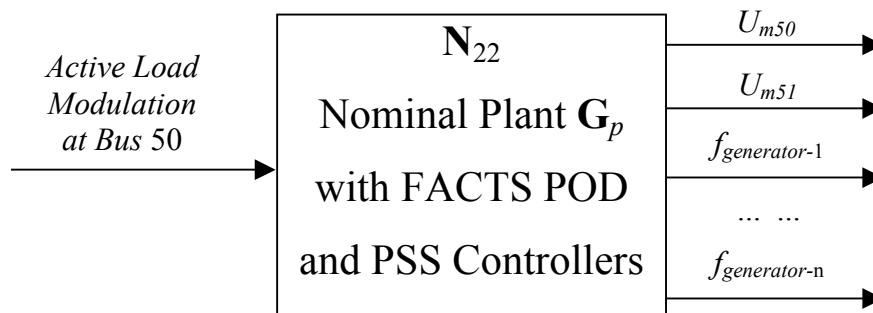


Figure 6.4 Block diagram for the evaluation of nominal performance: N_{22}

where N_{22} represents the power system with nominal controllers, i.e. conventional FACTS POD controller, PSS controllers, exciters and governors. The tie-bus voltages (U_{m50}, U_{m51}) and generator frequencies ($f_{generator-1} \sim f_{generator-n}$) are normalized outputs. The simulation result will be illustrated in Section 6.4.2 in detail.

Robust Stability criterion:

This criterion requires nominal stability together with the stability of \mathbf{F}_w . As shown in Equation 6.9, the only source of instability is the feedback term $(\mathbf{I} - \mathbf{N}_{11}\Delta)^{-1}$. The feedback system is robust stable to the uncertainties $\|\Delta\|_\infty \leq 1$ when [5,43,45]:

$$\|\mathbf{N}_{11}\|_\infty < 1 \quad (6.11)$$

where \mathbf{N}_{11} represents the transfer function from \mathbf{u}_Δ to \mathbf{y}_Δ .

The definition of \mathbf{N}_{11} will be discussed in detail in Section 6.4.4.

Robust Performance criterion:

This criterion requires robust stability together with [5,43,45]:

$$\|\mathbf{F}_w\|_\infty < 1 \quad (6.12)$$

As shown in Equation 6.9, \mathbf{F}_w is the transfer function between \mathbf{r}_{ex} and \mathbf{w}_{out} when the system closed with controls and uncertainties with $\|\Delta\|_\infty \leq 1$. In this study, all the exciters and the robust FACTS POD controllers are considered for the evaluation of the robust performance criterion.

6.3 FACTS robust loop-shaping POD controller design

There are many methods for the design of feedback controllers to provide robustness under system uncertainties. In this section, the robust loop-shaping FACTS damping

controller design is considered. Furthermore, the influences of conventional damping controllers on the system performance are also considered.

Considering coprime factor uncertainties, the FACTS robust loop-shaping controller is developed by employing the modern H_∞ robust controller design approach and the design procedure is given as follows:

- 1 Model reduction of the original power system
- 2 Loop-shaping of the reduced power system model
- 3 Robust loop-shaping FACTS POD controller design

6.3.1 Model reduction

In order to approximate the original high-order plant with a lower order state-space representation, model reduction is required. Particularly, for the design of robust controllers in large power systems, the necessity of model reduction arises in several places [45]:

- The purpose of power system robust controller design is to meet certain specifications, namely to damp certain modes of oscillations. Therefore, It is desirable to simplify the best available model with regards to the purpose to which the model is to be used.
- By employing modern H_∞ control method for which the complexity of the control law is not explicitly constrained, the order of the resultant controller is likely to be considerably greater than is truly needed [5, 53-54]. This high-order control may be too complex with regard to practical implementation and therefore, the model reduction is necessary.

A good model reduction algorithm must be both numerically robust and be able to address the closed-loop robustness issues [48-49]. In power system robust controller design, the proper model reduction can sometimes significantly reduce the controller order with little change in system performance [48-49,54]. As shown in Figure 6.5, different routines can be applied in realizing the model reduction [53]:

- Model reduction of the original high-order system model prior to controller design
- Reduction of the controller after the high-order controller design procedure.
- A combination of the above two routines.

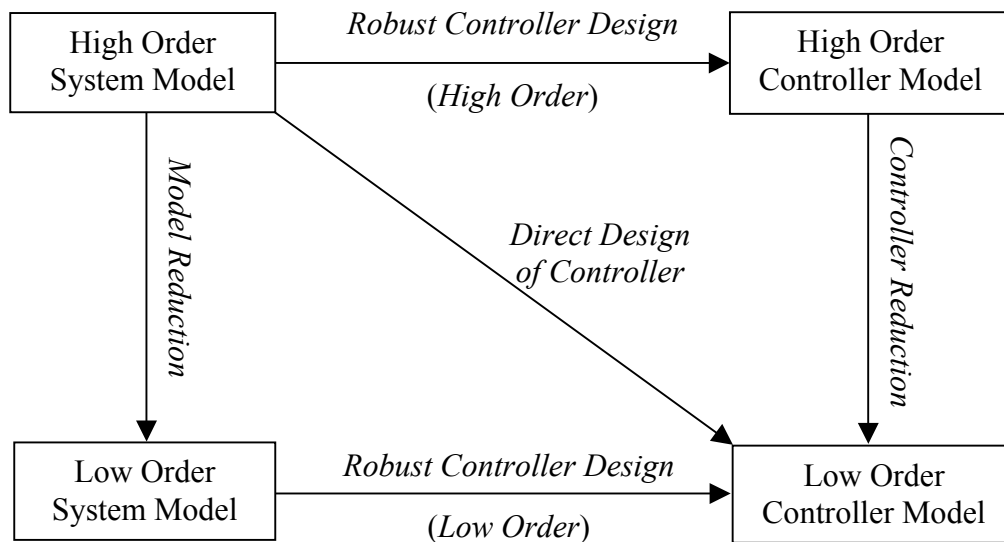


Figure 6.5 Different routines of model reduction

In this research, the model reduction is achieved as the following procedure:

- Firstly, the reduction of the original power system model is proceeded.
- Then, after the FACTS robust loop-shaping controller design, controller reduction is also applied.

The reduction of the original power system model is performed by means of balanced residue method [49]. Using this approach, all modes of interest (inter-area modes) can be preserved. Particularly in this study, the reduced system model has a high order (as shown in Section 6.4.3). After the H_∞ robust loop-shaping controller design procedure, the least order of robust loop-shaping controller must be equal to the order of the reduced system model. Therefore, the controller reduction is necessary. The balanced

truncation algorithm is applied because of its suitability for the controller reduction in feedback systems [49].

6.3.2 FACTS loop-shaping controller design

The power system with FACTS robust loop-shaping controller is shown in Figure 6.6, where G_p represents the reduced-order power system model and H_p represents the FACTS robust loop-shaping POD controller respectively. The controller design procedure is based on the method presented by Glover and McFarlane [47,54].

In order to optimize closed loop performance requirements, pre- and post-compensation of the plant model G_p should be first carried out. The objective of this process is to shape the open loop singular values of G_p prior to the robust controller design procedure.

$$G_{ps} = W_{post} \cdot G_p \cdot W_{pre} \quad (6.13)$$

where G_{ps} represents the shaped plant. W_{pre} and W_{post} are pre- and post-compensation function respectively. Usually, W_{post} is chosen as a constant and W_{pre} contains dynamic shaping. The closed loop system is shown in Figure 6.6.

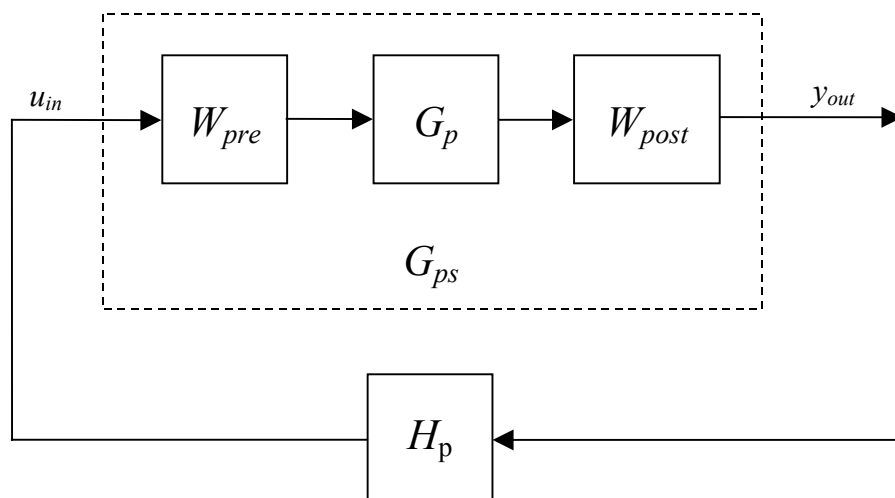


Figure 6.6 Loop-shaping of the plant

6.3.3 Robust loop-shaping design using coprime factors

The above-mentioned shaped plant G_{ps} with feedback control and uncertainties can be expressed in form of coprime factors of the plant shown in Figure 6.7 [5,47,54].

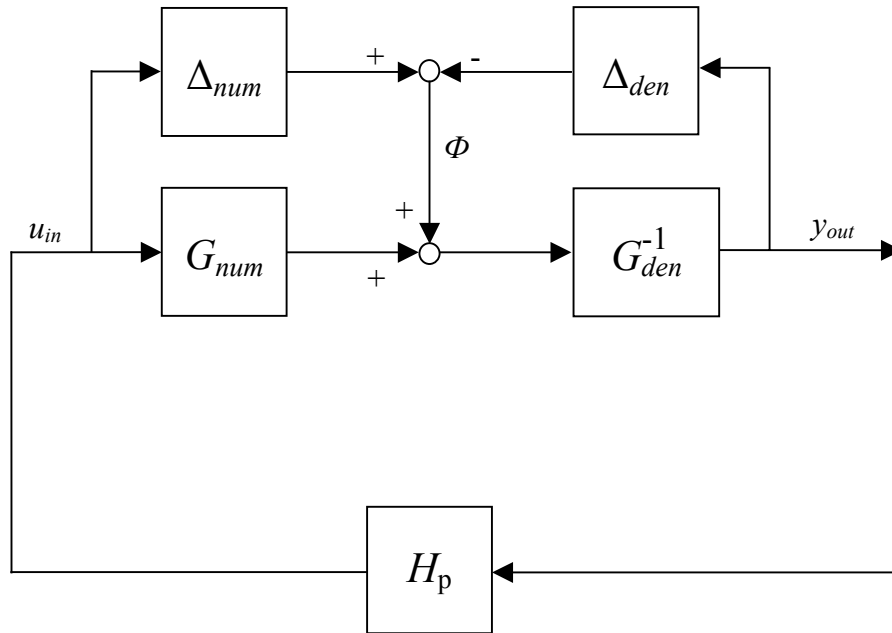


Figure 6.7 Plant with controller and coprime factor uncertainty

where H_p represents the FACTS robust loop-shaping damping controller that stabilizes the system G_{ps} .

In terms of the coprime factors:

$$G_{ps} = G_{den}^{-1} G_{num} \quad (6.14)$$

where the transfer function G_{num} and G_{den}^{-1} are assumed to be a stable left coprime factorization of G_{ps} . Both are stable and have no common zeros in the positive half s -plane. In this study, the normalized left coprime factors are computed using *Matlab μ -Analysis and Synthesis Toolbox* [49].

The perturbed plant transfer function of G_{ps} is

$$G'_{ps} = (G_{den} + \Delta_{den})^{-1} (G_{num} + \Delta_{num}) \quad (6.15)$$

where $\| [\Delta_{den} \quad \Delta_{num}] \|_{\infty} < \varepsilon$ ($\varepsilon \leq 1$) defines the level of uncertainty.

The transfer function M_p from $\begin{bmatrix} u_{in} \\ y_{out} \end{bmatrix}$ to Φ can be expressed as:

$$M_p = \begin{bmatrix} H_p (1 - G_{den}^{-1} G_{num} H_p)^{-1} G_{den}^{-1} \\ (1 - G_{den}^{-1} G_{num} H_p)^{-1} G_{den}^{-1} \end{bmatrix} = \begin{bmatrix} H_p (1 - G_{ps} H_p)^{-1} G_{den}^{-1} \\ (1 - G_{ps} H_p)^{-1} G_{den}^{-1} \end{bmatrix} \quad (6.16)$$

The stability property of the system shown in Figure 6.7 is robust if and only if the nominal feedback system is stable and

$$\gamma_p = \|M_p\|_{\infty} \leq \frac{1}{\varepsilon_p} \quad (6.17)$$

The lowest achievable value of γ_p and the corresponding maximum stability margin ε_p are given by Glover and McFarlane as:

$$\gamma_{p \min} = \varepsilon_{p \max}^{-1} = \left\{ 1 - \| [G_{den} \quad G_{num}] \|_H^2 \right\}^{-\frac{1}{2}} = (1 + \rho(\mathbf{XZ}))^{\frac{1}{2}} \quad (6.18)$$

where $\| \cdot \|_H$ denotes Hankel norm and ρ represents the spectral radius (maximum eigenvalue).

For a minimal state-space realization $(\mathbf{A}_{ps}, \mathbf{B}_{ps}, \mathbf{C}_{ps}, \mathbf{D}_{ps})$ of G_{ps} , \mathbf{Z} is the unique positive definite solution to the algebraic equation:

$$\begin{aligned} & \left(\mathbf{A}_{ps} - \mathbf{B}_{ps} \mathbf{S}^{-1} \mathbf{D}_{ps}^T \mathbf{C}_{ps} \right) \cdot \mathbf{Z} + \mathbf{Z} \cdot \left(\mathbf{A}_{ps} - \mathbf{B}_{ps} \mathbf{S}^{-1} \mathbf{D}_{ps}^T \mathbf{C}_{ps} \right)^T \\ & - \mathbf{Z} \mathbf{C}_{ps}^T \mathbf{R}^{-1} \mathbf{C}_{ps} \mathbf{Z} + \mathbf{B}_{ps} \mathbf{S}^{-1} \mathbf{B}_{ps}^T = 0 \end{aligned} \quad (6.19)$$

where

$$\begin{aligned} \mathbf{S} &= \mathbf{I} + \mathbf{D}_{ps}^T \mathbf{D}_{ps} \\ \mathbf{R} &= \mathbf{I} + \mathbf{D}_{ps} \mathbf{D}_{ps}^T \end{aligned} \quad (6.20)$$

and \mathbf{X} is the unique positive definite solution of the following algebraic equation:

$$\begin{aligned} & \left(\mathbf{A}_{ps} - \mathbf{B}_{ps} \mathbf{S}^{-1} \mathbf{D}_{ps}^T \mathbf{C}_{ps} \right)^T \cdot \mathbf{X} + \mathbf{X} \cdot \left(\mathbf{A}_{ps} - \mathbf{B}_{ps} \mathbf{S}^{-1} \mathbf{D}_{ps}^T \mathbf{C}_{ps} \right) \\ & - \mathbf{X} \mathbf{B}_{ps} \mathbf{S}^{-1} \mathbf{B}_{ps}^T \mathbf{X} + \mathbf{C}_{ps}^T \mathbf{R}^{-1} \mathbf{C}_{ps} = 0 \end{aligned} \quad (6.21)$$

A controller H_p which guarantees that:

$$\|M_p\|_{\infty} = \left\| \begin{bmatrix} H_p (1 - G_{ps} H_p)^{-1} G_{den}^{-1} \\ (1 - G_{ps} H_p)^{-1} G_{den}^{-1} \end{bmatrix} \right\|_{\infty} \leq \gamma_p \quad (6.22)$$

for a specified $\gamma_p > \gamma_{min}$ is given by state-space realization:

$$\begin{aligned} \mathbf{H}_p &= \left[\begin{array}{c|c} \mathbf{A}_{ps} + \mathbf{B}_{ps} \mathbf{H}_F + \gamma_p^2 (\mathbf{H}_L^T)^{-1} \mathbf{Z} \mathbf{C}_{ps}^T (\mathbf{C}_{ps} + \mathbf{D}_{ps} \mathbf{H}_F) & \gamma_p^2 (\mathbf{H}_L^T)^{-1} \mathbf{Z} \mathbf{C}_{ps}^T \\ \hline \mathbf{B}_{ps}^T \mathbf{X} & -\mathbf{D}_{ps}^T \end{array} \right] \\ \mathbf{H}_F &= -\mathbf{S}^{-1} (\mathbf{D}_{ps}^T \mathbf{C}_{ps} + \mathbf{B}_{ps}^T \mathbf{X}) \\ \mathbf{H}_L &= (1 - \gamma_p^2) \mathbf{I} + \mathbf{X} \mathbf{Z} \end{aligned} \quad (6.23)$$

Once the controller H_p is obtained, as can be seen from Figure 6.6, the loop-shaping controller H_{LS} for the reduced plant G_p can be expressed as:

$$H_{LS} = W_{pre} H_p W_{post} \quad (6.24)$$

In this study, the above-mentioned modern robust loop-shaping method is employed for the FACTS damping controller design. This method exploits the advantage of conventional loop-shaping and modern H_∞ robust controller design techniques. Furthermore, the FACTS robust loop-shaping damping controller is robust to uncertainties in a plant coprime factors and therefore, the influences of the other power system controllers can also be considered. The FACTS robust loop-shaping damping controller design is presented in Section 6.4 in detail.

6.4 Simulation results

The 16-machine system discussed in Chapter 3 is used in this section. A series FACTS device (TCSC) is located on the tie-line between area 3 and area 4.

To illustrate the performance of the FACTS controller, the PSSs are used only for the local modes of oscillation damping control and FACTS device serves as the inter-area oscillation damping controller.

The FACTS robust loop-shaping controller design and its robustness verification are performed as follows:

- First, the nominal stability and nominal performance of the power system are verified in Section 6.4.1 and 6.4.2.
- Then the FACTS robust loop-shaping controller design is proceeded in Section 6.4.3.
- In Section 6.4.4, the performance of the power system with FACTS robust loop-shaping controllers and exciters is verified under robust stability and robust performance criteria.
- Furthermore, in Section 6.4.5, non-linear simulation is also performed to validate the controller performance under large disturbances.

6.4.1 Nominal stability

This issue is the basic requirement for the robust controller design. As mentioned in Section 6.2.2, the nominal stability means the power system with the nominal control

has eigenvalues with only negative real parts and therefore the system is stable. The dominant eigenvalues of the power system with PSS controllers are shown in Figure 6.8.

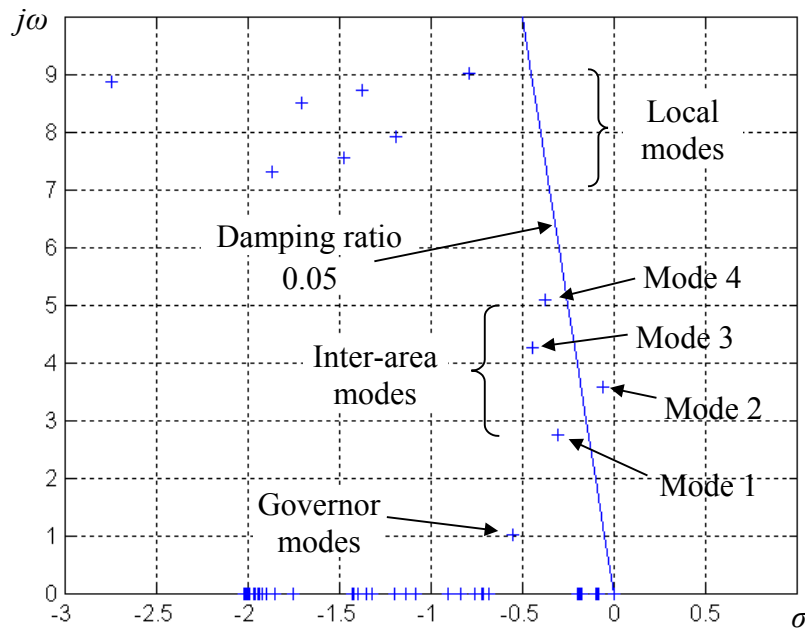


Figure 6.8 The dominant eigenvalues of the power system

It is obvious, with the conventional PSS controllers, the power system can be stable. However, the damping ratio of the inter-area mode 2 is not satisfactory. As discussed in Chapter 2, the damping behavior of the inter-area modes of oscillations can be modified using the FACTS controller:

$$H_{TCSC} = K_{FACTS} \cdot 100 \cdot \frac{5.0s}{1 + 5.0s} \cdot \frac{1}{1 + 0.05s} \cdot \left[\frac{1 + 0.1s}{1 + 0.5s} \right]^2 \quad (6.25)$$

The root-locus when K_{FACTS} varies from 0 to 400 is shown in Figure 6.9. As shown in the root-locus, FACTS controller has significant effects on the inter-area modes and exciter modes. To guarantee their damping ratios and avoid the adverse interactions between inter-area modes and exciter modes, the gain of FACTS controller K_{FACTS} is set to 50.

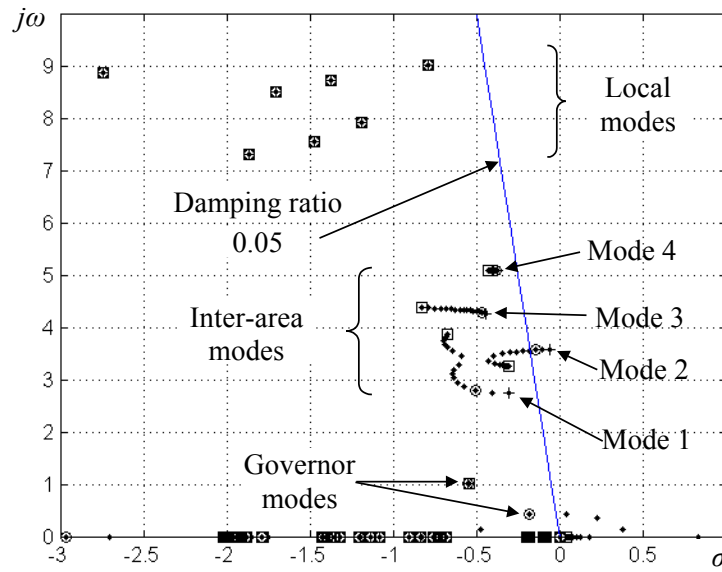


Figure 6.9 Root-locus of the FACTS POD controller when K_{FACTS} vary from 0 to 400

+ : $K_{FACTS} = 0$ o : $K_{FACTS} = 50$ \square : $K_{FACTS} = 400$

6.4.2 Nominal performance

To verify the nominal performance criterion discussed in Section 6.2.2.2, an active load modulation at bus 50 is considered.

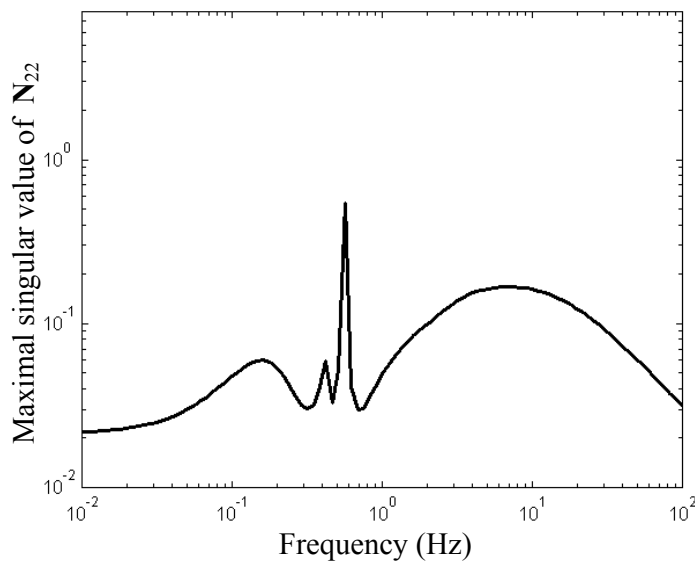


Figure 6.10 Maximum singular value plot of N_{22} of tie bus voltage magnitude and generator frequencies to active load modulation

The response of the tie-line bus (Bus 50 and 51) voltage magnitudes and frequencies of all the generators to the active load modulation is shown in Figure 6.10. Since the maximum singular value of \mathbf{N}_{22} is significantly less than unity, the nominal performance criterion is satisfied.

6.4.3 FACTS robust loop-shaping controller design

Since the requirements of nominal stability and nominal performance are satisfied, robust loop-shaping controller design can proceed. In this section, the FACTS robust loop-shaping POD controller design procedure shown in Section 6.3 is employed: system model reduction, robust loop-shaping controller design and controller reduction.

6.4.3.1 System model reduction

Using the balanced residue approach, the system order is reduced from 204 to 16.

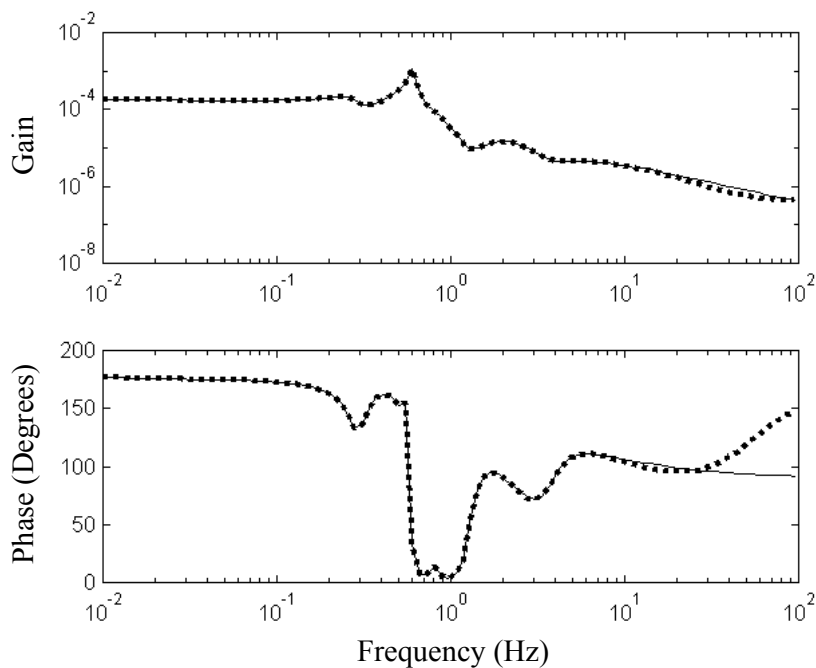


Figure 6.11 Bode diagram of the original and the reduced order system

⋯ : Original system model (Order=204)

— : Reduced system model (Order=16)

In the model reduction process, singular value Bode diagram provides the information needed to assure a given reduced model is sufficiently accurate within a prescribed bandwidth [48,49]. In this simulation, since robust loop-shaping controller is employed, the traditional Bode diagram is used to verify the performance of the model reduction. The Bode diagram shown in Figure 6.11 indicates the accuracy of the reduced model for low frequencies, which includes the inter-area oscillation frequencies (0.1~1Hz).

6.4.3.2 FACTS robust loop-shaping controller design

In this study, the FACTS robust loop-shaping controller H_{LS} is an additional controller to the conventional FACTS POD controller H_{TCSC} . The block diagram of the perturbed power system model with the FACTS robust POD controller is shown in Figure 6.12.

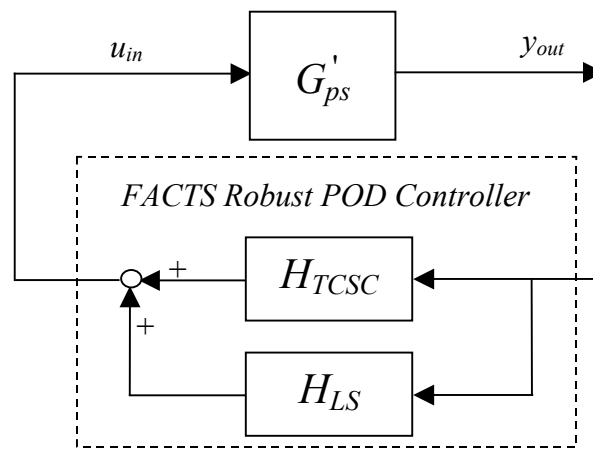


Figure 6.12 Power system with FACTS robust POD controller

where

H_{TCSC} represent the conventional FACTS POD controller

H_{LS} represent the FACTS robust loop-shaping controller

G'_{ps} represent the perturbed plant transfer function defined in Equation 6.15

Robust loop-shaping controller design and controller reduction

Using the algorithm discussed in Section 6.3, the robust loop-shaping controller design method calculates the amount of the increase in the uncertainty in the coprime factors before the system becomes unstable.

In this simulation, the post-compensation function W_{post} is chosen as a constant (unit transfer function). The pre-compensation function W_{pre} , which influences the dynamic shaping, is chosen according to the method given in [45] as:

$$W_{pre} = \frac{4s}{3s^2 + 2s + 1} \quad (6.26)$$

After the robust loop-shaping design procedure, the original loop-shaping controller with an order of 21 is obtained. Since this high-order controller is not practical for real power system control, the controller reduction is necessary. Using the balanced truncation controller reduction, the following reduced-order robust loop-shaping controller H_{LS_Red} is obtained:

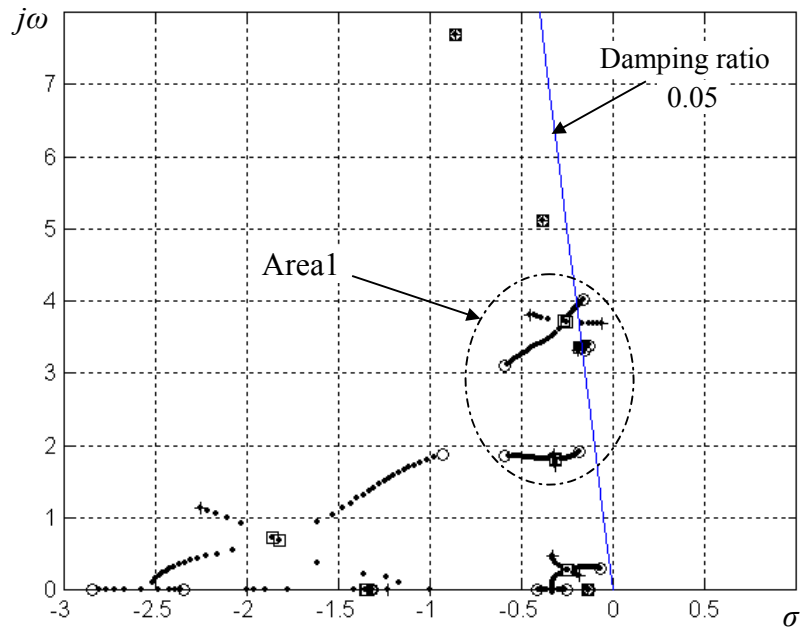
$$H_{LS_Red} = \frac{0.08s^5 + 0.064s^4 - 3.69s^3 - 1.91s^2 - 6.57s + 1.36}{s^6 + 2.4s^5 + 20.04s^4 + 32.55s^3 + 67.7s^2 - 54.4s + 10.4} \quad (6.27)$$

Performance of the robust loop-shaping controller

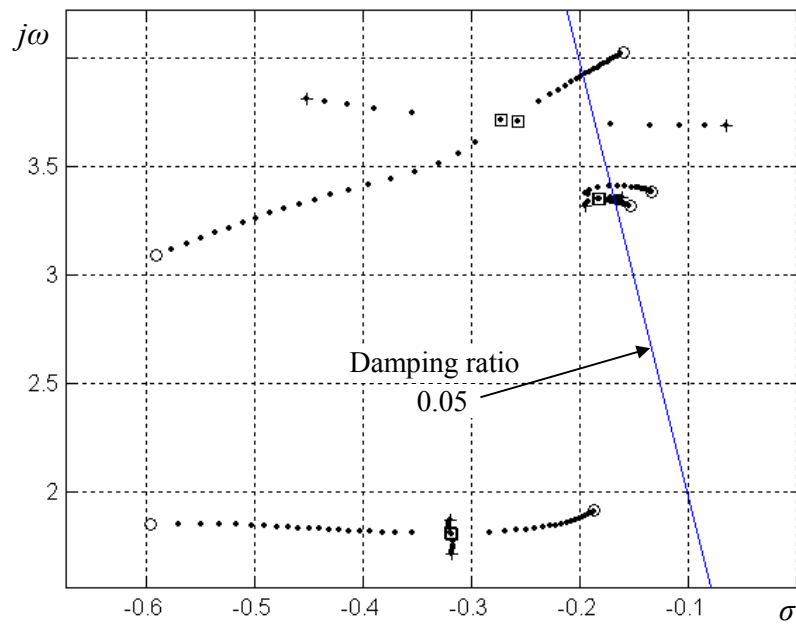
As shown in Equation 6.27, the gain of the FACTS robust loop-shaping controller is normalized to unity. In order to verify the performance of the robust loop-shaping controller with the variation of the controller gain, an artificial gain K_{LS} for the controller H_{LS_Red} is applied:

$$H_p = K_{LS} \cdot H_{LS_Red} \quad (6.28)$$

The root-locus when the gain of the robust loop-shaping controller K_{LS} varies from 0 to 5 is given in Figure 6.13.



(a) Root-locus



(b) Root-locus of Area 1 in Figure 6.13 (a)

Figure 6.13 Root-locus of the FACTS robust loop-shaping controller when controller gain K_{LS} varies from 0 to 5

+: $K_{LS} = 0$ □: $K_{LS} = 1$ ○: $K_{LS} = 5$

As can be seen from Figure 6.13, the FACTS robust loop-shaping controller with the unity gain ($K_{LS}=1$) has the best performance. Moreover, after the robust loop-shaping, the system becomes stable and the damping ratios are also favorable.

A successful design should have a stability margin greater than 25% [5,51]. In this simulation, the stability margin is achieved as 67.52% ($\gamma_{\min}=1.4180$). It is clear that the robust loop-shaping design is successful.

By employing the robust loop-shaping technology, the power system with FACTS POD controller is robust under coprime uncertainties. Since there are also other controllers in power system that have effects on the oscillation damping behavior, in Sections 6.4.4, the robust stability and robust performance criteria for the power system with exciters and FACTS POD controller are examined using the multiplicative output uncertainty.

6.4.4 Robust stability and robust performance

In this section, the multiplicative output uncertainty [44,49,54] is considered for the validation of the robust stability and robust performance criteria. The block diagram of the multiplicative output uncertainty model is shown in Figure 6.14.

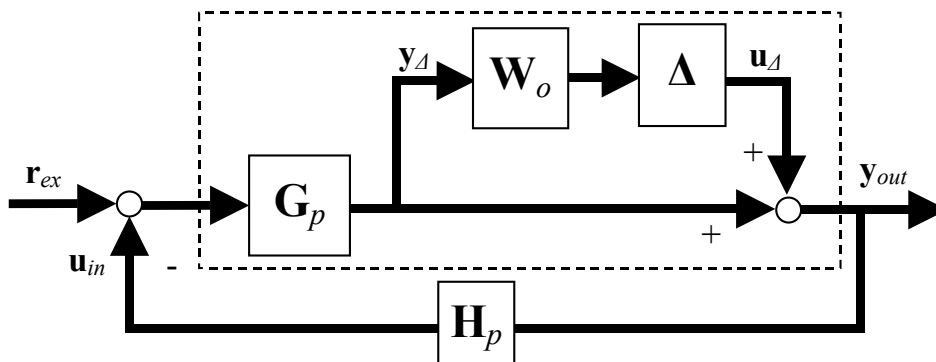


Figure 6.14 Feedback control system with multiplicative output uncertainty

where

\mathbf{H}_p represent FACTS robust POD controller and all the exciters

- \mathbf{r}_{ex} represent the reference inputs to the controllers
- \mathbf{W}_o represent output weighting functions which describe the uncertainties with frequency

According to the theory shown in [49,54] and Equation 6.9, the controller \mathbf{H}_p provide robust stability under the uncertainty of $\|\Delta\|_\infty \leq 1$ if:

$$\|\mathbf{N}_{11}\|_\infty = \|\mathbf{W}_o \mathbf{T}_C\|_\infty < 1 \quad (6.29)$$

where \mathbf{T}_C is the complementary sensitivity of the controlled plant:

$$\mathbf{T}_C = \frac{\mathbf{H}_p \mathbf{G}_p}{\mathbf{I} + \mathbf{H}_p \mathbf{G}_p} \quad (6.30)$$

and \mathbf{W}_o contains the weighting functions for the exciters and FACTS POD controller. The output weighting functions for the FACTS controller and for each exciter are given in Equations 6.31 and 6.32 respectively:

$$W_{o_FACTS}(s) = 0.1 \cdot \frac{1 + 1.45s}{1 + 0.00145s} \quad (6.31)$$

$$W_{o_exciter}(s) = 0.01 \cdot \frac{1 + 1.6s}{1 + 0.0016s} \quad (6.32)$$

Both output weighting functions are specified as a high pass filter. For the exciter, the uncertainty is 0.01 at low frequencies and increases to 10 at high frequencies. For the FACTS, the uncertainty is 0.1 at low frequencies and increases to 100 at high frequencies.

The maximum singular value of the transfer function corresponding to \mathbf{N}_{11} of Equation 6.9 is shown in Figure 6.15. Since all the maximal singular values of \mathbf{N}_{11} are less than unity at all frequencies, the system is robust stable with $\|\Delta\|_\infty \leq 1$.

The robust performance criteria can be proved using the closed loop transfer function of \mathbf{F}_w . In this study, \mathbf{F}_w can be expressed as following equation:

$$\mathbf{F}_w = \frac{\mathbf{G}_p(\mathbf{I} + \mathbf{W}_0\Delta)}{\mathbf{I} + \mathbf{H}_p\mathbf{G}_p(\mathbf{I} + \mathbf{W}_0\Delta)} \quad (6.33)$$

The maximum singular value of the transfer function \mathbf{F}_w is also shown in Figure 6.15. According to the robust performance criterion, since all the maximal singular values of \mathbf{F}_w are less than unity at all frequencies, the robust performance is favorable with $\|\Delta\|_\infty \leq 1$.

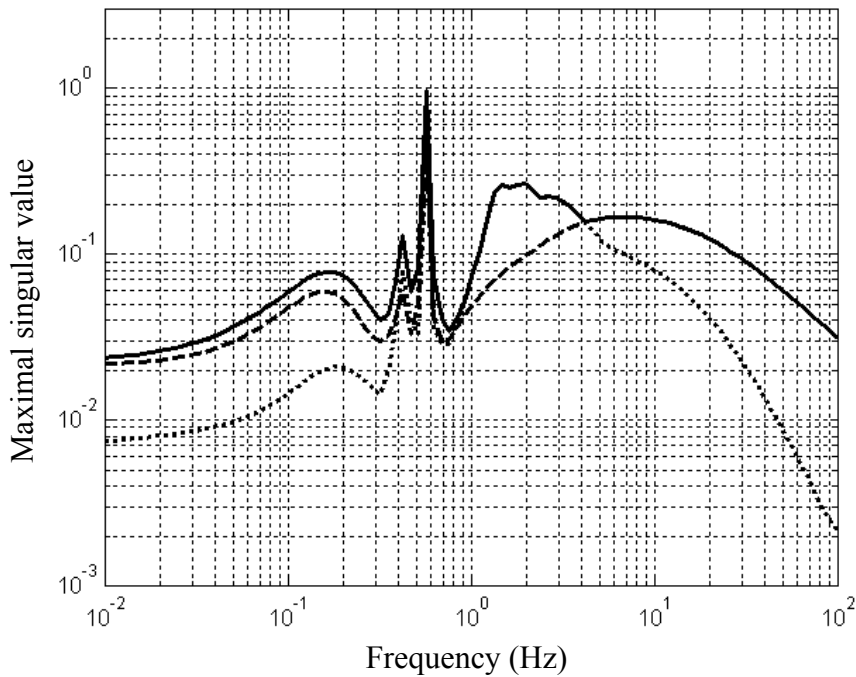


Figure 6.15 System performances

- : Nominal Performance
- : Robust stability with structured uncertainty (\mathbf{N}_{11})
- : Robust performance with structured uncertainty (\mathbf{F}_w)

6.4.5 Non-linear simulation results

To verify the performance of the FACTS robust POD controller under large disturbances, a short circuit of 100 ms duration at bus 50 is considered. The corresponding center of power angles of area 3 and area 4 are applied to evaluate the performance of the proposed controller. As shown in Figure 6.16, it is clear that using the proposed controller, the transient behavior of the power system is satisfactory.

The power system with only traditional FACTS POD controller can achieve almost similar transient behavior as the FACTS robust POD controller. However, the stability margin provided by the FACTS robust POD controller is achieved as 67.52% and it is much more than the conventional FACTS POD controller, which is only 31.55%.

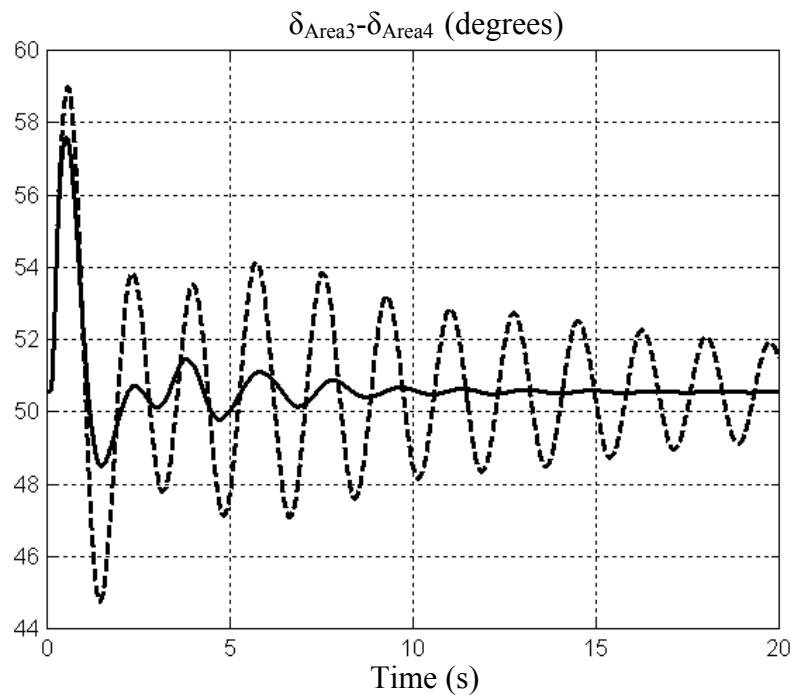


Figure 6.16 Non-linear simulation results

- : Without FACTS POD controller
- : With robust FACTS POD controller

6.5 Summary

This chapter presents the FACTS robust loop-shaping POD controller design scheme in large power systems. By applying the model reduction and modern robust loop-shaping control technique, the FACTS robust loop-shaping controller is realized. This robust loop-shaping controller exploits the advantages of both conventional loop-shaping and modern H_∞ robust control techniques. Moreover, it is a decentralized approach and practical for FACTS controller design in real large power systems.

The performance of the proposed control scheme has fulfilled the robust stability and robust performance criteria. Furthermore, non-linear simulation has proved that using the proposed controller, the power oscillation damping behavior is also satisfactory under large disturbances.

Although only the series FACTS device is simulated, this general control scheme is also applicable to other types of FACTS devices.

Chapter 7

Conclusions and Future Works

7.1 Conclusions

This dissertation mainly concerns with the damping of power system oscillations by using of the coordinated control of FACTS devices and conventional PSS controllers. Besides the damping control researches, the power flow regulation associated with FACTS controllers are also discussed. In conclusion, this dissertation has the following research achievements:

1 FACTS modeling and controller design

FACTS modeling: In this thesis, for power system steady-state and dynamic researches, FACTS devices are modeled using the current injection method. Furthermore, programs for both steady-state study and dynamic study of large power systems embedded with FACTS devices have been developed.

FACTS damping controller design: The FACTS damping controllers are developed using the residue method and local signals are employed as control input signals of FACTS devices. This residue approach is a practical method for FACTS damping controller design in real large power systems.

2 Optimal choice and allocation of FACTS devices

Many criteria can be employed for searching of optimal locations of FACTS devices. Practically, the main concerns for the allocation of FACTS devices are their economic and the dynamic effects. Therefore in this thesis, two criteria are presented:

Economic criterion: Provided optimal locations, FACTS devices can be applied to achieve the optimal power flow without any constraint violations and thus to increase the utilization of the lowest cost generation in power systems. In this thesis, using the genetic algorithms, the locations of the FACTS devices, their types and rated values are optimized simultaneously. The objective cost function, which consists of the investment costs for FACTS devices and the generation costs, is minimized using the proposed approach.

Steady-state stability criterion: Besides to the economic criterion based allocation approach, the residue method based FACTS allocation approach is also applied to the power system dynamic analysis.

3 Adaptive FACTS transient controller design using ANFIS technology

This objective deals with the development of adaptive FACTS transient stability controller using ANFIS technology. The approach adaptively activates the FACTS transient stability controller in large power systems during large disturbances. The design aspects and their implementation in form of fuzzy-adaptive switching controller are presented. Furthermore, ANFIS technology is employed for the parameter optimization of the proposed controller. This approach is realized in a large power system and it is proved to be an effective method for the adaptive transient control of FACTS devices.

4 Simultaneous coordinated tuning of FACTS damping controller and conventional PSS controllers

In this research, a novel method for the coordinated tuning of FACTS damping controller and the conventional PSS controllers has been developed based on non-linear optimization algorithm. Using this method, interactions among FACTS controller and PSS controllers are considered and their controller parameters are optimized simultaneously. This algorithm is a practical approach for optimal tuning of multi-controllers in large power systems.

5 Robust FACTS loop-shaping POD controller design in large power systems

This study deals with the FACTS robust loop-shaping POD controller design in large power systems. By applying the model reduction and modern robust loop-shaping control technique, the FACTS robust loop-shaping controller is realized. The FACTS robust loop-shaping controller exploits the advantages of both conventional loop-shaping and modern H_∞ robust control technique. Moreover, it is a decentralized approach and practical for FACTS robust controller design in real large power systems.

7.2 Future works

1 FACTS in the liberalized electricity market

In deregulated electricity market, the generation and network operation are unbundled activities. That means they are carried out by different companies. FACTS devices can be employed for a global optimization of the power flow states. Therefore, FACTS devices provide increasing controllability over the power flow for the independent system operators (ISO) or transmission system operators (TSO). The FACTS ability in

optimizing the power flow can be applied to solve following problems in electricity market:

- 1 Optimal power flow control in the liberalized electricity market
- 2 Congestion management using FACTS devices

These aspects should be considered in future works.

2 Implementation of the proposed methods in real power system

With the rapid development of power electronics, FACTS devices could be widely employed in power systems. Therefore, the system planning, operational procedure, coordinated tuning and coordinated control of FACTS devices become imperative tasks in real power systems. Future prospects should focus on the implementation of the proposed methods in practical power system applications.

Appendices

Appendix 1

Appendix 1.1 Derivation of Equation 2.28 (Based on Reference [19])

Consider the system shown in Figure 2.10 and assume the state space description of subsystem $H(s)$ as:

$$\begin{aligned} s\mathbf{x}(s) &= \mathbf{A}_H \mathbf{x}(s) + \mathbf{b}_H u(s) \\ y(s) &= \mathbf{c}_H \mathbf{x}(s) + \mathbf{d}_H u(s) \end{aligned} \quad (\text{A.1})$$

A formal solution of the state equations can be obtained:

$$H(s) = \mathbf{c}_H \mathbf{M}_H(s) \mathbf{b}_H + \mathbf{d}_H \quad (\text{A.2})$$

$$\mathbf{M}_H(s) = (s\mathbf{I} - \mathbf{A}_H)^{-1} \quad (\text{A.3})$$

According to Equation 2.22 and A.1, the complete matrix state matrix $\tilde{\mathbf{A}}$ has the form:

$$\tilde{\mathbf{A}} = \begin{bmatrix} \mathbf{A} + \mathbf{b}\mathbf{d}_H\mathbf{c} & \mathbf{b}\mathbf{c}_H \\ \mathbf{b}_H\mathbf{c} & \mathbf{A}_H \end{bmatrix} \quad (\text{A.4})$$

From Equation A.2 and A.4, the partial differential of $H(s)$ with respect to K_P is:

$$\begin{aligned} \frac{\partial H(s)}{\partial K_P} &= \frac{\partial \mathbf{c}_H}{\partial K_P} \mathbf{M}_H \mathbf{b}_H + \mathbf{c}_H \mathbf{M}_H(s) \frac{\partial \mathbf{A}_H}{\partial K_P} \mathbf{M}_H(s) \mathbf{b}_H \\ &\quad + \mathbf{c}_H \mathbf{M}_H(s) \frac{\partial \mathbf{b}_H}{\partial K_P} + \frac{\partial \mathbf{d}_H}{\partial K_P} \end{aligned} \quad (\text{A.5})$$

$$\frac{\partial \tilde{\mathbf{A}}}{\partial K_P} = \begin{bmatrix} \mathbf{b} \frac{\partial \mathbf{d}_H}{\partial K_P} \mathbf{c} & \mathbf{b} \frac{\partial \mathbf{c}_H}{\partial K_P} \\ \frac{\partial \mathbf{b}_H}{\partial K_P} \mathbf{c} & \frac{\partial \mathbf{A}_H}{\partial K_P} \end{bmatrix} \quad (\text{A.6})$$

From Equation 2.13, 2.14 and A.4, the eigenvectors of $H(s)$ can be derived:

$$\boldsymbol{\phi}_H = \mathbf{M}_H(\lambda_i) \mathbf{b}_H \mathbf{c} \boldsymbol{\phi}_i \quad (\text{A.7})$$

$$\boldsymbol{\psi}_H = \boldsymbol{\psi}_i \mathbf{b} \mathbf{c}_H \mathbf{M}_H(\lambda_i) \quad (\text{A.8})$$

Since

$$\frac{\partial \lambda_i}{\partial K_P} = \boldsymbol{\phi}_i \frac{\partial \mathbf{A}}{\partial K_P} \boldsymbol{\psi}_i \quad (\text{A.9})$$

therefore substituting A.6, A.7 and A.8 in A.9:

$$\frac{\partial \lambda_i}{\partial K_P} = \boldsymbol{\psi}_i \cdot [\mathbf{I} : \mathbf{b} \mathbf{c}_H \mathbf{M}_H(\lambda_i)] \cdot \begin{bmatrix} \mathbf{b} \frac{\partial \mathbf{d}_H}{\partial K_P} \mathbf{c} & \mathbf{b} \frac{\partial \mathbf{c}_H}{\partial K_P} \\ \frac{\partial \mathbf{b}_H}{\partial K_P} \mathbf{c} & \frac{\partial \mathbf{A}_H}{\partial K_P} \end{bmatrix} \cdot \begin{bmatrix} \mathbf{I} \\ \dots \dots \\ \mathbf{M}_H(\lambda_i) \mathbf{b}_H \mathbf{c} \end{bmatrix} \cdot \boldsymbol{\phi}_i \quad (\text{A.10})$$

With the multiplication of A.10 and substitution of A.5 with $s=\lambda_i$:

$$\frac{\partial \lambda_i}{\partial K_P} = \boldsymbol{\psi}_i \cdot \mathbf{b} \cdot \frac{\partial H(\lambda_i)}{\partial K_P} \cdot \mathbf{c} \cdot \boldsymbol{\phi}_i \quad (\text{A.11})$$

According to Equation 2.26, Equation A.11 can be expressed as the residue form:

$$\frac{\partial \lambda_i}{\partial K_P} = R_i \cdot \frac{\partial H(\lambda_i)}{\partial K_P} \quad (\text{A.12})$$

Equation A.12 is the same as Equation 2.28.

Appendix 1.2 FACTS POD controller optimized parameters

Parameter Value	K_P	T_w	$T_1=T_3$	$T_2=T_4$	C_{Max}	C_{Min}
Initial	0.5	3.0	0.05	0.05	0.1	-0.1
Optimized	1.82	3.0	0.02	0.15	0.1	-0.1

Appendix 1.3 Three machine power system parameter

Base Value: $V_B = 220kV$; $S_B = 1000MVA$;

Generators: $2H_1 = 2H_2 = 8s$; $2H_3 = 10$; $D_1 = D_2 = D_3 = 0.0$;

$T_{d01} = T_{d02} = 4.49s$; $T_{d03} = 6s$;

$X_{d1} = X_{d2} = 1.56(p.u.)$; $X_{d3} = 2(p.u.)$;

$X_{q1} = X_{q2} = 1.06(p.u.)$; $X_{q3} = 1.9$;

$X'_{d1} = X'_{d2} = 0.17(p.u.)$; $X'_{d3} = 0.25(p.u.)$;

Transformers: $X_{T1} = X_{T2} = X_{T3} = j0.305 (p.u.)$

Transmission lines: $Z_{l1} = Z_{l2} = Z_{l3} = 0.0 + j0.25 (p.u.)$

UPFCs: $U_{Oper} = 220kV$;

$U_{max1} = U_{max2} = 0.1U_m$; $U_{min1} = U_{min2} = -0.1U_m$;

Loads: $L_1 = L_2 = L_3 = 0.05 (p.u.)$; $L_4 = 0.65 (p.u.)$

Appendix 1.4 Fuzzy coordination controller

$$K_1=0.7, N_1=0.2$$

Appendix 2

Appendix 2.1 Generation cost function

Generator	Coefficients		
	α_0	α_1	α_2
G1	100	60	0.06
G2	100	50	0.05
G3	500	300	1.00
G4	100	15	0.02
G5	100	45	0.03

Appendix 2.2 Optimized settings of FACTS devices

	Line No.	From Bus	To Bus	FACTS Type	Rated Value
Case 1	10	5	6	SVC	10.5 Mvar
Case 2	5	2	5	TCSC	-22% X_{Line}

Appendix 3

Appendix 3.1 Membership functions

	MFs	$SW1$	$SW2$	$SW3$	$SW4$
Input1 ΔP_{Line}	S	-0.5548	-0.06164	0.1244	0.2479
	M	0.1226	0.2477	0.4544	0.4875
	B	0.3538	0.5164	1.294	1.788
Input2 $\Delta P_e/\Delta t$	S	-6.75	-0.75	2.00	3.0
	M	2.006	3.00	9.0	10.
	B	8.9997	10	15.75	21.75

Appendix 3.2 Linear functions of Sugeno model

i	p_i	q_i	r_i
1	-0.95	0.01	6.716
2	35.211	0.00989	6.010
3	22.1	0.59	0.0558
4	0.367	3.96	2.022
5	24.7	0.0295	3.648
6	-6.815	0.898	0.0815
7	3.12	0.039	6.108
8	0.445	1.97	0.464
9	0.073	0.8322	0.0751

Appendix 4

Appendix 4.1 Optimized controller parameters

PSS controller

No.	K_{PSS}	T_w	T_1	T_2	T_3	T_4	No.	K_{PSS}	T_w	T_1	T_2	T_3	T_4
G1	8.58	10	0.08	0.01	0.08	0.01	G9	8.97	10	0.05	0.01	0.05	0.02
G2	8.58	10	0.08	0.01	0.08	0.01	G10	9.27	10	0.08	0.01	0.08	0.02
G3	9.06	10	0.04	0.02	0.1	0.01	G11	6.00	10	0.08	0.03	0.05	0.01
G4	7.07	10	0.08	0.02	0.08	0.02	G12	8.58	10	0.08	0.01	0.08	0.01
G5	6.67	10	0.05	0.01	0.08	0.02	G13	8.06	10	0.04	0.01	0.05	0.01
G6	6.67	10	0.05	0.01	0.08	0.02	G14	8.06	10	0.04	0.01	0.05	0.01
G7	6.67	10	0.05	0.01	0.08	0.02	G15	8.06	10	0.05	0.01	0.04	0.01
G8	8.72	10	0.08	0.01	0.08	0.02	G16	7.51	10	0.03	0.02	0.05	0.01

FACTS controller

No.	K_{FACTS}	T_w	T_1	T_2	T_3	T_4
1	76.00	10	0.05	0.01	0.05	0.02

Appendix 4.2 Dominant eigenvalues

Parameter Modes	Eigenvalues After Optimization	Frequency (Hz)	Damping Ratio	
			Before Optimization	After Optimization
Exciter Mode	-0.77±0.99i	0.1588	0.42299	0.60833
Inter-Area Modes	-0.37±2.71i	0.43168	0.061066	0.1359
	-0.28±3.57i	0.56863	0.023607	0.076861
	-0.55±4.28i	0.68184	0.04534	0.12672
	-0.32±5.13i	0.81645	0.032769	0.061816
Local Modes	-10.1±6.78i	1.0795	0.83104	0.82941
	-1.46±7.48i	1.1901	0.82323	0.19182
	-10.4±7.51i	1.1953	0.052032	0.80991
	-1.34±7.61i	1.2111	0.034204	0.17397
	-1.35±8.05i	1.2811	0.80398	0.16554
	-8.41±8.05i	1.2815	0.15185	0.7225
	-1.62±8.53i	1.3581	0.76757	0.18628
	-7.997±8.8i	1.3992	0.058226	0.67288
	-1.3±8.89i	1.4144	0.066857	0.14482
	-2.53±8.96i	1.4257	0.76674	0.27133
	-0.82±9.06i	1.4426	0.037742	0.090167
	-9.28±9.82i	1.5622	0.076926	0.68684
	-1.2±10.24i	1.6308	0.69868	0.11671
	-9.08±10.8i	1.7258	0.038234	0.64183
	-3.5±10.9i	1.7388	0.084028	0.3049
-5.4±11.89i	1.8915	0.097096	0.41557	

References

- [1] N.G. Hingorani, L. Gyugyi, *Understanding FACTS – Concepts and technology of Flexible AC Transmission Systems*, IEEE Press, 2000. ISBN 0-7803-3455-8.
- [2] Y. H. Song, A. T. Johns. *Flexible AC Transmission Systems (FACTS)*, IEE Press, London, 1999. ISBN 0-85296-771-3.
- [3] Y. Guo, D.J. Hill, Y. Wang. "Global transient stability and voltage regulation for power systems", *IEEE Transactions on Power Systems*. VOL. 16, NO. 4. November 2001.
- [4] J.Y. Liu; Y.H. Song; P.A. Mehta, "Strategies for handling UPFC constraints in steady-state power flow and voltage control". *IEEE Transactions on Power Systems*. VOL. 15, May 2000, pp. 566–571.
- [5] G. Rogers, *Power System Oscillations*, Kluwer Academic Publishers, December 1999.
- [6] T.S. Chung, and Y.Z. Li, "A hybrid GA approach for OPF with consideration of FACTS devices", *IEEE Power Engineering Review*, pp. 47-57, February. 2001.
- [7] M. Noroozian, L. Angquist, M. Ghandari, and G. Anderson, "Use of UPFC for optimal power flow control", *IEEE Trans. on Power Delivery*, vol. 12, 1997, pp. 1629–1634.
- [8] A. Nabavi-Niaki and M.R. Iravani, " Steady-state and dynamic models of unified power flow controller (UPFC) for power system studies", *IEEE'96 Winter Meeting*, 1996.
- [9] S. Gerbex, R. Cherkaoui, and A. J. Germond, "Optimal location of multi-type FACTS devices in a power system by means of genetic algorithms," *IEEE Trans. Power Systems*, vol. 16, August. 2001, pp. 537-544.

- [10] T. T. Lie, and W. Deng, "Optimal flexible AC transmission systems (FACTS) devices allocation," *Electrical power & Energy System*, vol. 19, No. 2, 1997, pp. 125-134.
- [11] W. L. Fang, and H. W. Ngan, "Optimising location of unified power flow controllers using the method of augmented Lagrange multipliers," *IEE Proc.-Gener. Transm. Distrib.*, vol. 146, September. 1999, pp. 428-434.
- [12] K. S. Verma, S. N. Singh, and H. O. Gupta, "Location of unified power flow controller for congestion management," *Electric Power Systems Research*, vol. 58, 2001, pp. 89-96.
- [13] B. A. Renz, A. S. Mehraban, C. Schauder, E. Stacey, L. Kovalsky, L. Gyugyi, and A. Edris, "AEP unified power flow controller performance", *IEEE Trans. Power Delivery*, vol. 14, no. 4, November 1999, pp. 1374-1381.
- [14] L.J. Cai and I. Erlich, "Fuzzy coordination of FACTS controllers for damping power system oscillations, " *Modern Electric Power Systems Proc. of the International Symposium Wroclaw*, September 11-13, 2002, pp. 251-256.
- [15] X. Lei, D. Jiang and D. Retzmann, "Stability improvement in power systems with non-linear TCSC control strategies", *ETEP*, vol. 10, No. 6, November/December. 2000, pp. 339-345.
- [16] P. Kundur, *Power System Stability and Control*, EPRI, McGraw-Hill, 1994, ISBN 0-07-035958-X.
- [17] H.F. Wang, "Selection of robust installing locations and feedback signals of FACTS-based stabilizers in multi-machine power systems", *IEEE Trans. Power Systems*, vol. 14, May 1999, pp. 569-574.
- [18] N. Yang, Q.H. Liu, J.D. McCalley, "TCSC controller design for damping inter area oscillations", *IEEE Trans. Power Systems*, vol. 13, May 1998, pp. 1304-1310.
- [19] F.L. Pagola, I.J. Perez-Arriaga and G.C. Verghese, "On sensitivities, residues and participations: Applications to oscillatory stability and Control", *IEEE Trans. Power Systems*, vol. 4, May 1989, pp. 278-285.

- [20] X. Lei, E. N. Lerch, and D. Povh, "Optimization and coordination of damping controls for improving system dynamic performance", *IEEE Trans. Power Systems*, vol. 16, August 2001, pp. 473-480.
- [21] T. Coleman, M.A. Branch, and A. Grace. *Optimization Toolbox—for Use with Matlab*, The Mathworks Inc, 1999.
- [22] I. Erlich and H. Pundt. "Digital program for the simulation of electromechanic transients in the medium and long-term range , " 8th. PSCC Helsinki, August, 1984, pp. 19-24.
- [23] S. Limyingcharone, U. D. Annakkage, and N. C. Pahalawaththa, "Fuzzy logic based unified power flow controllers for transient stability improvement", *IEE Proc*, vol. 145, No. 3, 1998, pp. 225–232.
- [24] R. B. Chedid, S. H. Karaki and C. El-Chamali, "Adaptive fuzzy control for wind-diesel weak power systems," *IEEE Trans. on Energy Conversion*, vol. 15, No. 1, 2000, pp. 71–78.
- [25] *Fuzzy Logic Toolbox—for Use with Matlab*, The Mathworks Inc, 1999.
- [26] R. D. Zimmermann, and D. Gan, "Matpower - a Matlab power system simulation package, " User's Manual," , Version 2.0, Dec. 1997.
- [27] K. Habur, and D. O'leary, "FACTS - Flexible AC Transmission Systems, For cost effective and reliable transmission of electrical energy," <http://www.siemens.com/TransSys/pdf/CostEffectiveReliabTrans.pdf>.
- [28] P. Paterni, S. Vitet, M. Bena, and A. Yokoyama, "Optimal location of phase shifters in the French network by genetic algorithm," *IEEE Trans. Power Systems*, vol. 14, pp. 37-42, August. 1999.
- [29] E. J. Oliveira, J. W. M. Lima, and K. C. Almeida, "Allocation of FACTS devices in hydrothermal system," *IEEE Trans. Power Systems*, vol. 15, pp. 276-282, February. 2000.

- [30] F. D. Galiana, K. Almeida, M. Toussaint, J. Griffin, and D. Atanackovic, "Assessment and control of the impact of FACTS devices on power system performance, " *IEEE Trans. Power Systems*, vol. 11, no. 4, November 1996.
- [31] X. P. Wang, and L. P. Cao, *Genetic Algorithms – Theory, Application and Software Realization*, Xi'an Jiaotong University, Xi'an, China, 1998.
- [32] S. Forrest, G. Mayer-Kress, "Genetic algorithms, non-linear dynamical systems, and models of international security, " *Handbook of Genetic Algorithms*, Van Nostrand Reinhold, pp. 166-185, 1991
- [33] Y. Xiao, Y.H. Song, C.C. Liu, Y.Z. Sun, "Available transfer capability enhancement using FACTS devices, " *IEEE Transactions on Power Systems*, Vol. 18, pp. 305-312, February 2003.
- [34] K.F. Man, K.S. Tang, S. Kwong, *Genetic Algorithms*, Springer-Verlag London Berlin Heidelberg, 1999.
- [35] J. Shing, R. Jang, "ANFIS: Adaptive-network based fuzzy inference System, " *IEEE Transactions on SMC*, Vol. 23, pp. 665-685, May/June 1993.
- [36] M. Pavella, D. Ernst and D. Ruiz-Vega, *Transient Stability of Power Systems*, Kluwer Academic Publishers, 2000.
- [37] J. J. Sanchez-Gasca and J. H. Chow, "Power system reduction to simplify the design of damping controllers for inter-area oscillations," *IEEE Trans. Power Systems*, vol. 11, no. 3, pp. 1342–1349, August 1996.
- [38] P. Pourbeik and M. J. Gibbard, "Simultaneous coordination of Power-System Stabilizers and FACTS device stabilizers in a multimachine power system for enhancing dynamic performance, " *IEEE Trans. Power Systems*, vol. 13, no. 2, pp. 473–479, 1998.
- [39] D. Arnautovic and J. Medanic, "Design of decentralized multi-variable excitation controller in multi-machine power systems by projective con-trols, " *IEEE Trans. Energy Conversion*, vol. EC-2, no. 4, pp. 598–604, Dec. 1987.

- [40] Z.Y. Huang, Y.X. Ni, C. M. Shen, F.F. Wu, S.S. Chen, and B.L. Zhang, "Application of unified power flow controller in interconnected power systems— modeling, interface, control strategy, and case study", *IEEE Trans. on Power Systems*, vol. 15, No. 2, 2000, pp. 817–824.
- [41] A. J. F. Keri, X. Lombard, and A. A. Edris, "Unified power flow controller (UPFC): modeling and analysis", *IEEE Trans. on Power Delivery*, vol. 14, No. 2, April 1999, pp. 648-654.
- [42] Y. Y. Hong, W. C. Wu, "A new approach using optimization for tuning parameters of power system stabilizers, " *IEEE Trans. on Energy Conversion*, vol. 14, no. 3, pp. 780–786, 1999.
- [43] M. Klein, L.X. Le, G.J. Rogers, S. Farrokhpay and N.J. Balu, " H_∞ damping controller design in large power systems, " *IEEE Trans. on Power Systems*, vol. 10, pp. 158–166, 1995.
- [44] J. Doyle, B. Francis and A. Tannenbaum, *Feedback Control Theory*, Macmillan Publishing Co., 1990.
- [45] S. Skogestad and I. Postlethwaite, *Multivariable Feedback Control*, John Wiley & Sons Ltd., 1996.
- [46] G.N. Taranto and J.H. Chow, " A robust frequency domain optimisation technique for tuning series compensation damping controllers, " *IEEE Trans. on Power Systems*, vol. 10, pp. 1219–1225, 1995.
- [47] K. Glover and D. McFarlane, " Robust stabilization of normalized coprime factor plant descriptions with bounded uncertainty, " *Systems and Control Letters*, Vol. 11, pp. 167–172, 1989.
- [48] R.Y. Chiang and M.G. Safonov, *Matlab Robust Control Toolbox – User’s Guide*, The MathWorks, Inc, 1998.
- [49] G.J. Balas, J.C. Doyle, K. Glover, A. Packard and R. Smith, *μ -Analysis and Synthesis Toolbox – User’s Guide*, The MathWorks, Inc, 1998.

- [50] North American Electricity Reliability Council (NERC), "Available transfer capability – definitions and determinations," NERC Report June 1996.
- [51] F. Wang, G. B. Shrestha, "Allocation of TCSC devices to optimize total transmission capacity in a competitive power market". *Power Engineering Society Winter Meeting, IEEE*, Vol. 2, pp. 587–593, 28 January-1 February 2001.
- [52] K. S. Verma, S. N. Singh, and H. O. Gupta, "FACTS devices location for enhancement of total transfer capability,". *Power Engineering Society Winter Meeting, IEEE*, Vol. 2, pp. 522–527, 28 January-1 February 2001.
- [53] D.Y. Xue, *Control System Computer Simulation*, QingHua Press, China, December 1990.
- [54] K.M. Zhou and J.C. Doyle, *Essentials of Robust Control*, Prentice Hall, September 1997.
- [55] C. Rehtanz, *Autonomous Systems and Intelligent Agents in Power System Control and Operation*, Springer-Verlag Berlin Heidelberg New York, 2003. ISBN 3-540-40202-0.
- [56] Herbert. Wohlfahrt, "*Dämpfung von Leistungspendelungen in elektrischen Energieversorgungsnetzen*," Ph.D Thesis, University Dortmund, Germany, 12.10.1987.
- [57] Nathan. Schnurr, "Potential von multifunktionalen FACTS-Geräten zur Erhöhung der Übertragungskapazität und Pendeldämpfung im UCTE-Netz". *ETG-Tagung*, 7 October 2003.
- [58] Christian. Becker, "*Autonome Systeme zur koordinierenden Regelung von FACTS-Geräten*," Ph.D Thesis, University Dortmund, Germany, 12.02.2001.
- [59] N. Martins, "Impact of interactions among power system controls," *CIGRE Task Force 38.02.16 Report*, 1999, Paris.

List of Symbols

Latin Symbols

A	The n by n state matrix
$\mathbf{A}_0(\mathbf{x})$	The equality functions
A_1, A_2	Fuzzy sets in the antecedent
a_{kj}	A element of the state matrix A
\mathbf{A}_{ps}	State matrix for the shaped plant G_{ps}
$arg(R_i)$	Phase angle of the residue R_i
B	Control or input matrix with dimensions n by the number of inputs r
b	Input vector of a SISO system
B	Big set of fuzzified signal
$\tilde{\mathbf{B}}$	Mode controllability matrix
$\mathbf{B}_0(\mathbf{x})$	The inequality constrains
$\mathbf{B}_1(\mathbf{f})$	The inequality constrains for the conventional power flow
$\mathbf{B}_2(\mathbf{g})$	The inequality constrains for FACTS devices
b_{gen}	A parameter determining the degree of non-uniformity
\mathbf{B}_{ps}	Input matrix of the shaped plant G_{ps}
C	The output matrix of size m by n
c	Output vector of a SISO system
$\tilde{\mathbf{C}}$	Mode observability matrix
$c(\mathbf{f})$	The total investment costs of FACTS devices
$c_1(\mathbf{f})$	The average investment costs of FACTS devices
c_{1SVC}	Cost function for SVC ($US\$/kVar$)
c_{1TCSC}	Cost function for TCSC ($US\$/kVar$)
c_{1UPFC}	Cost function for UPFC ($US\$/kVar$)
$c_2(\mathbf{P}_G)$	The generation cost
C_{damp-s}	Signal from series FACTS damping controller
$C_{damp-sh}$	The signal from shunt FACTS damping controller
C_{FACTS}	Compensation value of the FACTS devices

$C_{FACTS-s}$	Compensation value of the series FACTS devices
$C_{FACTS-sh}$	Compensation value of the shunt FACTS devices
$C_{Initial}$	The initial compensation value of FACTS devices
C_{Max}	The maximum compensation value of FACTS devices
c_{max}	A large positive constant to convert the GA objective function
C_{ps}	Output matrix for the shaped plant G_{ps}
C_{TCPST}	The cost of TCPST (US\$)
c_{Total}	The overall cost objective function
D	The feed forward matrix of dimensions m by r
d_{ex}	External disturbance
d_{ex}	External disturbances
D_{ps}	Feedforward matrix for the shaped plant G_{ps}
d_{TCPST}	The positive constant representing the capital cost of the TCPST
e	Control error
E₀(z)	The equality constrains
E₁(f, g)	The conventional power flow equations
f	A vector that represent the variables of FACTS devices
$f_1(\mathbf{x})$	The objective function of the controller parameter optimization
$f(\mathbf{z})$	The objective function defined as CDI
F(z)	The inequality constrains
F_c	The matrix of coefficients in the ANFIS training
f_i	Output of the ANFIS layer 4
Fitness	The objective function of the GA
$Fitness_r$	The fitness of the r^{th} individual
$Fitness_{sum}$	The sum of fitness in population
F_w	The transfer function between \mathbf{r}_{ex} and \mathbf{w}_{out}
F_p	The transfer function of the sensor
g	The operating state of the power system
G(s)	Transfer function of the original power system
$G(s)$	Transfer function of a SISO system
G_d	The transfer function of the output disturbance
G_{den}^{-1}	Stable left coprime factorization of G_{ps}

$G_{jk}(s)$	The transfer function between the k^{th} input and the j^{th} output
G_{num}	Stable left coprime factorization of G_{ps}
G_p	The transfer function of the plant
\mathbf{G}_p	The plant transfer functions
G'_p	The transfer function of the perturbed plant
G'_{ps}	The perturbed plant transfer function of G_{ps}
$\mathbf{G}_{p11} \sim \mathbf{G}_{p33}$	Partitioned transfer functions for the plant \mathbf{G}_p
G_{ps}	The shaped plant transfer function of G_p
$H(s)$	The transfer function of the FACTS controller
$H_1(s)$	The transfer function for the lead-lag and wash-out blocks
H_k	The inertia constant of the k^{th} generator
H_{LS}	The transfer function of the robust loop-shaping controller
H_{LS_Red}	Transfer function of the reduced-order robust loop-shaping controller
$H_p(s)$	The transfer function of the controller
H_{TCSC}	The transfer function of the TCSC controller
\mathbf{H}_p	Feedback controller transfer functions
i	i^{th} mode of oscillation
\mathbf{I}	Identity matrix
IC	The installation costs of TCPST
\bar{I}_{UPFC}	The current flow through the UPFC.
K	Amplification part of factored form of $G_1(s)$
K_1	The calibration of the input signal to fuzzy-logic controller
K_{FACTS}	Amplification part of series FACTS POD controller
K_P	Amplification part (positive constant gain) of FACTS POD controller
K_{P-s}	The proportional part of the series FACTS PI-controller
K_{P-sh}	The proportional part of the shunt FACTS PI-controller
K_{PSS}	Amplification of PSS controller
L_p	The loop transfer function
m	The output vector length
M	Medium set of fuzzified signal
m_c	The number of compensation stages
M_p	The transfer function between $[u_{in} \quad y_{out}]$ to Φ

n	The number of states (the number of eigenvalues)
N_1	The calibration of the input signal to fuzzy-logic controller
N_{11}	The transfer function for the system closed with uncertainties
N_{12}, N_{13}	The transfer function in N_c
N_{22}	The transfer function between \mathbf{r}_{ex} and \mathbf{w}_{out} when $\Delta = 0$
N_c	The transfer function of the controlled plant
n_{ex}	Sensor noise
\mathbf{n}_{ex}	Sensor noises
n_{FACTS}	The number of FACTS devices to be located
n_{Ind}	The number of individuals of the population
$n_{Location}$	The possible locations for FACTS devices
ns	Sample time
n_{Type}	Types of FACTS devices
\mathbf{P}	Participation matrix
$\mathbf{p}_1 \sim \mathbf{p}_n$	Element in participation matrix
$p_1 \sim p_n$	Poles of $G_1(s)$
p_c	The probability of crossover
p_{ci}	The consequent parameter of the ANFIS training
P_G	The output of the generator (MW)
\mathbf{P}_G	A vectors that represent the the active power outputs of the generators
$P_{Generator1}$	The active power provided by generator 1
$P_{Generator2}$	The active power provided by generator 2
P_{ij}	Power flow through the transmission line i - j
p_{ki}	Participation factor
P_{Line}	Active power which flows through the series FACTS device
$P_{Line}^{(0)}$	The initial active power transferred through the FACTS device
$P_{Line}^{(ns)}$	Active power transferred through FACTS device at sample time ns
$P_{Line}^{(ns+1)}$	Active power transferred through FACTS device at sample time $ns+1$
P_{max}	The thermal limit of the transmission line where TCPST is installed
p_r	The proportion of the r^{th} individual on the roulette wheel
P_{ref-s}	Reference values of the active power
P_{UPFC1}	The input signal for UPFC POD controller 1

P_{UPFC2}	The input signal for UPFC POD controller 2
q_{ci}	The consequent parameter of the ANFIS training
Q_{Max}	Maximal reactive compensation of SVC
Q_{Min}	Minimal reactive compensation of SVC
Q_{SVC}	Reactive compensation of SVC
r	The input vector length
r_{ci}	The consequent parameter of the ANFIS training
r_{ex}	Reference or command input
\mathbf{r}_{ex}	Normalized reference inputs
rf	The rated value of FACTS device
r_{gen}	A random value in the range of $[0, 1]$
R_i	The residue of $G(s)$ at pole p_i
$rtcsc$	Coefficient represents the compensation degree of TCSC
$rupfc$	Coefficient represents the compensation degree of UPFC
$rtcpst$	Coefficient represents the compensation degree of TCPST
$rsvc$	Coefficient represents the compensation degree of SVC
$rtcsc_{max}$	Maximal compensation degree of TCSC
$rtcsc_{min}$	Minimal compensation degree of TCSC
S	Small set of fuzzified signal
SI	Premise parameters of ANFIS training
$S2$	Consequent parameters of ANFIS training
S_{FACTS}	Operating range of the FACTS devices ($MVar$)
S_k	The base power of the k^{th} generator
S_s	The sensitivity function
$SW1 \sim SW4$	The calibration of the input signal to fuzzy coordination controller
T_0	The pre-set time for the FACTS transient stability controller
t_1	The time range of the simulation
T_{1-PSS}	Lead time constant of PSS controller
T_{2-PSS}	Lag time constant of PSS controller
T_{3-PSS}	Lead time constant of PSS controller
T_{4-PSS}	Lag time constant of PSS controller
T_{d-s}	The delay time constant for series FACTS devices

T_{d-sh}	The delay time constant for shunt FACTS devices
t_{gen}	The current generation number
T_{gen}	The total generation number
T_{I-s}	The integral time constant of the series FACTS PI-controller
T_{I-sh}	The integral time constant of the shunt FACTS PI-controller
T_{lag}	The lag time constant
T_{lag-1}	The lag time constant for UPFC POD controller 1
T_{lag-2}	The lag time constant for UPFC POD controller 2
T_{lead}	The lead time constant
T_{lead-1}	The lead time constant for UPFC POD controller 1
T_{lead-2}	The lead time constant for UPFC POD controller 2
T_{m-s}	The measurement time constant for the series FACTS devices
T_{m-sh}	The measurement time constant for the shunt FACTS devices
T_s	The complementary sensitivity function
T_w	The washout time constant
T_{w1}	The washout time constant for UPFC POD controller 1
T_{w2}	The washout time constant for UPFC POD controller 2
T_{w-PSS}	Washout time constant of PSS controller
$u(s)$	Input of the power system
U_A	FACTS terminal voltage magnitude
U_{bus}	The bus voltage magnitude
u_i	The value of control output
U_i	Voltage magnitude on the sending end of the transmission line
$\overline{U}_i^{(t)}$	The sending end voltage of TCSC at the time t
u_{in}	Actuating signal, plant input
\mathbf{u}_{in}	Actuating signals, plant inputs
U_j	Voltage magnitude on the receiving end of the transmission line
$\overline{U}_j^{(t)}$	The receiving end voltage of TCSC at the time t
U_m	The rated voltage of the transmission line where the UPFC is installed
U_{max}	Maximal inserted voltage magnitude of TCPST and UPFC
U_{max1}	Maximal inserted voltage magnitude of the UPFC series part
U_{max2}	Maximal inserted voltage magnitude of the UPFC series part

U_{Max}^k	The upper range of x_k
$U_{max-pss}$	Maximal output voltage of PSS
U_{max-Sh}	Maximal inserted voltage magnitude of the UPFC shunt part
U_{min1}	Minimal inserted voltage magnitude of the UPFC series part
U_{min2}	Minimal inserted voltage magnitude of the UPFC series part
U_{Min}^k	The lower range of x_k
$U_{min-pss}$	Minimal output voltage of PSS
U_{s-pss}	Output voltage of PSS
U_{ref-sh}	Reference values of the bus voltage magnitude
\bar{U}_{Shunt}	Shunt voltage source of UPFC
\bar{U}_{TCPST}	Series voltage source of TCPST
\bar{U}_{UPFC}	Series voltage source of UPFC
\bar{U}_{UPFC1}	Inserted voltage of the UPFC1 series voltage source
\bar{U}_{UPFC2}	Inserted voltage of the UPFC2 series voltage source
\mathbf{u}_Δ	The input to the system from uncertainties
v_{Fuzzy}	Fuzzy-logic controller output signal
v_i	The value of control output
v_{out}	Sensor output
W_{pre}	Pre-compensation function
W_{post}	Post-compensation function
W_o	Output weighting functions
\mathbf{w}_{out}	Normalized outputs to specify system performance
$W_{o_exciter}$	Output weighting function for the exciters
W_{o_FACTS}	Output weighting function for FACTS
x	The ΔP_{Line} (input signal to fuzzy coordination controller)
\mathbf{x}	A vector that contains the parameters of the POD controller
\mathbf{X}	The unique positive definite solution to the algebraic Equation 6.21
$\mathbf{x0}$	Initial values for the controller parameters
x_1	Tracking error of the feedback control system
X_{ij}	Reactance of the transmission line $i-j$
x_{In}	Active power flow through UPFC (input to fuzzy-logic controller)
x_k	Gene selected for mutation

x'_k	The result of the mutation
X_{Line}	The reactance of the transmission line where the TCSC installed
X_{Max}	Maximal reactance of TCSC
X_{Min}	Minimal reactance of TCSC
X_{par}	A give parent
X_{TCSC}	Reactance of TCSC
$X_{TCSC}^{(0)}$	The TCSC reactance at the initial operating point
$X_{TCSC}^{(t)}$	The TCSC reactance at the time t
y	The $\Delta P_e / \Delta t$ (input signal to fuzzy coordination controller)
Y	Input signal to fuzzy coordination controller
\bar{y}	Coordination signal for FACTS transient and POD controllers
$y(s)$	Output of the power system
y_{mu}	Represents $x_k - U_{Min}^k$ and $U_{Min}^k - x_k$ in the process of mutation
y_{out}	The output from the plant to the controller
\mathbf{y}_{out}	The outputs from the plant to the controller
\mathbf{y}_Δ	The outputs of the system, which drives the uncertainty dynamics
\mathbf{z}	Vector of the parameters of the PSSs and FACTS POD controllers
\mathbf{Z}	The unique positive definite solution to the algebraic Equation 6.19
$\mathbf{z0}$	The pre-selected initial values of the POD controllers
$z_1 \sim z_n$	Zeros of $G_1(s)$
\mathbf{z}_c	The vector of consequent parameters in the ANFIS training
Z_{ij}	The total line impedance with TCSC
$Z_{ij}^{(0)}$	The initial influence of TCSC on the transmission line
$Z_{ij}^{(t)}$	The influence of TCSC on the transmission line at the time t
Z_{Line}	Impedance of the transmission line
Z_{Shunt}	Impedance of the UPFC (shunt side)

Greek Symbols

α	Operating angle of the UPFC series voltage source
α_0	Constant coefficient for generation cost function
α_1	Constant coefficient for generation cost function
α_2	Constant coefficient for generation cost function
α_c	T_{lag} / T_{lead}
β	Operating angle of the UPFC shunt voltage source
β_i	Multiplication of the fuzzified signals (firing strength of each rule)
$\overline{\beta}_i$	The average ratio of the rule's firing strength
γ	A specified achievable value
γ_p	Achievable value of feedback system
γ_{pmin}	Lowest achievable value of feedback system
$\delta_{Area1-2}(0, \mathbf{x})$	The initial power angle difference between the researched areas
$\delta_{Area1-2}(t, \mathbf{x})$	The power angle difference between the researched areas at the time t
δ_{13}	The power angle difference between G1-G3
δ_{23}	The power angle difference between G1-G3
Δ	The level of the uncertainty
Λ	The disturbance transfer functions
$\Delta(t, y)$	Returns a value in the range $[0, y]$
Δ_{den}	Defines the level of uncertainty in coprime factorization
Δ_{num}	Defines the level of uncertainty in coprime factorization
$\Delta\delta(t, \mathbf{x})$	The power angle difference from the original operating point
δ_{Area3}	Center of power angles of area 3
δ_{Area4}	Center of power angles of area 4
δ_i	The phase angle of the sending end voltage
$\Delta\bar{I}_i$	Injected current at the sending end of the transmission line
$\Delta\bar{I}_j$	Injected current at the receiving end of the transmission line
δ_j	The phase angle of the receiving end voltage
$\Delta P_e / \Delta t$	Input to fuzzy coordination controller defined in Equation 4.1

ΔP_{Line}	Input to fuzzy coordination controller defined in Equation 4.1
ΔQ_{is}	Injected reactive power at the sending end of transmission line
Δt	The time step between two sample points
$\Delta \mathbf{u}$	The input vector of length r
$\Delta \bar{U}_{FACTS}$	Series voltage source of FACTS model
$\Delta \mathbf{x}$	The state vector of length equal to the number of states n
$\Delta X_{TCSC}^{(t)}$	The change of the TCSC reactance at the time t
$\Delta \mathbf{y}$	The output vector of length m
$\Delta \omega$	Generator speed difference
ε	Level of uncertainty
ε_p	Stability margin
ε_{pmax}	Maximum stability margin
λ	Eigenvalue of matrix \mathbf{A}
λ_i	The i^{th} eigenvalue of matrix \mathbf{A}
$\mu(x)$	The fuzzified signal
ρ	The spectral radius (maximum eigenvalue)
Φ_i	The right eigenvector associated with the i^{th} eigenvalue
ϕ_{ki}	Right eigenvector element on the k^{th} row and i^{th} column of matrix Φ
ϕ_{ji}	Right eigenvector element on the j^{th} row and i^{th} column of matrix Φ
Φ	Right eigenvector matrix
φ_{com}	The compensation angle
Ψ	Left eigenvector matrix
Ψ_i	The left eigenvector associated with the i^{th} eigenvalue
ψ_{ik}	Left eigenvector element on the i^{th} row and k^{th} column of matrix Ψ
ω_i	The frequency of the researched mode of oscillation in <i>rad/sec</i>

List of Abbreviations

AEP	American Electric Power
ANFIS	Adaptive Network based Fuzzy Inference System
ASC	Advanced Series Capacitor
ATC	Available Transfer Capability
BPA	Bonneville Power Administration
CBM	Capacity Benefit Margin
CDI	Comprehensive Damping Index
COA	Center of Power Angles
FACTS	Flexible AC Transmission Systems
FIS	Fuzzy Inference System
GA	Genetic Algorithm
ISO	Independent System Operators
LSE	Least Square Estimation
MF	Membership Function
POD	Power Oscillation Damping
PSD	Power System Dynamic
PSS	Power System Stabilizer
SISO	Single input single output
SVC	Static Var Compensator
SSR	Subsynchronous Resonance
TCPST	Thyristor Controlled Phase Shifting Transformer
TCSC	Thyristor Controlled Series Capacitor
TRM	Transmission Reliability Margin
TSO	Transmission System Operators
TTC	Total Transfer Capability
TVA	Tennessee Valley Authority
UPFC	Unified Power Flow Controller
VSI	Voltage Source Inverter
WAPA	Western Area Power Administration

Curriculum Vitae

Personal data

Name: Lijun Cai
Gender: Male
Date, place of birth: September 29, 1970, Hebei Province, P.R. China
Nationality: Chinese
Marital status: Married

School education

1978~1982 Attended the Xian Xue Jie primary school
Baoding City, Hebei Province, P.R. China
1982~1988 Attended the No. 2 Middle and High School of
Baoding City, Hebei Province, P.R. China

Studies

1988~1992 Undergraduate student
Department of Electric Engineering
North China Institute of Electric Power
1994~1997 Graduate student
Department of Electric Engineering
North China Electric Power University

Work experience

- | | |
|------------|--|
| 1992~1994 | Teach and research assistant
Specialized at Power System Diagnosis
Department of Electric Engineering
North China Institute of Electric Power |
| 1997~2000 | Lecturer and researcher
Specialized in Power System Monitoring and Control
Department of Electric Engineering
North China Electric Power University |
| Since 2000 | Research assistant
Department of Electric Engineering
University Duisburg-Essen, Germany |

Published Papers

Journal Paper

- 1 L.J. Cai and I. Erlich, " Simultaneous Coordinated Tuning of PSS and FACTS Damping Controllers in Large Power Systems, " accepted for publication in *IEEE Transactions on Power Systems*.

Papers in Proceedings

- 1 L.J. Cai and I. Erlich, "Fuzzy coordination of FACTS controllers for damping power system oscillations, " *Modern Electric Power Systems Proc. of the International Symposium Wroclaw*, September 11-13, 2002, pp. 251-256.
- 2 L.J. Cai and I. Erlich, "Optimal Choice and Allocation of FACTS Devices using Genetic Algorithms, " Paper published in *ISAP (Intelligent Systems Application to Power Systems) 2003*, Lemnos, Greece, August 31 – September 3, 2003.
- 3 L.J. Cai and I. Erlich, "Simultaneous Coordinated Tuning of PSS and FACTS Controller for Damping Power System Oscillations in Multi-Machine Systems, " Paper published in *IEEE Bologna Power Tech*, June 23-27, 2003.
- 4 L.J. Cai and I. Erlich, "Coordination between transient and damping controller for series FACTS devices using ANFIS technology, " Paper published in *IFAC Symposium on Power Plants & Power Systems Control 2003*, June 9-12, Seoul, Korea.

Developed Programs

- 1 Implementation of FACTS devices in *PC_PSD* (Power System Dynamics) program for both steady-state and dynamic analyses.
- 2 Implementation of FACTS devices in *Matpower* program for optimal power flow analysis.
- 3 Implementation of Genetic Algorithms in *Matpower* program for optimal FACTS allocation analysis.
- 4 Implementation of UPFC and TCPST in *Power System Toolbox* program for both steady-state and dynamic analyses.